BIOZENTRUM
Universität Basel
The Center for Molecular Life Sciences

Heterogeneity of inflammation and host metabolism in a typhoid fever model

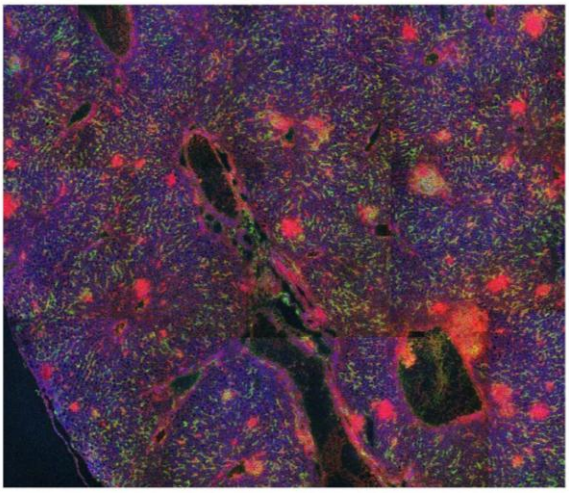

Inauguraldissertation
zur
Erlangung der Würde eines Doktors der Philosophie
vorgelegt der
Philosophisch-Naturwissenschaftlichen Fakultät
der Universität Basel
von

Anne Kathrin Schemmer

aus Münster in Westfalen, Deutschland

Basel, 2012

Originaldokument gespeichert auf dem Dokumentenserver der Universität Basel
edoc.unibas.ch

Dieses Werk ist unter dem Vertrag „Creative Commons Namensnennung-Keine kommerzielle Nutzung-Keine Bearbeitung 2.5 Schweiz“ lizenziert. Die vollständige Lizenz kann unter
creativecommons.org/licences/by-nc-nd/2.5/ch
eingesehen werden.

creative commons

Namensnennung-Keine kommerzielle Nutzung-Keine Bearbeitung 2.5 Schweiz

---

Sie dürfen:

das Werk vervielfältigen, verbreiten und öffentlich zugänglich machen

Zu den folgenden Bedingungen:

Namensnennung. Sie müssen den Namen des Autors/Rechteinhabers in der von ihm festgelegten Weise nennen (wodurch aber nicht der Eindruck entstehen darf, Sie oder die Nutzung des Werkes durch Sie würden entlohnt).

Keine kommerzielle Nutzung. Dieses Werk darf nicht für kommerzielle Zwecke verwendet werden.

Keine Bearbeitung. Dieses Werk darf nicht bearbeitet oder in anderer Weise verändert werden.

- Im Falle einer Verbreitung müssen Sie anderen die Lizenzbedingungen, unter welche dieses Werk fällt, mitteilen. Am Einfachsten ist es, einen Link auf diese Seite einzubinden.
- Jede der vorgenannten Bedingungen kann aufgehoben werden, sofern Sie die Einwilligung des Rechteinhabers dazu erhalten.
- Diese Lizenz lässt die Urheberpersönlichkeitsrechte unberührt.

Die gesetzlichen Schranken des Urheberrechts bleiben hiervon unberührt.

Die Commons Deed ist eine Zusammenfassung des Lizenzvertrags in allgemeinverständlicher Sprache: http://creativecommons.org/licenses/by-nc-nd/2.5/ch/legalcode.de

Haftungsausschluss:
Die Commons Deed ist kein Lizenzvertrag. Sie ist lediglich ein Referenztext, der den zugrundeliegenden Lizenzvertrag übersichtlich und in allgemeinverständlicher Sprache wiedergibt. Die Deed selbst entfaltet keine juristische Wirkung und erscheint im eigentlichen Lizenzvertrag nicht. Creative Commons ist keine Rechtsanwaltsgesellschaft und leistet keine Rechtsberatung. Die Weitergabe und Verlinkung des Commons Deeds führt zu keinem Mandatsverhältnis.

Quelle: http://creativecommons.org/licenses/by-nc-nd/2.5/ch/ Datum: 3.4.2009

Genehmigt von der Philosophisch-Naturwissenschaftlichen Fakultät
auf Antrag von

Prof. Dr. Dirk Bumann und Prof. Dr. Christoph Dehio

Basel, den 27.März 2012

Prof. Dr. Martin Spiess
Dekan

Table of contents

Abstract

Systemic infections can lead to severe inflammation and altered host metabolism. These host responses are being extensively studied, but their spatial relationships in infected tissues remain largely unknown.

The goal of this thesis was to investigate the spatial organization of metabolic and inflammatory patterns in *Salmonella*-infected tissues and to elucidate the impact of host heterogeneity on host-*Salmonella* interactions in a murine typhoid fever model.

We showed that antimicrobial effector mechanisms such as generation of ROS and RNS occurred predominantly in granulomatous lesions. However, a substantial fraction of *Salmonella* resided outside of these lesions and was therefore not covered by these antimicrobial regions. Heterogeneous exposure to RNS induced distinct, locally adapting *Salmonella* subpopulations (see chapter 2.1).

We also investigated host metabolic enzyme activities in various tissue regions. Using a novel combination of immunostaining with enzyme histochemistry, we showed that granulomas had a distinct metabolic profile with a high capacity for generation of NADPH, an essential substrate for local generation of bacteriostatic/bactericidal ROS and RNS. Indeed, adaptation of GFP-based live/dead discrimination revealed extensive *Salmonella* killing that predominantly occurred in granulomas (see chapter 2.2).

The spatial segregation of live *Salmonella* from regions with massive killing also offered a potential explanation why surface-associated *Salmonella* antigens, but not internal antigens that are inaccessible in live *Salmonella*, were required for protective immunity (see chapter 2.3).

In conclusion, this thesis revealed markedly heterogeneous conditions in *Salmonella*-infected host tissues that had profound impact on disease mechanisms, infection control, and immunity.

1. Introduction

1.1 Host immune responses to Gram negative bacterial infection

The human body consists of 10^{13} cells, while it is colonized by 10^{14} bacteria. Evidently, bacteria play an important role and it is therefore crucial to understand host-bacterial interactions. Commensal bacteria, which naturally colonize the body, can be neutral or even beneficial for human health. In contrast, pathogenic bacteria cause damage to the host.

Before a bacterial infection can be established, natural barriers such as epithelial and mucosal tissues have to be crossed. Bacteria mostly enter through orifices of the body, but cuts and wounds can also allow direct entry into the blood stream. Harm during an infection can be caused by the release of bacterial toxins which have the potential to damage host tissues. Damage can be also caused more indirectly by bacterial components whose recognition by the immune system leads to the initiation of inflammatory processes.

Acute inflammation is defined by five criteria, which are pain, redness, swelling, heat and loss of function. Vasodilation of blood vessels leads to increased blood flow and vessels become more permeable to plasma and leukocytes, which leads to swelling and redness.

Inflammation can be beneficial for the host, fostering elimination of the pathogen. However, overshooting inflammation can lead to extensive tissue damage, sepsis or multi-organ failure, conditions which are detrimental or even lethal to the host (Oberholzer et al., 2001).

Once bacteria are located within host tissues, they are in most cases rapidly recognized based on their pathogen-associated molecular patterns (PAMPs), which can be of different molecular nature, for example lipids, carbohydrates, proteins or bacterial CpG DNA. Some pattern recognition receptors (PRRs) that identify these foreign molecules are expressed on the surface of innate immune cells (Kumar et al., 2011) but also parenchymal cells (Liu et al., 2002). As an example, Gram negative bacteria can be recognized by their lipopolysaccharide (LPS) which is scavenged by LBP, the lipopolysaccharide binding protein. The LBP complex then binds to CD14, which is a membrane protein on macrophages and other cell types, or circulates as a soluble protein in the blood stream. The LPS-CD14 complex binds to Toll-like receptor four (TLR4), which belongs to a group of transmembrane PRRs (Rock et al., 1998).

Other PRRs are expressed in the cytoplasm, for example NOD1, which recognizes diaminopimelic acid, a peptidoglycan component that is specific to Gram negative bacteria.

Ligand binding to the receptor initiates an intracellular signaling cascade. This ultimately triggers proinflammatory transcription factors including NFκB and AP-1 to translocate into the nucleus where they initiate expression of target genes, such as cytokines and chemokines. The secretion of these inflammatory mediators leads to the onset of inflammation. Signals from the affected tissue stimulate endothelial cells of the microvasculature to express adhesion molecules (selectins) and to secrete chemokines that are then bound on the cell surface and presented to leukocytes (Molteni et al., 2006).

Leukocytes patrolling the blood tether and roll on these activated endothelial cells by binding of surface glycoproteins to endothelial selectins. Repeated binding and loosening of these interactions rolls the cells towards the inflamed tissue. It also enables sensing of the chemokines which leads to the activation of integrins on the leukocyte surface (Takada et al., 2007). Integrins interact with ligands of the inflamed vasculature, intercellular adhesion molecules (ICAMs) and vascular cell adhesion molecules (VCAMs). These interactions allow the leukocyte to increase binding to the endothelium and to further slow down (see figure 1).

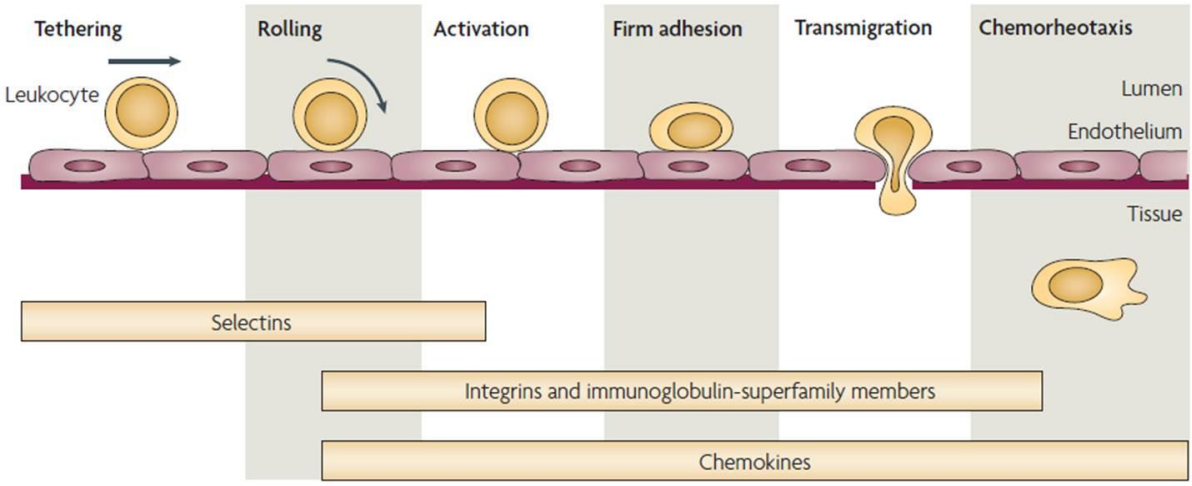

Figure 1. Leukocyte extravasation. Adapted from Weber et al. (Weber et al., 2007).

Cells then transmigrate in an amoeboid fashion through the endothelial layer into the tissue (Muller, 2003) and follow the chemokine gradient towards the site of inflammation. The process

described is called leukocyte extravasation and is dominated by phagocytes, mostly neutrophils and macrophages which are recruited from bone marrow, blood or spleen (Swirski et al., 2009).
In conjunction with physical migration these cells undergo a change in expression patterns and physiological properties. Stimulated by cytokines and chemokines, cells change from a resting to a primed, or elicited state. Transmigration and TLR stimulation leads to further activation. Resolution of inflammation finally promotes anti-inflammatory, alternatively activated cells (Gordon and Martinez, 2010).
Neutrophils, also named polymorphonuclear leukocytes (PMNs), are the first cells to be recruited to the site of infection and are the most abundant type of granulocytes. They derive from myeloid progenitor cells in the bone marrow (Klion and Nutman, 2004). Neutrophils enter the blood in a mature, but dormant state until they are recruited into the tissue (Borregaard, 2010). Transmigration leads to neutrophil activation, indicated by increased transcriptional activity (Theilgaard-Monch et al., 2004).
Upon contact with a bacterium, neutrophils can engulf it, forming a new cell compartment, the phagosome. In addition, the content of cytoplasmic granules can be released into the phagosome in a process called degranulation. Azurophil granules contain bactericidal proteins, such as serine proteases and myeloperoxidase, an enzyme that generates hypochloric acid from hydrogen peroxide and chloride ions. So-called specific granules store collagenase, lactoferrin, other enzymes and antimicrobial peptides. Neutrophils can also form extracellular traps (NETs), which are extracellular fibers mainly composed of chromatin, to scavenge bacteria (Brinkmann et al., 2004).
Upon stimulation, neutrophils also generate superoxide during the so-called oxidative burst, which indicates an increased uptake of oxygen. The enzyme NADPH oxidase reduces molecular oxygen by transferring electrons from NADPH. The enzyme assembles from cytoplasmic and membrane- associated subunits upon stimulation (Robinson, 2009) (see figure 2).

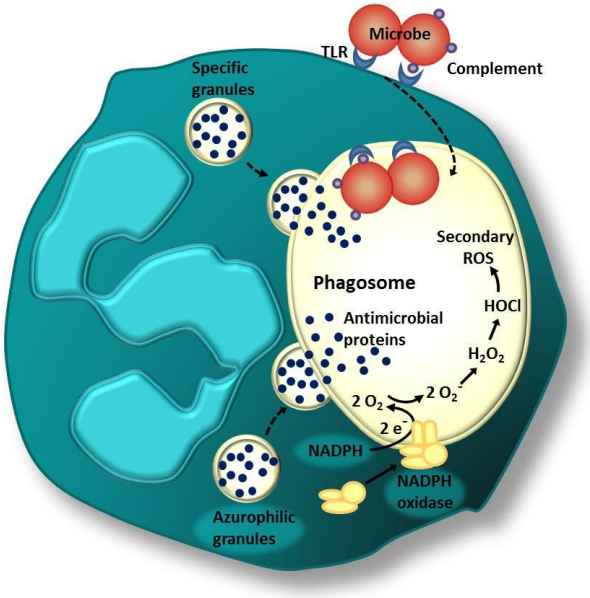

Figure 2. Events during the oxidative burst in neutrophils. Production of NADPH and enhanced O_2 consumption lead to ROS formation by the NADPH oxidase, which assembles at the membrane. (Adapted from Kobayashi and DeLeo (Kobayashi and DeLeo, 2009).

Superoxide can undergo spontaneous or enzymatic dismutation to form hydrogen peroxide. The reaction with ferrous iron generates hydroxyl radicals. All these compounds represent reactive oxygen species (ROS). ROS are responsible for oxidative stress; they damage proteins, DNA and lipids. If ROS truly are the causative agents of bacterial killing in phagocytes still remains a subject of discussion (Slauch, 2011).

The concentrations of superoxide and hydrogen peroxide estimated in a model of the phagosome are too low to be bactericidal, when compared to *in vitro* data. These experiments on the other hand probably fail to sufficiently mimic the real *in vivo* situation. Bacteria may be exposed to much higher stress in the phagosome, related to synergistic ROS actions and close proximity to the source of ROS production (Fang, 2011).

On the other hand, ROS may not be themselves bactericidal, but the NADPH oxidase could rather function indirectly by pumping electrons inside the phagosome. This should lead to a compensatory flux of potassium ions which is essential for the activation of granule enzymes by dissociation from the negatively charged granule membrane (Segal, 2005). However, this model remains controversial (2010; Thrasher and Segal, 2011). Neutrophils also express the inducible nitric oxide synthase (iNOS), although to a lower extent than macrophages. iNOS generates

nitric oxide (NO) in a reaction that also consumes NADPH. NO can give rise to other reactive nitrogen species (RNS) and it can react with superoxide to form the highly reactive peroxynitrite. Beside their function as microbicidal agents, ROS and RNS are important signaling and regulatory molecules under physiological conditions and during inflammation (D'Autreaux and Toledano, 2007; Nathan, 2003).

In addition to these putatively beneficial actions of host-derived ROS and RNS, these species are also highly dangerous for the producing phagocytes and neighboring host cells. Cells protect themselves by the use of detoxifying enzymes including catalases and peroxidases, which scavenge hydrogen peroxide, and superoxide dismutases (SOD) that neutralize superoxide. In addition, the glycine-cysteine-glutamate tripeptide glutathione (GSH) can scavenge various radicals via the thiol group of cysteine. Oxidized glutathione reacts with a second glutathione molecule to form reduced GSSG and water. GSH can be regenerated via glutathione reductase with NADPH. Therefore, NADPH not only plays a key role in generation of ROS and RNS, but also in antioxidant defense (see figure 3). Other antioxidants such as α-tocopherol or carotinoids also aid in limiting ROS/RNS damage (Splettstoesser and Schuff-Werner, 2002).

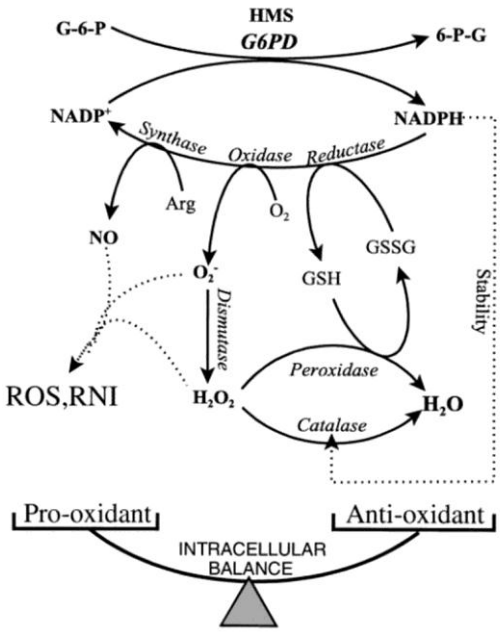

Figure 3. Intracellular redox balance. Adapted from Spolarics (Spolarics, 1998).

As described, neutrophils do not rely on a single weapon against bacteria, but employ a set of oxygen-dependent and independent mechanisms to be effective. Because they produce highly cytotoxic compounds, they are also potentially dangerous for the host tissue. A short lifespan of one to two days maximum inside the tissue limits tissue damage and renders dead neutrophils a main component of pus during an infection (Kantari et al., 2008).

Macrophages represent another important type of professional phagocytes, which derive from monocytic progenitor cells in the bone marrow. Monocytes circulate in the blood and differentiate into macrophages and dendritic cells during tissue recruitment (Galli et al., 2011). In contrast to neutrophils, macrophages are abundant even in healthy tissues, as a population of resident macrophages. Important physical barriers like the skin, gastrointestinal tract or the respiratory system, but also internal organs like the liver harbor especially large populations of macrophages. These cells are essential for clearance of cellular debris and thus in the first place have janitorial functions (Mosser and Edwards, 2008). They also serve for immune surveillance, protecting the tissue from invading microorganisms (Knolle and Gerken, 2000). In case of an infection, pathogens are rapidly recognized by macrophages which leads to the initiation of inflammation and subsequent recruitment of another type of macrophages, so-called inflammatory macrophages from the blood, to the site of infection, where they are subsequently activated. Compared to resident macrophages, inflammatory macrophages are more proficient in uptake, killing and subsequent removal of bacteria, although not as efficient as neutrophils. After macrophage phagocytosis of bacteria, the resulting phagosomes fuse with lysosomes, compartments that contain acid hydrolase and other digestive enzymes as well as the NADPH oxidase complex. This enzyme enables macrophages to exhibit an oxidative burst, similar to neutrophils. Inflammatory macrophages that are characterized by high expression of the cell surface marker Ly6C, also express the inducible nitric oxide synthase (iNOS), particularly when stimulated by IFN-γ and exposed to bacterial LPS.

Macrophages activated in this manner serve for host defense and are called classically activated, or M1 macrophages. Besides this classical activation, other subtypes of macrophages are known, which are summarized as alternatively activated, or M2 cells (Vats et al., 2006). Interleukin-4 (IL-4) stimulated cells are termed wound-healing macrophages and mainly function in the secretion of extracellular matrix components, while regulatory macrophages produce IL-10 and are

strongly anti-inflammatory (Mosser and Edwards, 2008). These fundamental differences in function are associated with physiological differences (see below).

In contrast to neutrophils macrophages also play an important role for adaptive immunity in presenting bacterial antigens to lymphocytes. The main antigen-presenting cell types (APCs) however are dendritic cells which can be derived from myeloid progenitor cells or macrophages (Banchereau and Steinman, 1998).

A critical aspect of fighting bacterial infections is the local restriction of infection, in order to prevent a systemic spread of the disease. Infected cells and origins of inflammation are named infectious or inflammatory foci. These foci attract neutrophils, leading to neutrophil-rich abscesses, and later macrophages by chemokine gradients as previously described. It is thought that these lesions form in order to restrict the inflammation to small areas, thus protecting the surrounding tissue from collateral damage and prevent bacterial dissemination. Neutrophils and macrophages form tight clusters in which they cooperate and stimulate each other by the secretion of cytokines, enhancing their antimicrobial properties (Silva, 2011). This gives rise to high local concentrations of proinflammatory cytokines, which are required for the maintenance of lesion structure (Co et al., 2004), and also high concentrations of toxic agents produced by the leukocytes.

In a dynamic process that involves the recruitment of further macrophages and lymphoid cells, these foci maturate into granulomas. A granuloma is an organized structure, consisting of an inner core of partially necrotic neutrophils and macrophages and an outer ring of macrophages, T and B cells. Granuloma formation represents a typical response to chronic infections such as tuberculosis, but also acute *Salmonella* or *Listeria* infections (Sheppard et al., 2003).

Despite the probably hostile environment of infection foci/granulomas, some bacteria manage to evade host killing and can even spread further into the tissue. It is not fully understood, how the host defense mechanisms can be subverted and if granuloma formation really benefits the host or sometimes even the pathogen, as has been suggested for *Mycobacterium* (Flynn, 2004).

1.2 Host metabolic responses to bacterial infection

Leukocyte metabolism

The activity of a cell depends on its metabolism. Only if the suitable nutrients are taken up and transformed into energy and cell components, the cell can function according to its physiological role.

Leukocytes have distinct patterns of metabolism. For example, in order to phagocytose and kill bacteria and to defend themselves against collateral damage, activated phagocytes have another metabolic profile than resting cells. To study the metabolism of these cells, they have been isolated and analyzed *ex vivo*, but there is sparse information about *in situ* metabolic activities of these cells.

Macrophages have been described as metabolically active cells, comprising high protein and lipid turnover (Newsholme et al., 1996). Non-activated, elicited peritoneal macrophages show a pattern of high glucose consumption and glycolytic flux as well as high activities for hexose monophosphate shunt (HMP shunt) enzymes. Beside glucose, also glutamate and fatty acids serve as main nutrients for these cells. Most of the glucose is fermented to lactate and glutamate and fatty acids are also not fully oxidized. Nonetheless, activities of TCA cycle enzymes suggested a potentially high, yet unexploited capacity for this pathway (Calder, 1995; Newsholme et al., 1996). In contrast to peritoneal macrophages that reside in a hypoxic environment, alveolar macrophages, which are exposed to higher oxygen concentrations, exhibit elevated TCA cycle and respiratory activity. They can change their physiology in response to different oxygen concentrations, which reveals the metabolic plasticity of this cell type (Nizet and Johnson, 2009; Simon et al., 1977).

During classical macrophage activation, NADPH oxidase causes an increase of O_2 consumption (oxidative burst) but also an increased demand for NADPH. The main source for NADPH is the oxidative branch of the HMP shunt. An increased HMP shunt activity has been described for phagocytosing macrophages, compared to resting cells (Costa Rosa et al., 1995). A parallel increase in glucose uptake and hexokinase activity to provide more glucose-6-phosphate (G6P) has also been demonstrated (Newsholme et al., 1996). Increased uptake is partly facilitated by the enhanced expression of glucose transporters (GLUTs) (Calder et al., 2007).

However, the dominant metabolic change during macrophage activation is a strong increase in glycolytic flux to meet the enhanced energy demand during activation. This metabolic program is controlled by the hypoxia-inducible factor (HIF)-1α, which is stabilized by NFκB expressed in macrophages and induces the expression of glycolytic enzymes (Cramer et al., 2003; Garedew et al., 2010; Shapiro et al., 2011). NO, produced by iNOS, impairs mitochondrial function (Garedew and Moncada, 2008). NO renders mitochondria non-functional, but the mitochondrial membrane potential has to be maintained in order to prevent the induction of apoptosis. Therefore, large quantities of ATP are hydrolyzed by ATP synthase inside the mitochondrial membrane in order to maintain the proton-motive force (Garedew et al., 2010). In accordance with this metabolic pattern, oxidative phosphorylation (OXPHOS) enzymes are down-regulated (Rodriguez-Prados et al., 2010). Uptake of fatty acids (FA) and fatty acid oxidation are also lowered during classical activation (Vats et al., 2006) (see figure 4).

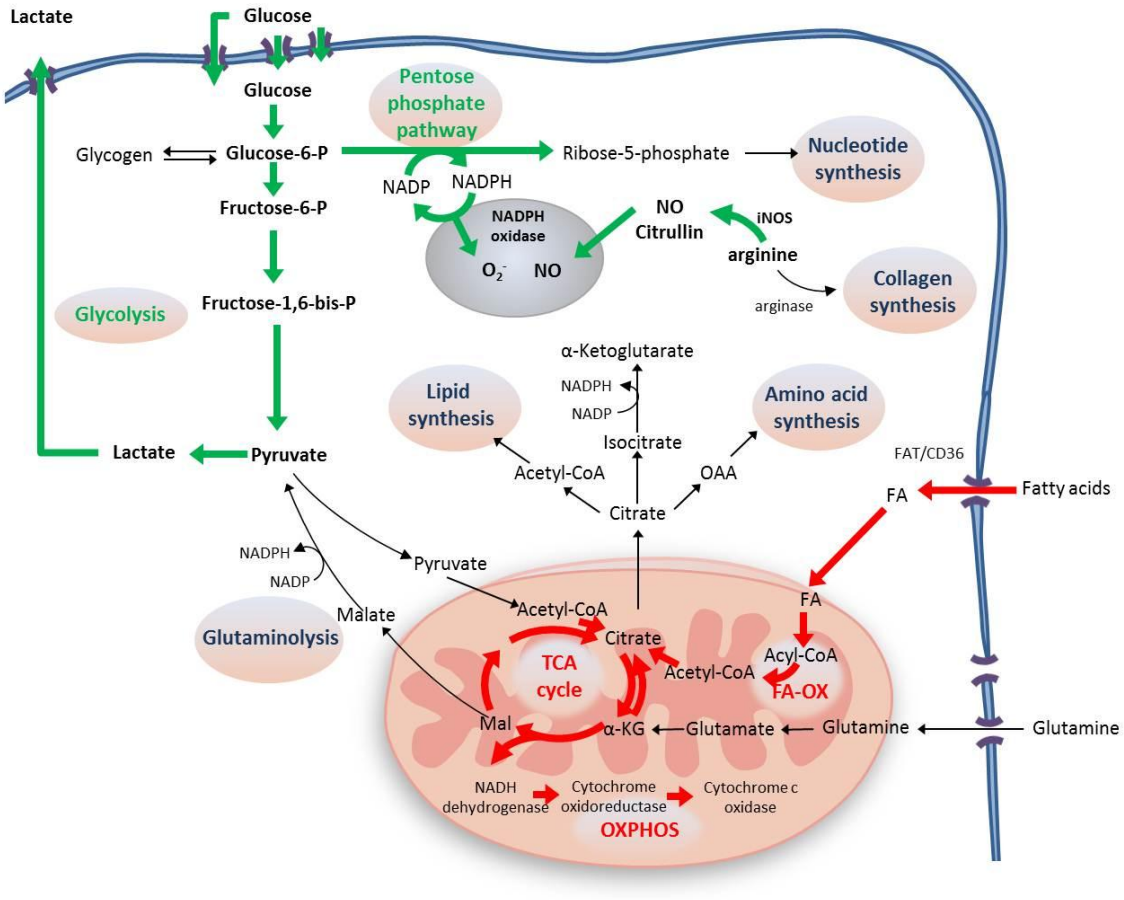

Figure 4. Metabolism of M1 classically activated macrophages. Green lines indicate up-regulated pathways; red lines indicate down-regulated pathways. Modified from Levine and Puzio-Kuter (Levine and Puzio-Kuter, 2010).

Alternatively activated macrophages such as wound-healing macrophages exhibit a less pronounced increase in glycolysis, but highly increase their capacity for the TCA cycle and oxidative phosphorylation (Odegaard et al., 2007; Rodriguez-Prados et al., 2010), fatty acid uptake and oxidation (Vats et al., 2006). On the molecular level, this metabolic switch can be induced by the response to IL-4 through the activation of signal transducer and activator of transcription 6 (STAT6) and PPAR-γ coactivator-1b (PGC-1β) that induce fatty acid oxidation and synthesis of mitochondria (Vats et al., 2006) (see figure 5).

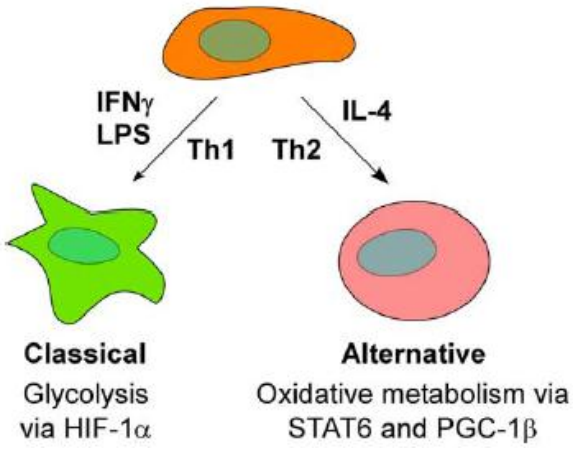

Figure 5. Model for regulation of macrophage activation by metabolic regulators (Vats et al., 2006).

The activity of the NADPH oxidase decreases during alternative activation (Balce et al., 2011). By enhanced expression of arginase 1, L-arginine is deprived from the reaction catalyzed by the iNOS. Both changes lead to an impairment of ROS and RNS production, accounting for the anti-inflammatory character of this cell-type (Varin and Gordon, 2009) (see figure 6).

The largest population of fixed tissue macrophages, called Kupffer cells (KCs), resides in the liver and represents approximately 70% of all macrophages in the body. Compared to peritoneal macrophages, these macrophages exhibit less anaerobic glycolysis and higher capacity for TCA cycle activity. Again, activation by pro-inflammatory cytokine TNF-α can prime KCs, leading to increases in glucose utilization and glycolytic flux. Upon a second, phagocytic, stimulus or by activation with phorbol myristate acetate (PMA) these cells additionally exhibit an increase in HMP shunt activity (Spolarics et al., 1991). However, resident macrophages are usually less responsive to inflammatory signals and exhibit a lower capacity for the production of ROS and proinflammatory mediators, compared to infiltrating inflammatory macrophages (Laskin et al., 2001). During infection, resident macrophages also clear dead neutrophils, which can even induce an Il-10 mediated alternative activation (Holub et al., 2009).

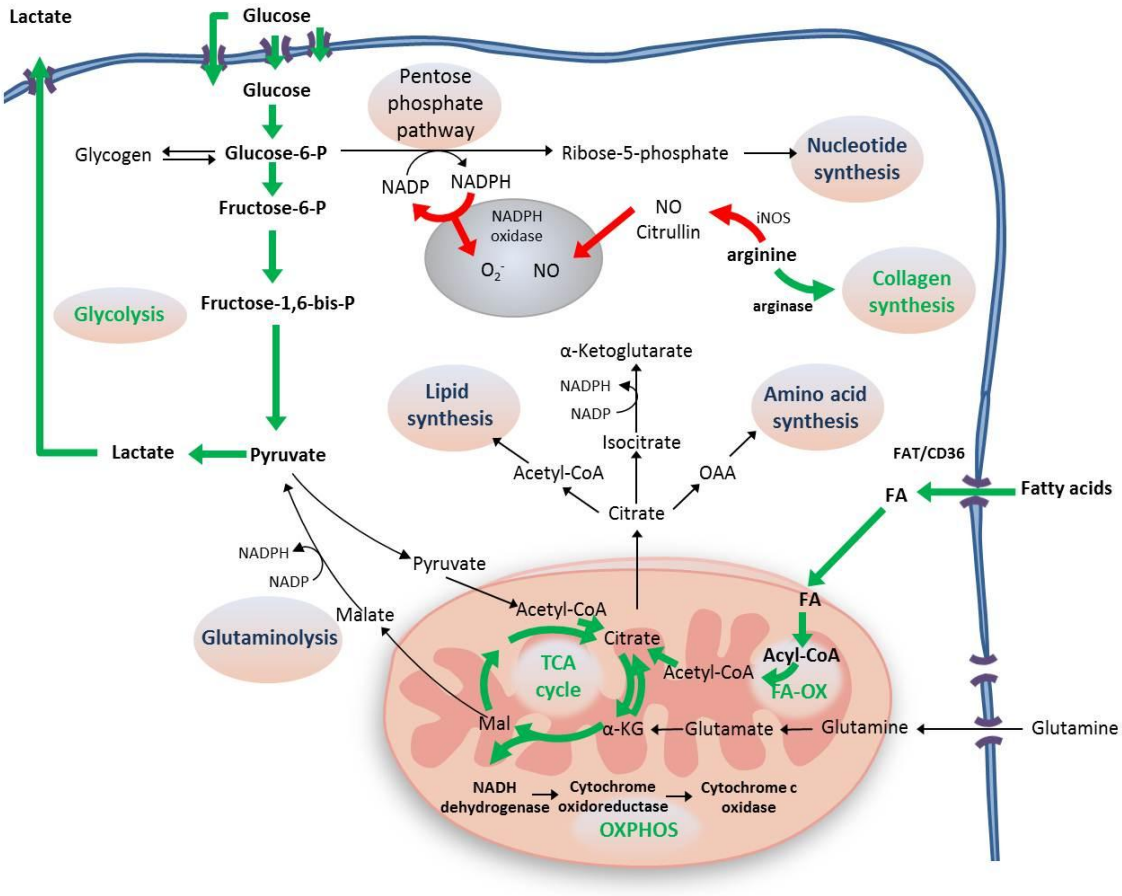

Figure 6. Metabolism of M2 alternatively activated macrophages. Green lines indicate up-regulated pathways; red lines indicate down-regulated pathways. Modified from Levine and Puzio-Kuter (Levine and Puzio-Kuter, 2010).

Compared to macrophages, metabolism of neutrophils has been less well studied. Neutrophils have a less flexible metabolic pattern and already exhibit high glucose consumption and glycolytic flux in the resting state (Shapiro et al., 2011). The TCA cycle is not important for the gain of energy in this cell type. Upon phagocytosis, ATP levels drop, probably in response to enhanced energy demand, but glucose utilization and glycolysis remains constant (Borregaard and Herlin, 1982). It was generally assumed that neutrophils possess only few and small mitochondria, but in fact they exhibit a complex mitochondrial network throughout the cytoplasm (Fossati et al., 2003). However, mitochondria do not serve for oxidative phosphorylation and rather play a role in apoptosis (Kobayashi and DeLeo, 2009; Peachman et al., 2001).

Granuloma metabolism

The metabolic profile of granulomas has been studied in animal models of mycobacterial infection (MTB). Positron emission tomography (PET) reveals granulomas as areas of increased glucose uptake and enhanced metabolic activity (Davis et al., 2009).

Enzyme histochemistry revealed activity of almost all central carbon metabolism enzymes investigated (Cerny, 1980; Wertheimer, 1967). A recent study on excised granulomas revealed increases in various metabolites, suggesting that granulomas have a distinct metabolism from uninfected tissue. In accordance with the metabolism described for isolated neutrophils and macrophages, the more abundant metabolites such as lactate, glutathione and alanine are indicative of glycolysis, HMP shunt and TCA cycle activities (Somashekar et al., 2011). Furthermore, transcriptional profiling and lipid analysis have identified MTB granulomas as areas of lipid accumulation. The detected abundance of free cholesterol (CHO), cholesterol esters (CE) and triglycerides (TG) is indicative of enhanced uptake of low-density lipoproteins (oxLDL) by macrophages (Kim et al., 2010).

Global metabolic derangements during systemic infection

To account for the enhanced energy demand of the leukocytes during infection, the body needs to provide nutrients in a sufficient amount. Indeed, increased concentration of free glucose (hyperglycemia) in the blood is a consequence of systemic infections. In later stages of disease, glucose is consumed in high rates resulting in hypoglycemia and the concentration of lactate is increased (hyperlactatemia) (Spitzer et al., 1988; Trager et al., 2003).

As a central regulator of glucose and lipid homeostasis, the liver has a key role in the redistribution of nutrients. Resident KCs produce TNF-α and other pro-inflammatory cytokines. These are secreted into systemic circulation or act on endothelial cells and hepatocytes via paracrine interactions. Parenchymal hepatocytes possess receptors for inflammatory mediators. TNF-α mediates the development of insulin resistance, which promotes a rearrangement in liver metabolism (Dhar and Castillo, 2011). Hepatocytes respond by a shift from glycolysis towards gluconeogenesis (Dhainaut et al., 2001). The central enzyme of gluconeogenesis, the glucose-6-phosphatase, shows a rapid up-regulation, but decreased expression during the later phase of sepsis (Maitra et al., 2000).

Glycogen storages are depleted during sepsis. Increased glycogen phosphorylase activity has been found in *in vivo* models of sepsis (Pastor et al., 1995), while decreased activity of glycogen

synthase as well as decreased availability of G6P have been described in an *in vitro* model of sepsis (Wallington et al., 2008). Most likely, the complex *in vivo* situation involves the actions of glucoregulatory hormones, cytokines and paracrine interactions of hepatocytes and Kupffer cells, which have been shown to stimulate glycogenolysis via prostaglandin secretion (Casteleijn et al., 1988). Resident and infiltrating leukocytes exhibit an increased uptake of glucose, while hepatocytes do not change glucose consumption (Meszaros et al., 1991).

Other metabolic changes involve increased protein synthesis, mainly for the synthesis of acute phase proteins in hepatocytes (Dhainaut et al., 2001).

The concentration of free fatty acids (FFA) can be elevated during sepsis, because FFA are mobilized from adipose tissue. Enhanced uptake by the liver leads to enhanced *de novo* TG synthesis, storage of big fat droplets inside hepatocytes and elevated TG concentrations in the blood (hypertriglyceridemia) while fatty acid oxidation is decreasing (Bechmann et al., 2011; Khovidhunkit et al., 2004). Cytokines such as TNF-α inhibit lipoprotein lipase, therefore additionally decreasing the clearance of TG (Spitzer et al., 1988). Lipoprotein metabolism changes towards the promotion of inflammation and atherogenesis (Khovidhunkit et al., 2004).

The changes in lipid metabolism during infection have been suggested to aid host defense against the pathogen (Frazier et al., 2009). It has been found that oxidized lipids function as modulators of LPS signaling during infection (Walton et al., 2003). Moreover, TG-rich lipoproteins can bind and neutralize LPS *in vitro* (Barcia and Harris, 2005) and *in vivo* (Netea et al., 2009) which might limit overshooting immune responses. Macrophages store higher amounts of TGs and cholesterol when confronted with LPS (Funk et al., 1993), and thus lipoproteins may also play a role in feeding immune cells (Feingold et al., 1998; Khovidhunkit et al., 2004).

On the other hand, the metabolic changes described in this section also have a negative side to the host. Prolonged hypermetabolism and energy expenditure lead to depletion of storages, resulting in under-supply of central organs like the brain and can lead to multiple organ-failure. Therefore, metabolic changes are ambiguous and have a wide range of effects.

Interestingly, there is evidence that modulation of metabolism might actually support immunity and host defense during infection (Erkkila et al., 2005; Ferreira et al., 2008; Svec and Porter, 1998).

Open questions

The current knowledge about leukocyte metabolism in the context of inflammation is mainly derived from *in vitro* experiments with a particular type of primary macrophages (peritoneal) or aberrant cancer cell lines. Metabolism of major classes of infiltrating leukocytes during inflammation may be different, as these are predominantly neutrophils and inflammatory macrophages, which have been less well studied.

Moreover, most studies used cell culture models, which might differ from more relevant conditions within inflamed tissues. Infiltrating leukocytes form high-ordered structures (granulomas) that might have distinct metabolic patterns, although existing *in vivo* data are still fragmentary. Finally, the functional relevance for host defense against pathogens remains unclear. To investigate all these issues, a suitable *in vivo* model is required.

1.3 Murine typhoid fever as a model system to study metabolism during infection

***Salmonella* infection biology**

The murine typhoid fever model is well suited as a model system to study host immunological and metabolic responses to infection. The causative bacterium *Salmonella* provokes a typical host response, leading to fast leukocyte infiltrations in liver and spleen and formation of granulomatous lesions as well as typical metabolic responses to bacteremia.

Salmonella is a Gram negative, facultative intracellular bacterium that can survive inside host macrophages and dendritic cells after phagocytosis, which allows intracellular replication and dissemination throughout the whole body. This leads to fever and sepsis in susceptible mice (Nramp $^{-/-}$), resembling human typhoid fever (Santos et al., 2001; Vidal et al., 1993).

In the mouse model, *Salmonella typhimurium* is either applied orally, intraperitoneally or intravenously. Depending on the route of infection, *Salmonella* is confronted with different host cell types.

If ingested orally in a sufficiently high dose, it passes the gastrointestinal tract and invades specialized epithelial cells lining the intestinal wall (M cells), dendritic cells and enterocytes of the gut. Genes required for invasion are encoded on the *Salmonella* pathogenicity island 1 (SPI-1) (Vazquez-Torres et al., 1999). These genes encode for a Type Three Secretion System (T3SS)

and effectors which facilitate invasion. In peritoneum and blood, the bacterium is ingested by patrolling $CD18^+$ phagocytes. After uptake, *Salmonella* senses intracellular nutrient limitation and expresses genes of the pathogenicity island 2 (SPI-2), which encode for a second T3SS and effectors, enabling intracellular survival and proliferation, predominantly in macrophages (Abrahams and Hensel, 2006).

Salmonella subverts host immune functions, which largely depends on the capability of intracellular replication. SPI-2 effectors are thought to prevent the fusion of the phagosome with NADPH oxidase (Phox) and iNOS-containing vesicles, which makes the compartment that is also called *Salmonella*-containing vacuole (SCV), a safe place for the bacterium (Chakravortty et al., 2002; Vazquez-Torres et al., 2000) although a recent study could not confirm the relevance of the SPI-2 encoded T3SS for stress defense (Aussel et al., 2011). To what extent *Salmonella* is negatively affected by oxidative and nitrosative stress *in vivo* is also not fully understood (Aussel et al., 2011).

In addition to NADPH oxidase, mitochondria could also significantly contribute to ROS production (mROS) and hence bactericidal activity. A TLR-mediated mechanism that recruits mitochondria to the phagosome and increases production of mROS has been described recently (West et al., 2011).

Salmonella possesses a set of redundant catalases, peroxiredoxins and superoxide dismutases to neutralize ROS. RNS are detoxified mainly by Hmp, a flavohemoprotein. The formation of peroxynitrite is indirectly prevented by the action of the antioxidant enzymes. Efficient repair systems remove damaged nucleotides in DNA (Fang, 2011; Henard and Vazquez-Torres, 2011).

Salmonella in the liver

Salmonella reaches its main sites of proliferation and persistence, liver and spleen, via the bloodstream. In the case of intravenous application, *Salmonella* may arrive extracellularly as well as inside phagocytes. Up to 70 percent of injected bacteria have been found after ten minutes inside the liver (Dhainaut et al., 2001). The liver receives blood from the intestine via the portal vein as well as blood from the systemic circulation via the portal artery. All hepatic vessels are lined by endothelial cells which are highly endocytic. Incoming bacteria or infected phagocytes are endocytosed by this cell type and by Kupffer cells, the resident macrophage population in liver (Gao et al., 2008; Nemeth et al., 2009). As intestinal blood always carries components of gut bacteria to the liver, Kupffer cells (KCs) are continuously exposed and more

tolerant to LPS and other bacterial components compared to other macrophages. However, high LPS concentrations still lead to KC secretion of proinflammatory mediators (Bilzer et al., 2006). Infiltrating neutrophils and inflammatory macrophages form inflammatory foci around the infected macrophages (Richter-Dahlfors et al., 1997). Inside infected tissues, *Salmonella* grows exponentially to high loads. Depending on the initial dose and the route of infection, *Salmonella typhimurium* infection in susceptible mice is fatal within 5 to 10 days.

Salmonella proliferates in macrophages, but may also reside in dendritic cells and neutrophils (Geddes et al., 2007). On the other hand, there is evidence that neutrophils are essential for the control of *Salmonella* infection and more efficient in killing of this pathogen (Cheminay et al., 2004; Conlan, 1997). Nonetheless, it has not been conclusively demonstrated in which phagocyte subsets *Salmonella* predominately replicates in liver and spleen, and which cell types preferentially kill the bacterium.

Metabolic changes during murine typhoid fever

Mice challenged with *Salmonella typhimurium* exhibit some of the typical host metabolic changes described for sepsis, such as glycogen depletion and hypertriglyceridemia.

Following intraperitoneal challenge with a very high dose of *Salmonella* in mice, initial increases in liver gluconeogenesis (glucose-6-phosphatase) and glycogenolysis (glycogen phosphorylase) were observed after two hours, while enzyme activities dropped again 18 hours after infection (Sakaguchi et al., 1980). This is in good accordance with observations for other models of sepsis (Maitra et al., 2000). In serum, a fast increase of free glucose and FFA one hour post infection was followed by subsequent decreases at later timepoints. Accumulation of TG in serum was accompanied by decreased serum lipoprotein lipase activity (Sakaguchi et al., 1980), again in agreement with other sepsis models (Spitzer et al., 1988). Also the increase in lactate concentrations in serum which has been described in sepsis can be seen in this model (Trager et al., 2003).

In a study using Swiss-Webster mice, injected with 7.5×10^1, 7.5×10^4 and 7.5×10^6 bacteria respectively, the activity of three particular enzymes was investigated. Pyruvate kinase, tryptophan oxygenase and tyrosine aminotransferase activities were shown to increase in all scenarios of infection, indicative of enhanced glycolysis, decreased gluconeogenesis, and enhanced amino acid metabolism in accordance with some other sepsis models (Snyder, 1971). One significant difference of rodent animal models to human sepsis is the development of

hypercholesteremia (Khovidhunkit et al., 2004). Cholesterol-lowering statins can ameliorate *Salmonella* infection in Balb/c mice, but changes in cholesterol concentrations have not been monitored (Catron et al., 2004).

A recent metabolomics approach was conducted with C75BL/6 mice that were infected orally with 7.5×10^7 bacteria. Elevated hepatic metabolite concentrations were indicative of increased hormone metabolism in the liver. Metabolites of sugar metabolism and general carbohydrate metabolism were decreased (Antunes et al., 2011).

The information summarized here represents individual studies which used rather different experimental conditions (mouse strain, inoculation dose, route of administration and timepoints of sample preparation) and remain fragmentary. A detailed and experimentally consistent analysis of host metabolism in mouse typhoid fever is still lacking.

1.4 Goal of the thesis

Systemic infections give rise to global inflammatory and metabolic responses. This is indicated by inflammatory mediators in the circulation, immune cells recruited from reservoirs in the body and altered host metabolism.

Although these systemic inflammatory and metabolic responses are studied well in cell culture and tissue homogenates, information about the topology of infiltrates and local metabolic alterations in infected tissues are sparse. Information has been obtained from different *in vitro* and *in vivo* models of infection and sepsis, but an integrated analysis of potential links of inflammation and metabolism is lacking.

Therefore the goal of this thesis was to study these aspects and their mutual relationships in a single *in vivo* model of mouse typhoid fever. Since only few methods for colocalization of metabolic activities and inflammatory processes in tissues were available, development of suitable techniques was a part of this goal.

Specific aims:

- To visualize the topology of inflammation in *Salmonella*-infected liver and spleen
- To develop methods to visualize metabolic activities in specific cell types *in situ*
- To use these methods to determine the local interconnection of metabolism, inflammation and infection control in *Salmonella*-infected liver

2. Results

2.1 *Salmonella* response to nitric oxide demonstrates diverse host / pathogen interactions in vivo

Burton NA, Schemmer AK, Schmidt A, Bumann D

(Manuscript in preparation)

Summary:

In this paper, we show that *Salmonella*-infected host tissues are highly heterogeneous, which is demonstrated by the differential expression of inducible nitric oxide synthase (iNOS).
iNOS was expressed in inflammatory macrophages localizing to the periphery of granulomatous lesions. To determine the local response to nitric oxide (NO) stress by *Salmonella*, an hmpA-promotor-gfp fusion was constructed. By the use of this reporter strain we could show that *Salmonella* forms dim and bright subpopulations *in vivo* that correlated with local iNOS expression, suggesting differential nitrosative stress sensed by *Salmonella* subpopulations in the tissue. Bright and dim *Salmonella* populations were sorted and their proteomes analyzed. Bright bacteria showed a signature of adaptive changes towards NO detoxification and repair of NO-induced damage.

In this study we demonstrate that *Salmonella* is confronted with heterogeneous host environments *in vivo* and adapts to local stress conditions. Our approach shows how bacterial subpopulations from distinct host environments can be isolated and analyzed.

Statement of my work:

I contributed to this work by the analysis of iNOS expression in $Ly6C^+$ macrophages and detection of nitrosative damage in granulomatous lesions in liver and spleen. These findings were crucial for the development of the entire project.

Salmonella response to nitric oxide demonstrates diverse host / pathogen interactions in vivo

Neil A. Burton[1], Anne K. Schemmer[1], Alexander Schmidt[2], Dirk Bumann[1]*

[1]Focal Area Infection Biology and [2]Proteomics Core Facility, Biozentrum, University of Basel, CH-4056 Basel, Switzerland

*To whom correspondence should be addressed. E-mail: dirk.bumann@unibas.ch

Running title: Host-induced *Salmonella*-heterogeneity

Abstract

During infection, pathogens colonize complex host tissues harboring diverse microenvironments that might promote pathogen subpopulations with distinct properties and fate. However, experimental strategies to unravel this complexity are largely lacking. Here, we combined fluorescent biosensors, confocal microscopy, flow cytometry, and proteomics, to map reactive nitrogen species (RNS) stress and *Salmonella* responses in infected mouse tissues. The results revealed heterogeneous expression of inducible nitric oxide synthase generating high RNS stress for only part of the entire *Salmonella* population. Exposed *Salmonella* up-regulated a specific set of defense proteins that lowered their RNS burden. Additional data suggested that *Salmonella* exposure and responses to reactive oxygen species were also inhomogeneous. Together, these findings demonstrate surprisingly diverse host conditions and locally adapting *Salmonella* subpopulations that may be important for disease development and control. Our general approach should be applicable to uncover heterogeneous host/pathogen interactions in many infectious diseases.

Introduction

During infection, pathogens encounter complex host environments with distinct anatomical structures and inhomogeneous inflammation. The diverse microenvironments likely provide a wide range of growth conditions for pathogens. Pathogen adaptation to different local conditions could contribute to the emergence of pathogen subpopulations with distinct properties and fates such as high tolerance to antimicrobials resulting in treatment failure (*1-5*), slow or no proliferation (dormancy) causing chronic infections (*6-10*), or hypervirulence (*11, 12*). However, experimental evidence for host-induced pathogen heterogeneity is scarce (*13, 14*) since most current approaches to study infectious diseases are based on bulk analyses of tissue homogenates that fail to capture the spatial complexity of host environments. Here, we addressed this issue in a well-characterized mouse typhoid fever model that closely mimics human disease (*15*). Specifically, we focused on the generation of reactive nitrogen species (RNS), an important antimicrobial host mechanism that depends on the host enzyme inducible nitric oxide synthase (iNOS) (*16-20*).

Results and Discussion

As expected (*21, 22*), immunostaining of *Salmonella*-infected spleen revealed strong expression of iNOS in infected spleen red pulp (Fig. 1A) and liver (Fig. S1A). This staining was specific for iNOS since infected iNOS-deficient mice showed only faint background staining (data not shown). Immunohistochemistry with an antibody to nitrotyrosine indicated nitrosative protein damage in regions with high iNOS expression (Fig. 1B) as observed previously (*22*), suggesting that iNOS generated physiologically relevant levels of reactive nitrogen species (RNS).

Salmonella was distributed throughout the spleen red pulp in regions with widely different iNOS concentration (Fig. 1C,D). It was initially surprising to detect some *Salmonella* in regions with little iNOS expression, since *Salmonella* infection induces rapid NO production in mouse macrophages in cell culture experiments (*23*). However, in vivo, iNOS was predominantly expressed by Ly-6C^{hi} inflammatory macrophages (but not Ly-6G^{hi} neutrophils) in structured inflammatory lesions called granulomas as observed previously (*21, 22*) (Fig. 1A; Fig. S1A). Infiltration and granuloma formation/maturation is a comparatively slow process (*24*) that might have lagged behind the continuous *Salmonella* spreading to new infection foci (*25*).

Host microenvironments with differential iNOS expression might expose *Salmonella* to a wide range of RNS stress levels, triggering corresponding *Salmonella* RNS defense responses. To test this hypothesis, we developed an integrated experimental approach (Fig. 2). Specifically, we generated an NO-responsive fluorescent *Salmonella* biosensor (Fig. 2A). We examined biosensor responses in host microenvironments with high and low iNOS expression using confocal microscopy (Fig. 2B). We sorted *Salmonella* biosensor subpopulations with differential response levels from infected tissues and comprehensively analyzed their properties using proteomics (Fig. 2C).

A key component of this strategy was the construction of an NO-responsive *Salmonella* biosensor (Fig. 2A). For this purpose, we constructed a transcriptional fusion of the *hmpA* promoter and a *gfp::ova* reporter gene (specific sequence coordinates are described in Supporting Materials and Methods). The *hmpA* promoter is regulated by the NO-sensitive transcription factor NsrR (*26, 27*), and can be induced in infected macrophages in an iNOS-dependent manner (*28*). *gfp::ova* encodes an unstable variant of the green fluorescent protein (GFP) (*29*) that reports on current promoter activities instead of integrating over extended time periods like stable GFP (*30*). When transformed into *Salmonella*, this P*hmpA::gfp::ova* construct

expressed increasing amounts of GFP upon in vitro stimulation with acidified nitrite (Fig. 3A), a commonly used source of NO (*31, 32*), as expected (*33*). To obtain sufficient signal to noise for in vivo analysis, we used a multi-copy plasmid construct. To enable in vivo detection of biosensor *Salmonella* regardless of actual GFP expression, we co-expressed red fluorescent mCherry from the native chromosomal *sifB* promoter, which is constitutively active during systemic infection (*29*).

Infection of mice revealed normal biosensor *Salmonella* growth in infected host tissues with no plasmid loss within the first five days of infection as observed previously for similar constructs (*34*). Flow cytometry of infected spleen and liver homogenates revealed uniformly mCherry-positive biosensor *Salmonella* (Fig. 3B; Fig. S2) that had, however, widely varying GFP levels (Fig. 3C; Fig. S1B). Such heterogeneous expression patterns were reproducibly observed although the proportions of dim and bright *Salmonella* varied somewhat between spleen and liver, and among independently infected mice (Fig. 3C; Fig. S1B). In contrast to the *hmpA* promoter, two different promoters in otherwise identical transcriptional *gfp::ova* fusions showed narrow unimodal *Salmonella* in vivo expression patterns (Fig. 3D). This suggested that heterogeneous GFP expression in the biosensor *Salmonella* reflected variations in *hmpA* promoter activity and not a noisy *gfp::ova* reporter gene, variations in plasmid copy number, or artifacts in flow cytometry of tissue homogenates.

High *hmpA* promoter activity in a *Salmonella* subpopulation was dependent on RNS generated by host iNOS, since *Salmonella* had homogeneously low GFP levels in iNOS-deficient mice compared to congenic control mice (Fig. 3E; Fig. S1C). These data also demonstrated that alternative RNS sources such as host endothelial nitric oxide synthase (eNOS) or *Salmonella* nitrate respiration (*35-37*), as well as other possible stimuli had at most minor impact on biosensor activities.

Low GFP expression in part of the population could have resulted from inactivating mutations in the expression construct. However, GFP^{dim} *Salmonella* that had been isolated ex vivo by flow cytometric sorting, rapidly up-regulated GFP expression when stimulated with acidified nitrite in vitro (Fig. 3E), indicating that they retained a functional RNS-responsive promoter fusion. Moreover, re-infection of naïve mice with either GFP^{dim} or GFP^{bright} ex vivo purified *Salmonella* fractions, yielded identical heterogeneous *Salmonella* GFP expression patterns including both dim and low subpopulations in spleen four days later (data not shown). These observations

indicated that heterogeneous *hmpA* promoter activities reflected *Salmonella* responses to inhomogeneous in vivo RNS stress levels.

Indeed, confocal microscopy of tissue sections revealed a strong regional link between host iNOS expression and *Salmonella* biosensor GFP expression (Fig. 3G,H). Specifically, mCherry-positive but GFP^{dim} *Salmonella* resided predominantly in tissue regions with low host iNOS expression, whereas mCherry-positive GFP^{bright} *Salmonella* mostly resided in granuloma-associated regions with high iNOS expression. Some GFP^{bright} *Salmonella* apparently resided in host cells with low iNOS expression but had iNOS-positive host cells in their close vicinity, likely reflecting the fact that NO can diffuse freely through cellular membranes (*38*). Based on in vitro data for NO diffusion from macrophages, we determined iNOS density within a radius of 15 µm around individual *Salmonella* to account for this (*39*).

Together, these data indicated that inhomogeneous host iNOS expression generated diverse RNS levels that were sensed by local *Salmonella* subpopulations.

Most of our data were obtained for a typhoid fever model in genetically susceptible mice. However, we also observed patchy host iNOS expression and heterogeneous *Salmonella hmpA* promoter activities during early infection of genetically resistant 129/Sv mice (Fig. S3), suggesting that inhomogeneous RNS stress and heterogeneously responding *Salmonella* subpopulations are a general feature of systemic salmonellosis.

Heterogeneous GFP content revealed distinct *Salmonella* subpopulations that might differ in additional properties. Comprehensive analysis of pathogen in vivo subpopulations had been challenging because suitable purification methods were lacking. Here, we could overcome these difficulties by combining our *Salmonella* biosensor approach with high-speed flow cytometric sorting. We sorted several million GFP^{dim} and GFP^{bright} biosensor *Salmonella* from infected spleen homogenates under conditions that largely preserved *Salmonella* in vivo protein content (*40*). *Salmonella* sorting efficiencies varied somewhat between individual experiments but interestingly, recovery of colony-forming units was similar for GFP^{dim} and GFP^{bright} *Salmonella* (Fig. S4), suggesting that both subpopulations maintained similar viability despite their differential RNS stress exposure. Shot-gun mass spectrometry-based proteome analysis of these sorted subpopulations enabled us to identify peptides corresponding to approximately 1000 proteins at a false discovery rate of 1%, with substantial overlap in identifications over 4 independent biological replicates. We used a “label free quantification” method (*41*) to establish

the relative abundances of proteins in GFP^{dim} and GFP^{bright} populations and the "iBAQ" method (*42*) to calculate absolute quantities for these proteins (see Supporting Materials and Methods).

Comparison of protein profiles (Fig. 4A) revealed that GFP was more abundant in GFP^{bright} *Salmonella* whereas mCherry was equally abundant in both subpopulations in agreement with flow cytometry data (Fig. 4A). Surprisingly, subpopulation protein profiles were otherwise remarkably similar with just 3 *Salmonella* proteins showing more than threefold enrichment in the GFP^{bright} population; HmpA, YtfE and Hcp, which function as an NO dioxygenase (*43, 44*), an iron sulphur cluster repair protein (*45*) and a hydroxalamine reductase (*46*) respectively. All three proteins are subject to NsrR repression, and are highly expressed upon NO exposure in vitro and in cell culture infections (*26, 47*)(*32, 48*). These proteome signatures thus indicated a highly specific *Salmonella* response to local in vivo RNS stress. NsrR regulation in biosensor *Salmonella* could be affected by the multi-copy plasmid-encoded P*hmpA* fusion that could titrate NsrR (*49*). However, proteins HmpA, YtfE, and Hcp all had similar average in vivo copy numbers in biosensor *Salmonella* and control *Salmonella* lacking this multi-copy fusion (Fig. 4B) indicating that NsrR titration by multi-copy P*hmpA* had no detectable impact in our biosensor *Salmonella*.

Up-regulation of HmpA, YtfE, and Hcp could protect RNS exposed *Salmonella*. To test this hypothesis, we generated a *Salmonella hmpA ytfE hcp* mutant and transformed it with the P*hmpA::gfp::ova* plasmid. In vitro, the resulting biosensor *Salmonella* Δ3 showed increased sensitivity and response levels to acidified nitrite compared to wildtype biosensor *Salmonella* (Fig. 4C), which likely reflected the lack of NO dioxygenase (HmpA)-mediated NO detoxification (*47*). In vivo, flow cytometry of infected spleen and liver revealed a wider range of P*hmpA* activities and a larger portion of GFP^{bright} *Salmonella* Δ3 than was observed for wild type *Salmonella* (Fig 4C; Fig. S1B). This suggested increased RNS stress in exposed Δ3 subpopulations consistent with their lack of RNS defense proteins. Increased RNS stress was also supported by up-regulation of four additional RNS-associated proteins in the GFPbright *Salmonella* Δ3 subpopulation (Fig. 4D, E). NorV and NorW (comprising an alternate NO detoxification pathway (*50, 51*), STM1808 and YoaG, are all up-regulated by NO under certain in vitro conditions (*48*) but had shown either no enrichment (NorV, NorW; STM1808), or lower enrichment (YoaG) in the corresponding wild type population (Fig. 4E). We also observed a moderate enrichment of Isc proteins implicated in iron sulphur cluster biogenesis in GFP^{bright} *Salmonella* Δ3 (Fig. S5),

consistent with iron sulphur clusters representing cellular targets of NO, and the up-regulation of the *isc* operon by NO in vitro (*48*).

Despite their compromised RNS defense, RNS-exposed GFP^{bright} *Salmonella* Δ3 maintained similar viability compared to the less exposed GFP^{dim} *Salmonella* Δ3 subpopulation (Fig. S4). This was also supported by the overall high virulence of *Salmonella* Δ3 (competitive index against parental wildtype *Salmonella*, CI = 0.87 ± 0.1) consistent with previous data for the individual genes in genetically susceptible mice (*27, 32*). A *Salmonella hmpA ytfE hcp hcr norVW yoaG yeaR* STM1273 STM1808 *nrfABCDEFG nfnM cadABC metQ* mutant lacking several additional RNS stress-associated *Salmonella* proteins (*27, 45, 46, 48, 52, 53*) was significantly attenuated (CI value against parental wildtype at day 4 post infection, 0.41 ± .27; *P*=0.0058, two-tailed t-test on log-transformed data), but still maintained relatively high virulence. This could reflect yet additional redundant defense systems against NO stress (*54, 55*), a generally limited efficacy of iNOS derived products to control *Salmonella* growth during acute infection (*56-58*), and/or the fact that only a *Salmonella* subpopulation was exposed to substantial NO levels resulting in small effects in bulk virulence measurements such as competitive indices.

In addition to RNS, *Salmonella* also encounters stresses such as reactive oxygen species (ROS), cationic antimicrobial peptides, and digestive host enzymes during infection (*59*). Indeed, our proteome data revealed a number of proteins indicative for diverse stress responses, but their abundance was similar in RNS-exposed and unexposed *Salmonella* subpopulations suggesting limited correlation between the various stresses. As an example, the *katG*-encoded catalase HPI that detoxifies high levels of hydrogen peroxide (*60*), was present in *Salmonella* in vivo at an abundance of 2800 ± 500 copies per cell, regardless of RNS exposure (abundance ratio of GFP^{bright} vs. GFP^{dim} *Salmonella* P*hmpA::gfp::ova*, 0.95 ± 0.1). Surprisingly, however, a P*katG::gfp::ova* fusion, that responded homogeneously to reactive oxygen species in vitro, as expected (*61*), had clearly heterogeneous activities in infected spleen and liver (Fig. S6). This suggested ROS as an independent inhomogeneous stress for *Salmonella* in infected tissues. The superposition of multiple inhomogeneous stresses could result in a large diversity of locally adapting *Salmonella* subpopulations. Moreover, pathogen heterogeneity might be further enhanced by internal stochastic noise in pathogen transcription (*62-64*). On the other hand, the apparent inability of the host to combat the entire *Salmonella* population with high correlated stresses might limit the efficacy of these and other antimicrobial effector mechanisms.
All these issues might represent exciting areas for future research.

Conclusion

In summary, mapping of host RNS stress generation through iNOS and local *Salmonella* adaptations at the single cell level revealed that complex structure of infected host tissues can promote diverse host/pathogen interactions with important implications for disease development and control. Our general approach to discover spatially heterogeneous host-pathogen interactions should be applicable to many other infectious diseases.

References and notes

1. W. McDermott, *Yale J Biol Med* **30**, 257 (Feb, 1958).
2. K. Lewis, *Nat Rev Microbiol* **5**, 48 (Jan, 2007).
3. H. H. Lee, J. J. Collins, *Nat Chem Biol* **8**, 6 (Jan, 2012).
4. B. B. Aldridge *et al.*, *Science* **335**, 100 (Jan 6, 2012).
5. K. N. Adams *et al.*, *Cell* **145**, 39 (Apr 1, 2011).
6. D. M. Monack, A. Mueller, S. Falkow, *Nat Rev Microbiol* **2**, 747 (Sep, 2004).
7. C. E. Barry, 3rd *et al.*, *Nat Rev Microbiol* **7**, 845 (Dec, 2009).
8. J. D. McKinney *et al.*, *Nature* **406**, 735 (Aug 17, 2000).
9. K. R. Allison, M. P. Brynildsen, J. J. Collins, *Nature* **473**, 216 (May 12, 2011).
10. S. Helaine *et al.*, *Proc Natl Acad Sci U S A* **107**, 3746 (Feb 23, 2010).
11. M. Ackermann *et al.*, *Nature* **454**, 987 (Aug 21, 2008).
12. L. A. Knodler *et al.*, *Proc Natl Acad Sci U S A* **107**, 17733 (Oct 12, 2010).
13. G. Fenhalls *et al.*, *Infect Immun* **70**, 6330 (Nov, 2002).
14. G. J. Ryan *et al.*, *PLoS One* **5**, e11108 (2010).
15. R. L. Santos *et al.*, *Microbes Infect* **3**, 1335 (Nov-Dec, 2001).
16. C. Nathan, M. U. Shiloh, *Proc Natl Acad Sci U S A* **97**, 8841 (Aug 1, 2000).
17. C. Bogdan, *Nat Immunol* **2**, 907 (Oct, 2001).
18. F. C. Fang, *Nat Rev Microbiol* **2**, 820 (Oct, 2004).
19. A. R. Richardson *et al.*, *PLoS Pathog* **5**, e1000451 (May, 2009).
20. C. A. Henard, A. Vazquez-Torres, *Front Microbiol* **2**, 84 (2011).
21. S. A. Khan *et al.*, *Microb Pathog* **30**, 29 (Jan, 2001).
22. K. Umezawa *et al.*, *Infect Immun* **65**, 2932 (Jul, 1997).
23. A. Vazquez-Torres, J. Jones-Carson, P. Mastroeni, H. Ischiropoulos, F. C. Fang, *J Exp Med* **192**, 227 (Jul 17, 2000).
24. A. Richter-Dahlfors, A. M. Buchan, B. B. Finlay, *J.Exp.Med.* **186**, 569 (1997).
25. P. Mastroeni, A. Grant, O. Restif, D. Maskell, *Nat Rev Microbiol* **7**, 73 (Jan, 2009).
26. N. P. Tucker *et al.*, *PLoS One* **3**, e3623 (2008).
27. I. S. Bang *et al.*, *J Biol Chem* **281**, 28039 (Sep 22, 2006).
28. B. D. McCollister *et al.*, *Immunobiology* **212**, 759 (2007).
29. C. Rollenhagen, M. Sorensen, K. Rizos, R. Hurvitz, D. Bumann, *Proc.Natl.Acad.Sci.U.S.A* **101**, 8739 (2004).

30. A. Zaslaver *et al.*, *Nat Methods* **3**, 623 (Aug, 2006).
31. K. Y. Rhee, H. Erdjument-Bromage, P. Tempst, C. F. Nathan, *Proc Natl Acad Sci U S A* **102**, 467 (Jan 11, 2005).
32. C. C. Kim, D. Monack, S. Falkow, *Infect Immun* **71**, 3196 (Jun, 2003).
33. P. Mukhopadhyay, M. Zheng, L. A. Bedzyk, R. A. LaRossa, G. Storz, *Proc Natl Acad Sci U S A* **101**, 745 (Jan 20, 2004).
34. D. Bumann, *Mol Microbiol* **43**, 1269 (Mar, 2002).
35. X. B. Ji, T. C. Hollocher, *Biochem Biophys Res Commun* **157**, 106 (Nov 30, 1988).
36. N. J. Gilberthorpe, R. K. Poole, *J Biol Chem* **283**, 11146 (Apr 25, 2008).
37. G. Rowley *et al.*, *Biochem J* **441**, 755 (Jan 15, 2012).
38. P. Pacher, J. S. Beckman, L. Liaudet, *Physiol Rev* **87**, 315 (Jan, 2007).
39. A. M. Leone, V. W. Furst, N. A. Foxwell, S. Cellek, S. Moncada, *Biochem Biophys Res Commun* **221**, 37 (Apr 5, 1996).
40. D. Becker *et al.*, *Nature* **440**, 303 (Mar 16, 2006).
41. A. Schmidt *et al.*, *Mol Syst Biol* **7**, 510 (1038).
42. B. Schwanhausser *et al.*, *Nature* **473**, 337 (May 19, 2011).
43. M. J. Crawford, D. E. Goldberg, *J Biol Chem* **273**, 12543 (May 15, 1998).
44. P. R. Gardner, A. M. Gardner, L. A. Martin, A. L. Salzman, *Proc Natl Acad Sci U S A* **95**, 10378 (Sep 1, 1998).
45. M. C. Justino, C. C. Almeida, M. Teixeira, L. M. Saraiva, *J Biol Chem* **282**, 10352 (Apr 6, 2007).
46. M. T. Wolfe, J. Heo, J. S. Garavelli, P. W. Ludden, *J Bacteriol* **184**, 5898 (Nov, 2002).
47. N. J. Gilberthorpe, M. E. Lee, T. M. Stevanin, R. C. Read, R. K. Poole, *Microbiology* **153**, 1756 (Jun, 2007).
48. A. R. Richardson *et al.*, *Cell Host Microbe* **10**, 33 (Jul 21, 2011).
49. N. Filenko *et al.*, *J Bacteriol* **189**, 4410 (Jun, 2007).
50. A. M. Gardner, R. A. Helmick, P. R. Gardner, *J Biol Chem* **277**, 8172 (Mar 8, 2002).
51. P. C. Mills, G. Rowley, S. Spiro, J. C. Hinton, D. J. Richardson, *Microbiology* **154**, 1218 (Apr, 2008).
52. S. Spiro, *Biochem Soc Trans* **34**, 200 (Feb, 2006).
53. J. M. Bower, M. A. Mulvey, *J Bacteriol* **188**, 928 (Feb, 2006).
54. D. Chakravortty, I. Hansen-Wester, M. Hensel, *J.Exp.Med.* **195**, 1155 (2002).

55. C. E. Vine, J. A. Cole, *Biochem Soc Trans* **39**, 213 (Jan, 2011).
56. P. Mastroeni *et al.*, *J Exp Med* **192**, 237 (Jul 17, 2000).
57. J. K. White, P. Mastroeni, J. F. Popoff, C. A. Evans, J. M. Blackwell, *J Leukoc Biol* **77**, 311 (Mar, 2005).
58. C. A. Henard, A. Vazquez-Torres, *Infect Immun*, (Feb 6, 2012).
59. G. Dougan, V. John, S. Palmer, P. Mastroeni, *Immunol Rev* **240**, 196 (Mar, 2011).
60. J. A. Imlay, *Annu Rev Biochem* **77**, 755 (2008).
61. C. Lu, C. R. Albano, W. E. Bentley, G. Rao, *Biotechnol Bioeng* **89**, 574 (Mar 5, 2005).
62. M. B. Elowitz, A. J. Levine, E. D. Siggia, P. S. Swain, *Science* **297**, 1183 (Aug 16, 2002).
63. I. Hautefort, M. J. Proenca, J. C. Hinton, *Appl Environ Microbiol* **69**, 7480 (Dec, 2003).
64. E. Rotem *et al.*, *Proc Natl Acad Sci U S A* **107**, 12541 (Jul 13, 2010).

Acknowledgements

We are grateful to John Mekalanos, Philippe Sansonetti, Lalita Ramakrishnan, and members of Bumann laboratory for constructive comments. We thank M. Rosas for help in preparing Figure 2. This work was supported by grants from Deutsche Forschungsgemeinschaft (SPP1316 Bu971/6) and Swiss National Fonds (3100A0-121834/1).

Figures

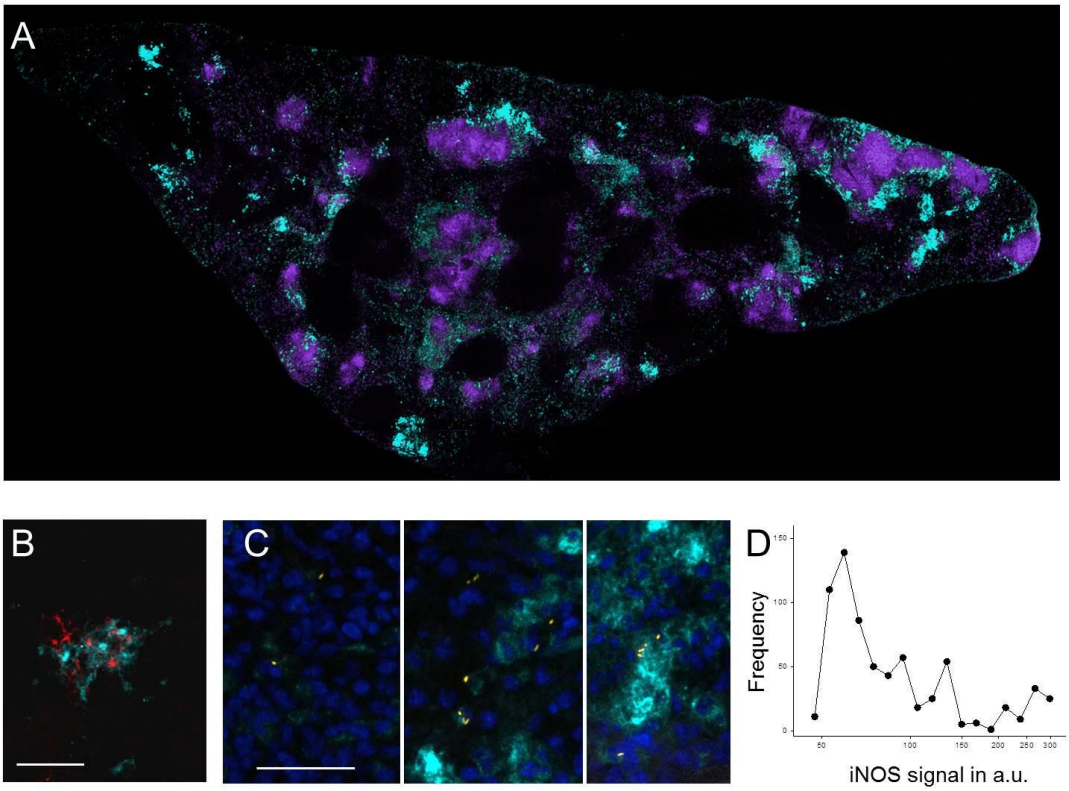

Fig. 1. Inhomogeneous expression of inducible nitric oxide synthase (iNOS) around individual *Salmonella* in infected mouse spleen. (**A**) Overview of a spleen cryosection stained for iNOS (cyan) and the neutrophil marker GR-1 (magenta). The unstained dark areas represent white pulp. Similar results were obtained for four independently infected mice. (**B**) iNOS expression (cyan) co-localized with nitrosative damage as indicated by 3-nitrotyrosine (red). The scale bar represents 30 µm. (**C**) *Salmonella* (yellow) resided in regions with low, medium, or high iNOS expression (cyan). Nuclei are shown in blue. The scale bar represents 30 µm. Similar results were obtained for four independently infected mice. (**D**) Quantification of iNOS expression around 690 individual *Salmonella*. Data represent mean iNOS signals within a radius of 15 µm to account for free diffusion of NO through host cell membranes (*39*). Control sections from iNOS-deficient mice showed average background signals in the range of 50 to 70 arbitrary units. Two additional data sets revealed similar broad distributions.

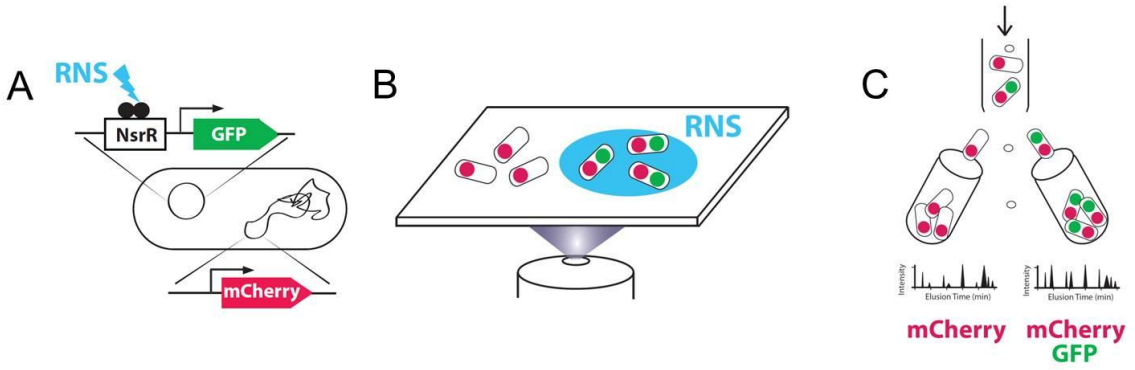

Fig. 2. Schematic representation of biosensor approach to discover heterogeneous host / *Salmonella* interactions. (**A**) Biosensor *Salmonella* express the green fluorescent protein (GFP) from a stress-responsive plasmid-encoded promoter. In addition, the red fluorescent protein mCherry is expressed from a constitutively active chromosomal promoter. This biosensor shows red fluorescence under basal conditions but yellow fluorescence (red plus green) upon exposure to stress. (**B**) Confocal microscopy of infected tissue sections validates biosensor *Salmonella* responses to local host stress (cyan). (**C**) Responding and non-responding *Salmonella* are separated by flow cytometry sorting based on their differential fluorescence. The different *Salmonella* subpopulations are analyzed by mass spectrometry-based proteomics.

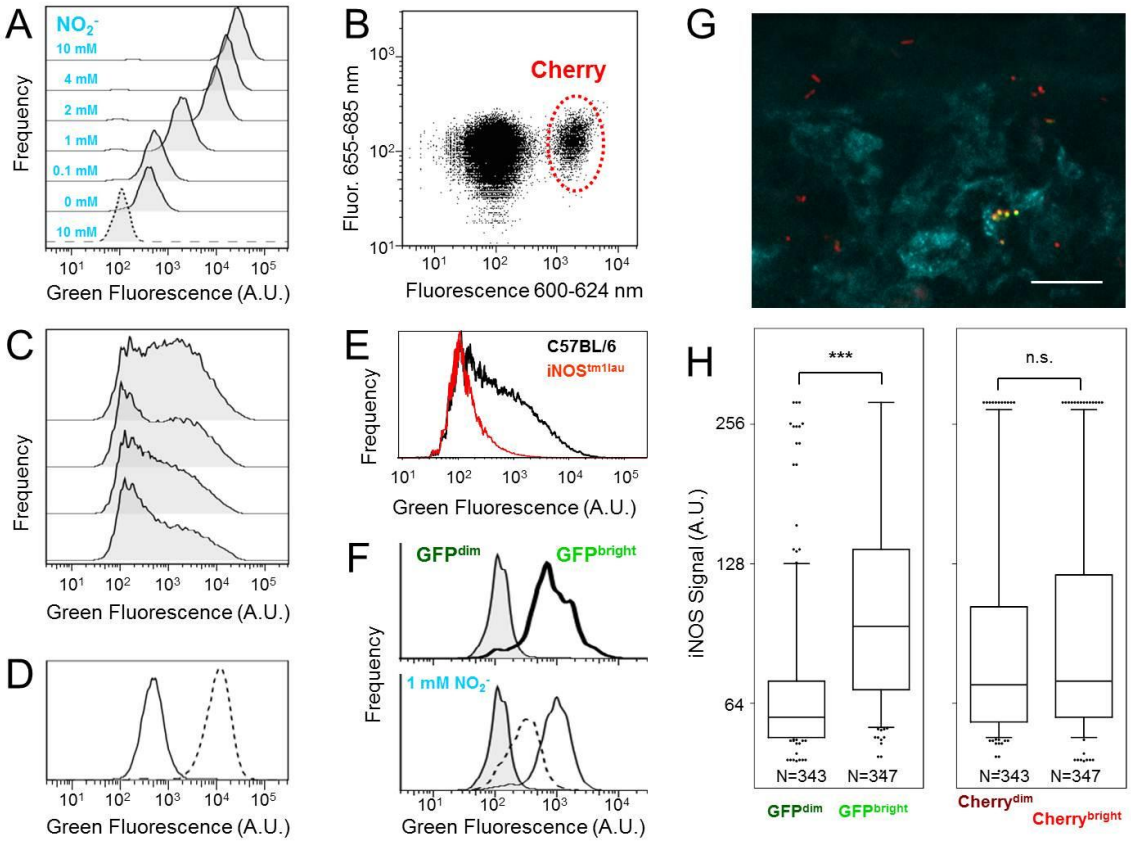

Fig. 3. Biosensor *Salmonella* reveal heterogeneous exposure to reactive nitrogen species in infected mouse spleen. (**A**) Response of *Salmonella* carrying a P*hmpAp::gfp::ova* fusion to in vitro stimulation with acidified nitrite. The dashed curve represents background fluorescence of control *Salmonella* without GFP. Histograms of green fluorescence intensities (502-524 nm) after excitation with a 488 nm laser are shown. (**B**) Flow cytometry of infected spleen revealed homogeneous mCherry expression of biosensor *Salmonella* (excitation with 561 nm laser). The mCherry gate was analyzed for GFP co-expression. Spleen homogenates from control mice infected with *Salmonella* not expressing mCherry, did not show any particles in this gate (Fig. S2). (**C**) GFP expression of biosensor *Salmonella* in spleen of individual independently infected mice. (**D**) In vivo activities of P*glpA::gfp::ova* (straight line) and P*sopD2::gfp::ova* fusions (dashed line). (**E**) GFP expression of biosensor *Salmonella* in spleen of iNOS deficient and congenic wildtype mice. (**F**) GFP^{dim} and GFP^{bright} subpopulations of biosensor *Salmonella* carrying P*hmpA::gfp::ova* were sorted from spleen homogenates by flow cytometry and re-analyzed (upper panel). The GFP^{dim} fraction (shaded area) was stimulated in vitro with acidified nitrite

(lower panel) for 30 min (dashed line) or 120 min (straight line). (**G**) Local biosensor *Salmonella* responses in infected spleen (cyan, iNOS; red, mCherry; green, GFP). (**H**) Quantification of iNOS signal within a 15 µm radius around GFP^{dim} and GFP^{bright} biosensor *Salmonella*. As a control, *Salmonella* with slightly different Cherry expression were also analyzed. The data are represented as box plots (central line is the median; the box includes the central 50%; the whiskers include the central 90%; ***, $P< 0.001$; n.s., not significant; Mann-Whitney-U test). A similar link between host iNOS expression and local *Salmonella* responses was observed in two additional data sets.

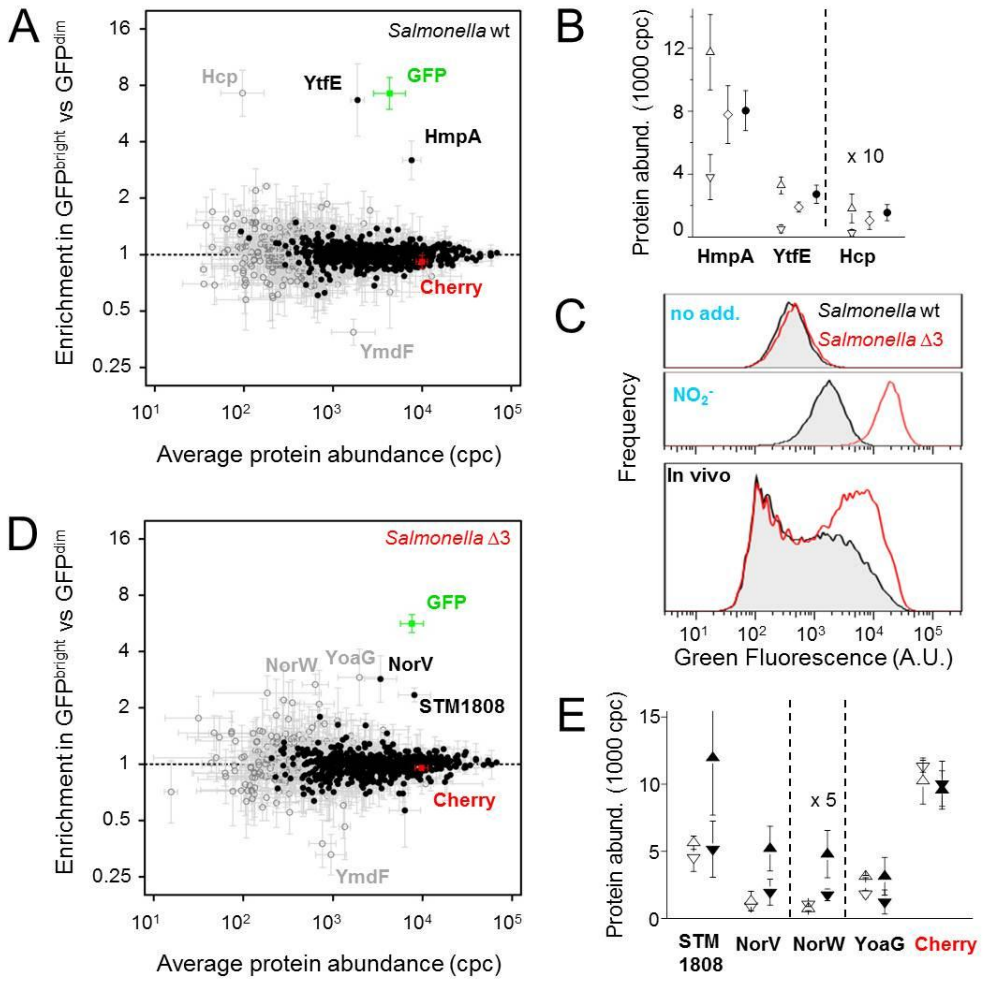

Fig. 4. Specific adaptations in *Salmonella* subpopulations exposed to differential reactive nitrogen species stress. (**A**) Proteome comparison of GFP^{bright} and GFP^{dim} biosensor *Salmonella* subpopulations sorted from infected spleen (cpc, copies per *Salmonella* cell). Mean values ± SD for proteins detected in all 4 independently infected mice (filled circles), or at least 2 out of 4 mice (open circles) are shown. (**B**) Comparison of HmpA, YtfE, and Hcp in vivo abundance in biosensor *Salmonella* (down triangles, GFP^{dim} subpopulation; up triangles, GFP^{bright} subpopulation; diamonds, average) and control ex vivo sorted *Salmonella* without a multi-copy P*hmpA* fusion (filled circles). Values for Hcp were multiplied with 10 for better visualization. (**C**) Comparison of P*hmpAp::gfp::ova* activities in wildtype *Salmonella* and the triple mutant *Salmonella hmpA ytfE hcp* (Δ3) in vitro (upper panel) and in infected spleen (lower panel). Similar data were obtained for two independently infected mice. (**D**) Proteome comparison of

GFP^{bright} and GFP^{dim} *Salmonella* Δ3 subpopulations sorted from infected spleen (cpc, copies per *Salmonella* cell). Mean values ± SD for proteins detected in all 3 independently infected mice (filled circles), or at least 2 out of 3 mice (open circles) are shown. (**E**) Comparison of protein abundances in GFP^{dim} (down triangles) and GFP^{bright} (up triangles) subpopulations of wildtype *Salmonella* (filled symbols) and *Salmonella* Δ3 (open symbols). Values for NorW were multiplied with 5 for better visualization.

Supporting Material

Materials and Methods

Bacterial strains, media and chemicals

Salmonella strains used in this study were derived from *Salmonella enterica* serovar Typhimurium SL1344 *hisG rpsL xyl* (*1*). Unless otherwise stated *Salmonella* were cultured at 37°C with aeration (200 rpm) in LB low salt (5 g/l NaCl), or on LB low salt agar plates, with addition of the following antibiotics where appropriate: streptomycin (90 µg/ml); ampicillin (100 µg/ml); kanamycin (50 µg/ml); chloramphenicol (25 µg/ml).

Cloning and mutagenesis

A region of chromosomal DNA of *Salmonella (enterica serovar typhimurium)* incorporating a promoter region of interest, as defined (*2*), was PCR amplified and ligated into a *Bam*HI, *Xba*I digest of pMW82 (*3*). The extents of the different promoter regions used, relative to the ATG of the named gene, were as follows: *hmpAp* (SL1344_2518) -403 to +73; *glpAp* (SL1344_2253) -343 to +127; *sopD2p* (SL1344_0909) -388 to +218; *katGp* (SL1344_4056) -240 to +61. Correct insertion of the promoter fragment upstream of *gfp_ova* in pMW82 was confirmed by restriction digest of purified plasmids and sequencing over the full insert region and flanking sites. The finished constructs were expected to produce "operon-like" fusions, in which the transcribed mRNA contains a short peptide corresponding to the start of the gene downstream of the promoter of interest, prior to a stop codon in the plasmid vector, and then a strong ribosome binding site to reinitiate translation of GFPova. The lower copy *hmpAp*GFPova pSC101 derived vector was constructed by PCR amplifying the full *hmpAp::gfp_ova* construct in pMW82 and ligating this into a *Bam*HI, *Sbf*I digest of pUA66 (*2*).

Gene replacement mutagenesis of *Salmonella* was carried out as described (*4*). All mutations were P22 transduced into a relevant recipient strain and confirmed by PCR over the modified genomic region.

A chromosomal fusion of the native *sifB* promoter with mCherry was constructed as described for a similar GFPmut2 fusion at this locus (*5*). Correct insertion of mCherry was confirmed by PCR, and expression of mCherry was verified by growing cells overnight in inducing media

(MOPS medium (*6*) buffered to pH 5.5 with 100 mM 2-(N-morpholino)ethanesulfonic acid (MES; Sigma-Aldrich), and containing 10 µM $MgCl_2$).

Mice infections

All animals were handled in strict accordance with good animal practice and all animal work was approved by local animal care and use committee (license 2239, Kantonales Veterinäramt BS).

BALB/c mice and 129/Sv mice were purchased from Charles River Laboratories. B6.129P2-$Nos2^{tm1Lau}$/J mice deficient in iNOS (stock number: 002609; (*7*)) were purchased from the Jackson laboratory along with age- and sex-matched C57BL/6J congenic control mice (Stock number: 000664). At the time of infection animals were 10-12 weeks old. Mice were infected by tail vein injection of 400-700 *Salmonella* in 100 µl PBS. Prior to infection *Salmonella* were grown to late log phase in LB low salt (OD 1.6) and washed 3 times in PBS. Mice were euthanized 4-5 days after infection. Spleens and livers were recovered from sacrificed animals. *Salmonella* were plated both before and after infection to verify input numbers and the final tissue loads. Where relevant, competitive index values were established to determine virulence of *Salmonella* mutants as described (*8*) .

Immunohistochemistry of infected spleen and liver

For all experiments other than for nitrotyrosine staining, 2-3 mm thick portions were cut from freshly recovered spleen and liver and immediately transferred to 1 ml fresh 4% paraformaldehyde at 4°C. After 4 hours fixation, samples were washed 3 times in ice cold PBS and then a further 4 times in ice cold PBS with progressively higher sucrose concentrations from 10%- 40%. After overnight incubation in 40% sucrose PBS at 4°C, the tissue portions were rapidly frozen in embedding media (Tissue-Tek® O.C.T; Sakura), left overnight at -80°C, and then stored at -20°C. 16-20 µm thick sections were cut using high Profile Microtome Blades (Leica 818) in a cryostat (Leica 1800 cryocut) at -14°C and dried either directly onto coated coverslips (BD BioCoat™), or coated slides (SuperFrost Plus, Thermo Scientific) at room temperature. In the case of nitrotyrosine staining, sections were immediately frozen in embedding media without fixation. Sections were then fixed in acetone before staining.

Sections were blocked in 1% blocking reagent (Invitrogen) and 2% mouse serum (Invitrogen) in TBST (0.05% Tween-20 in 1x TBS, pH7.4), and then stained with primary and secondary antibodies made up at a 1:100 dilution in TBST + 1% blocking reagent for 1 hour and 30 minutes,

respectively, with standard washing steps in TBST. The primary antibodies used were as follows: rabbit anti-iNOS (Acris antibodies; Cat: iNOS-A); rat biotin conjugated anti-Ly6GC (Becton Dickinson; Cat: 553124); goat anti-nitrotyrosine (Alpha Diagnostics; Cat: NITT13-S). A variety of secondary antibodies were used depending on the application (Molecular probes; Cat. A-21443; S11225; A-21206; D20698). In the case of nitrotyrosine staining, a horseradish peroxidase kit (Molecular probes; Cat: T-20936) was used as a tertiary antibody to amplify the signal. Sections were mounted onto glass slides using a glycerol based DABCO mounting medium (90% glycerol, 24.5 mg/ml DABCO (1,4-Diazabicyclo[2.2.2]octane) in PBS, pH7.4). All staining procedures were done immediately prior to microscopic analysis on a Leica SP5 confocal microscope (Biozentrum, Imaging Core Facility), using 20x and 63x glycerol objectives (400 Hz scan; 1024x1024 pixels; Airy 1 pinhole). Image analysis was done using FIJI. The average GFP and mCherry pixel fluorescence was quantified for individual *Salmonella* outlined in single planes of a z stack of images taken at 189x magnification (0.5 µm step size). Individual *Salmonella* were assigned an iNOS exposure score by quantifying the average iNOS stain pixel intensity (using an Alexa 647 conjugated secondary antibody) on a sum projection of the z stack from images taken at 20x magnification in a circle of 15 µm radius centred on the *Salmonella* cell. This procedure was used to account for reported diffusion of high NO concentrations beyond the confines of a single NO producing macrophage (*9*).

Flow cytometry analysis and sorting of *Salmonella*

Spleen homogenates were prepared for flow cytometry as described (*10*), with a few additional steps to maximise *Salmonella* recovery as follows: After *Salmonella* were separated from large host cell debris in an initial slow speed centrifugation step (500 x g, 5 min, 4°C), pelleted host cell debris was re-homogenised in 3 ml fresh homogenisation buffer (0.17% Triton x-100, 10 µM $CaCl_2$, 170 µg/ml chloramphenicol in PBS) using the flat end of a sterile plastic syringe, re-spun at slow speed (500 x g, 5 min, 4°C), and the supernatant combined with that recovered from the first centrifugation. *Salmonella* in the combined supernatants was then pelleted at high speed (12,000 x g, 12 min, 4°C), thoroughly re-suspended in half the volume (3 ml) of fresh homogenisation buffer, and finally passed through a 30 µm pre-separation filter (MACS; Miltenyi Biotech). Liver homogenates were prepared in a similar fashion, using double the volume of homogenisation buffer to account for the increased tissue mass, and applying the fast speed

centrifugation step 4-5 times in order to remove excess lipids in the liver homogenate which otherwise interfere with flow cytometry.

Relevant spectral parameters of 10,000 to 50,000 *Salmonella* were recorded in a FACS Fortessa II equipped with 488 nm and 561 nm lasers (Becton Dickinson), using thresholds on SSC and FSC to exclude electronic noise, and a broad mCherry recording gate to exclude the bulk of contaminating host particles (Fig 3B; Fig. S2). Data processing was done in FloJo.

For downstream proteomic analyses samples were sorted in a FACS Aria III equipped with 488 nm and 561 nm lasers (Becton Dickinson) into GFP^{dim} and GFP^{bright} populations separated by the line of median GFP intensity of a population. Although this median line shifted slightly for different biological replicates, we noted that the GFP^{bright} population was always distinct from the whole population observed in an iNOS mouse. Sorted samples were collected into 1 ml homogenisation buffer and *Salmonella* were maintained at 4°C throughout. Once the sorted volume reached 10 ml, additional chloramphenicol was added to account for the drop in concentration during sorting. Sorted S*almonella* were pelleted in protein LoBind microcentrifuge tubes (Eppendorf) by centrifugation at 4°C (12,000 x g) and stored at -80°C until further processing.

NO induction assays

A culture harbouring a relevant reporter construct was grown to mid log phase in LB buffered to pH 5.7 with 100 mM MES prior to a 1 to 20 dilution into fresh pre-warmed media to which various concentrations of $NaNO_2$ (Sigma-Aldrich) had been added 30 min earlier as a NO donor compound (*11*). Samples were collected at various time intervals after dilution, fixed in 1% Histofix/PBS (Roth), and 20,000 events recorded by flow cytometry (BD Fortessa II) using bacterial SSC FSC characteristics to exclude noise.

Re-induction of ex vivo GFP^{dim} *Salmonella* harbouring the *hmpAp::gfp_ova* construct was done by sorting 100,000 GFP^{dim} and 100,000 GFP^{bright} *Salmonella* from infected spleen homogenate at 4°C, and diluting 12’500 cells directly into 4 tubes containing 1.125 ml MOPS medium buffered to pH 5.7 with MES and containing 1 mM $NaNO_2$. The contents of one tube, plus a portion of GFP^{bright} cells were fixed immediately with formaldehyde as a time zero reference, while the remaining 3 tubes were transferred to 37°C shaker (200 rpm) and fixed 15, 30 and 2 hours after induction. As a control, a similar number of cells were diluted into LB pH 5.7 without $NaNO_2$,

transferred to the 37°C shaker and fixed a similar time points. Samples were analysed exhaustively by flow cytometry (BD Aria III).

Proteomics

Preparation of tryptic peptides and analysis by LC-MS/MS was done essentially as described (*12*) with some modifications. Given the limited sample material Protein LoBind tubes and pipette tips (Axygen) were used throughout the procedure. Frozen FACS sorted *Salmonella* pellets were resuspended in 15 µl lysis buffer (100 mM NH_4HCO_3, 8M urea, 0.1% RapiGest™) and sonicated for 2x 30 sec. The released proteins were reduced and alkylated, and first digested for 4 hours with sequencing grade LysC peptidase (10 ng/µl; Promega) before overnight trypsin digestion. The detergent was cleaved by adding 2M HCl and 5% TFA to final concentrations of 50 mM and 0.5% respectively, and incubating for 45 min at 37°C. Prior to centrifugation to remove the cleaved detergent (14,000 x g, 10 min, 4°C) a mixture containing 32 heavy labelled reference peptides were added to the samples (5x 10^{-5} fmoles per *Salmonella* for expected "high" abundance proteins, 5x 10^{-6} fmoles per *Salmonella* for expected "low" abundance proteins; Table S1). The recovered peptides were desalted on C18 reverse-phase spin columns (Macrospin columns, Harvard apparatus), dried under vacuum and subjected to directed LC-MS/MS using an LTQ-Orbitrap-Velos instrument (Thermo-Fischer Scientific). The amount of material analysed in a single shot in the MS depended on the infection load, and corresponded to peptides derived from between 5x 10^5 and 2x 10^6 sorted *Salmonella*, plus contaminating mouse material which escaped detection in the cell sorter (*10*). In order to increase the number of *Salmonella* protein identifications, MS-sequencing was focused on previously identified peptides from *Salmonella* using the recently developed inclusion list driven workflow (*12*). Each sample was analysed twice in succession in the MS to verify technical reproducibility. Peptides and proteins were database searched against the SL1344 genome sequence (ftp://ftp.sanger.ac.uk/pub/pathogens/Salmonella/) including 206 frequently observed contaminants (among them mCherry and GFPova), all mouse entries from SwissProt (version 57.12) and all sequences in reversed order (total 42502 entries) using the Mascot search algorithm. The false discovery rate was set to 1% for protein and peptide identifications. In addition to *Salmonella* proteins a substantial number of mouse proteins were identified in the samples as previously noted (*10*). The relative abundance of *Salmonella* proteins in GFP^{dim} and GFP^{bright} populations sorted from the same mouse were established using a "label free

quantification method" (*13*). Specifically, the MS1 spectra were aligned between runs and mouse proteins and contaminants excluded from further analysis. Using Progenesis software (Nonlinear Dynamics), the peak heights of peptides uniquely derived from a given protein were established and summed in each sample. Summed peak heights were normalized across samples to the average of all proteins (assuming the same total abundance of proteins in each sample), and the technical replicate values averaged. A log10 ratio was then calculated for all identified proteins between the GFP^{dim} and the GFP^{bright} sample defining the fold enrichment in the GFP^{bright} sample. For those proteins identified across different biological replicates run on different days, these log10 ratios were averaged and a standard deviation cut-off of 0.2 applied on this parameter to exclude noisy data. We noted that abundance differences calculated by this method were typically also reflected by a difference in spectral counts (data not shown). Absolute quantities were determined for those 18-20 "anchor" proteins that were detected along with a corresponding labelled AQUA peptide (STab.5) using the Trans-Proteomic Pipeline (TPP,V4.4.0). We then used the iBAQ method (*14*) to establish absolute quantities of all remaining protein identifications, with a linear model error of between 47 and 60%.

Supporting Figures

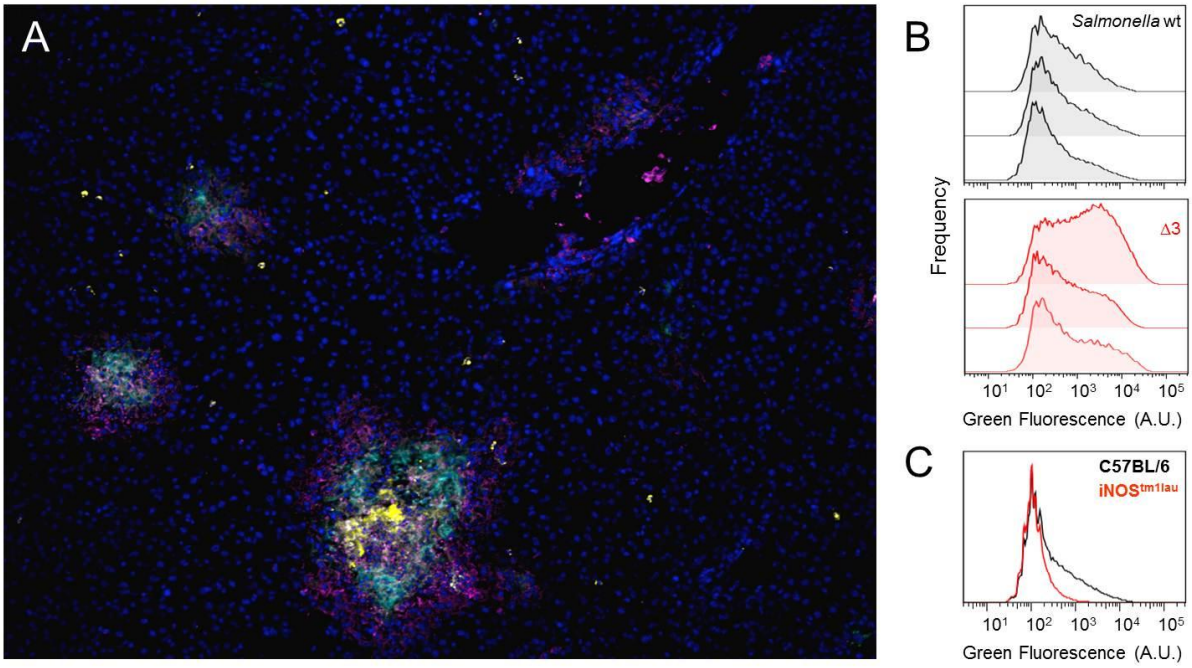

Fig. S1. Inhomogenous RNS stress and heterogeneous *Salmonella* adaptation in infected mouse liver. (**A**) Immunohistochemistry of a liver cryosection (cyan, iNOS; yellow, Ly-6G; magenta, Ly6C; blue, nuclei). (**B**) GFP expression of wildtype *Salmonella* (upper panel), or *Salmonella* Δ3 mutant (lower panel) carrying a *hmpA::gfp_ova* fusion in liver of independently infected mice.

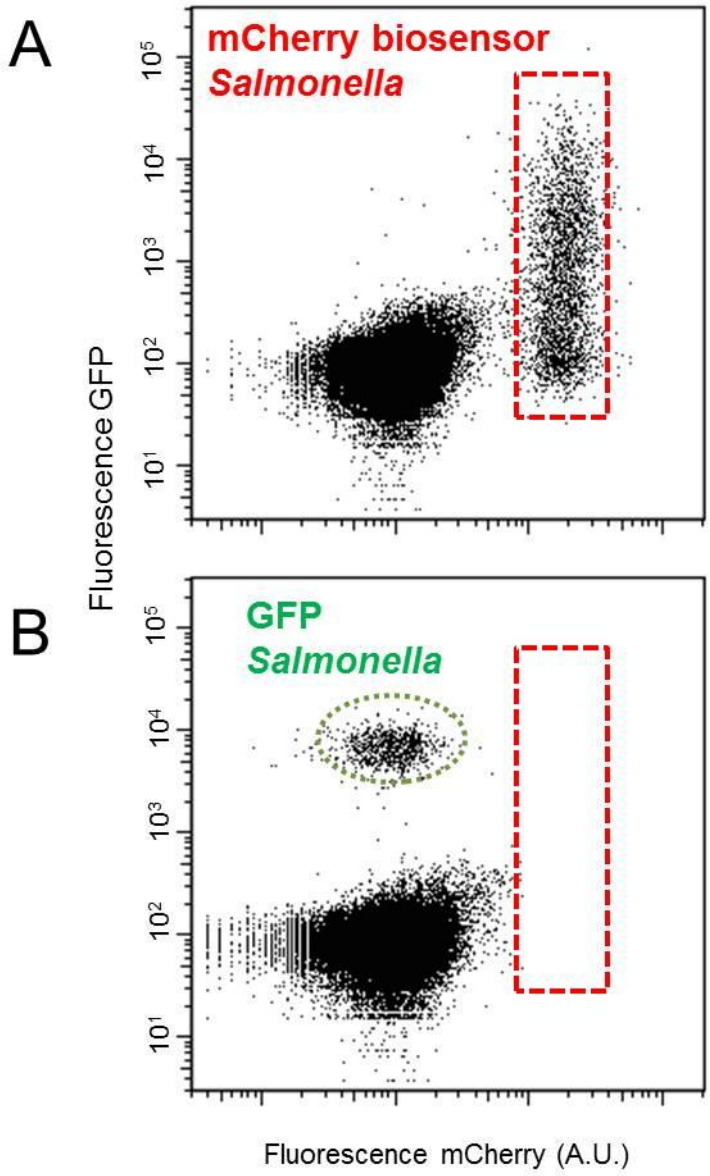

Fig. S2. mCherry is constitutively expressed in *Salmonella* biosensor expressing different levels of GFP and is detected orthogonally to GFP by flow cytometry. **(A)** Spleen homogenate infected with *Salmonella* biosensor strain harbouring P*hmpA*::*gfp::ova* and expressing mCherry from the endogenous *sifB* promoter. **(B)** Spleen homogenate infected with *Salmonella* expressing GFP from the endogenous *sifB* promoter, but no mCherry. All data were first gated on *Salmonella* scatter properties.

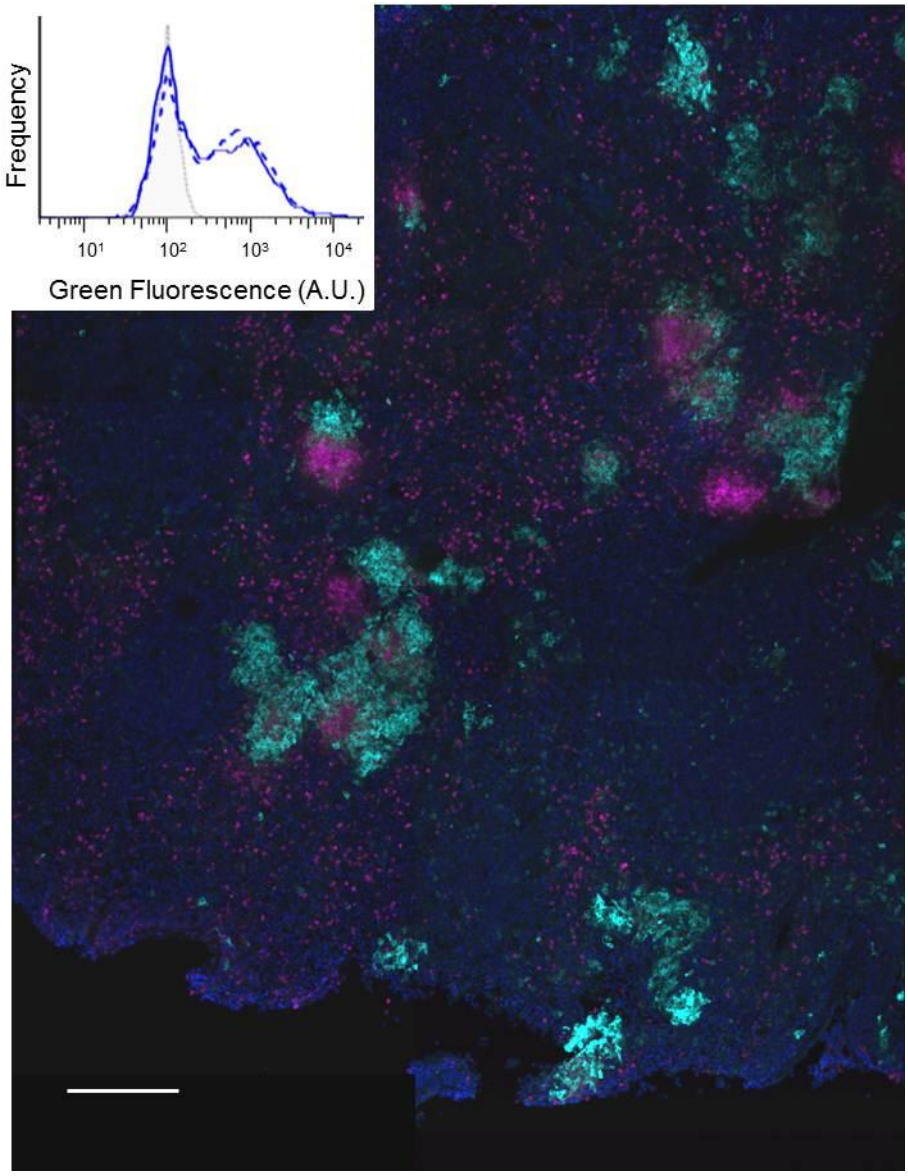

Fig. S3. Inhomogeneous RNS stress in genetically resistant 129/Sv mice. The image shows iNOS expression (cyan), neutrophils (magenta), and nuclei (blue) in infected spleen. The scale bar represents 200 µm. The inset shows activity of a P*hmpA::gfp::ova* fusion in spleen of two independently infected mice (blue lines) and background fluorescence of *Salmonella* without GFP (shaded area).

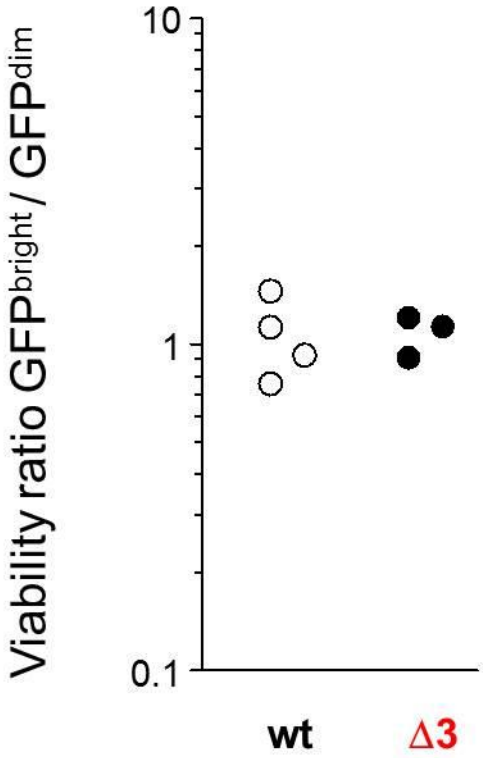

Fig. S4. Viability of ex vivo sorted GFP^{bright} and GFP^{dim} subpopulations of wildtype *Salmonella* and *Salmonella* Δ3 mutant. Values represent the ratio of plating efficiencies of sorted *Salmonella* from individual independently infected mice.

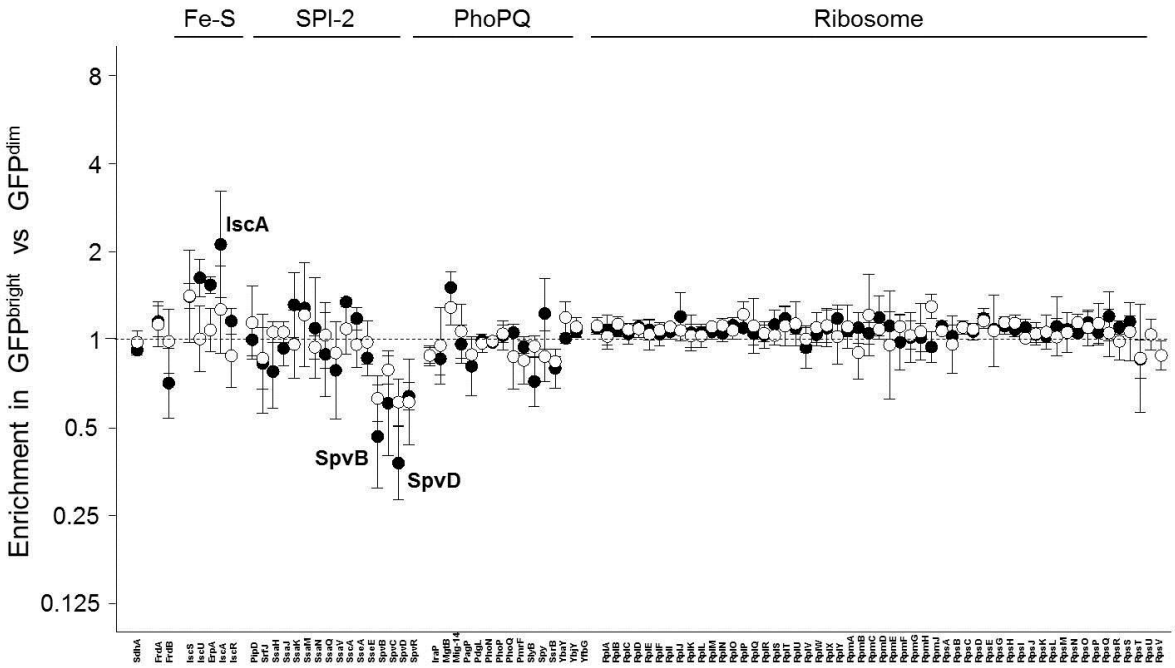

Fig. S5. Regulation of candidate proteins in subpopulations of wildtype *Salmonella* (open circles) or *Salmonella* Δ3 mutant (filled circle) in infected spleen.

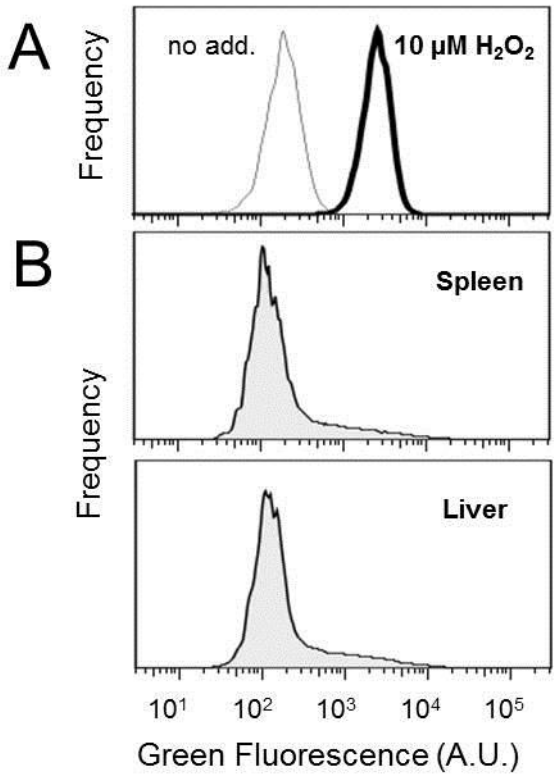

Fig. S6. Activity of P*katG*::*gfp*::*ova* construct in *Salmonella* **(A)** in vitro in absence and presence of hydrogen peroxide stress, and **(B)** during infection of spleen (upper histogram) or liver (lower histogram).

Supporting references

1. S. K. Hoiseth, B. A. Stocker, Aromatic-dependent Salmonella typhimurium are non-virulent and effective as live vaccines. *Nature* **291**, 238 (May 21, 1981).
2. A. Zaslaver *et al.*, A comprehensive library of fluorescent transcriptional reporters for Escherichia coli. *Nat Methods* **3**, 623 (Aug, 2006).
3. D. Bumann, R. H. Valdivia, Identification of host-induced pathogen genes by differential fluorescence induction reporter systems. *Nat Protoc* **2**, 770 (2007).
4. K. A. Datsenko, B. L. Wanner, One-step inactivation of chromosomal genes in Escherichia coli K-12 using PCR products. *Proc Natl Acad Sci U S A* **97**, 6640 (Jun 6, 2000).
5. C. Rollenhagen, M. Sorensen, K. Rizos, R. Hurvitz, D. Bumann, Antigen selection based on expression levels during infection facilitates vaccine development for an intracellular pathogen. *Proc Natl Acad Sci U S A* **101**, 8739 (Jun 8, 2004).
6. F. C. Neidhardt, P. L. Bloch, D. F. Smith, Culture medium for enterobacteria. *J Bacteriol* **119**, 736 (Sep, 1974).
7. V. E. Laubach, E. G. Shesely, O. Smithies, P. A. Sherman, Mice lacking inducible nitric oxide synthase are not resistant to lipopolysaccharide-induced death. *Proc Natl Acad Sci U S A* **92**, 10688 (Nov 7, 1995).
8. C. R. Beuzon, D. W. Holden, Use of mixed infections with Salmonella strains to study virulence genes and their interactions in vivo. *Microbes Infect* **3**, 1345 (Nov-Dec, 2001).
9. A. M. Leone, V. W. Furst, N. A. Foxwell, S. Cellek, S. Moncada, Visualisation of nitric oxide generated by activated murine macrophages. *Biochem Biophys Res Commun* **221**, 37 (Apr 5, 1996).
10. D. Becker *et al.*, Robust Salmonella metabolism limits possibilities for new antimicrobials. *Nature* **440**, 303 (Mar 16, 2006).
11. P. Mukhopadhyay, M. Zheng, L. A. Bedzyk, R. A. LaRossa, G. Storz, Prominent roles of the NorR and Fur regulators in the Escherichia coli transcriptional response to reactive nitrogen species. *Proc Natl Acad Sci U S A* **101**, 745 (Jan 20, 2004).
12. A. Schmidt *et al.*, Absolute quantification of microbial proteomes at different states by directed mass spectrometry. *Mol Syst Biol* **7**, 510 (2011).

13. L. N. Mueller, M. Y. Brusniak, D. R. Mani, R. Aebersold, An assessment of software solutions for the analysis of mass spectrometry based quantitative proteomics data. *J Proteome Res* **7**, 51 (Jan, 2008).

14. B. Schwanhausser *et al.*, Global quantification of mammalian gene expression control. *Nature* **473**, 337 (May 19, 2011).

2.2 Metabolic bias for extensive *Salmonella* killing in inflammatory foci

Schemmer AK, Schmidt A, Bumann D

(Manuscript in preparation)

Summary:

Inflammatory and metabolic responses to systemic infections are well understood. Nonetheless, detailed information about the spatial context of inflammation and metabolism inside infected tissues and possible consequences to the pathogen is lacking.

In this study, we used the mouse model of typhoid fever to investigate local patterns of metabolism and inflammation in liver tissue. To visualize metabolism of specific cell types *in situ,* a method to combine enzyme histochemistry and immunostaining was developed. In addition, infiltrating and resident phagocytes were purified by flow cytometry and analyzed by proteomics. We used cytosolic GFP as a viability marker to distinguish live and dead *Salmonella.*

The results revealed that granulomas which were formed by infiltrating leukocytes had a distinct metabolic pattern compared to the surrounding tissue, including resident tissue macrophages. The observed metabolic profile indicated a higher local capacity for generation of NADPH. Proteome analysis of phagocyte subpopulations independently confirmed these results. Indeed, NADPH-dependent oxidative and nitrosative damage occurred predominantly in these regions, and this correlated with preferential *Salmonella*-killing in granulomas.

In conclusion, this study provided evidence that host metabolism and inflammation were highly heterogeneous in *Salmonella*-infected host organs with important implications for infection control.

Statement of my work:

I generated all data presented in this manuscript except for the *ex vivo* proteome that was acquired and analyzed by Alexander Schmidt and visualized by Julien Limenitakis. Janine Zankl assisted in cell sorting. I wrote the manuscript together with Dirk Bumann.

Metabolic basis for extensive *Salmonella* killing in inflammatory foci

Anne Kathrin Schemmer, Alexander Schmidt and Dirk Bumann

(Manuscript in preparation)*

**This manuscript includes preliminary proteome data. Additional experiments are planned to verify the presented results.*

Abstract

Infection can cause fundamental changes in host tissue metabolism and inflammation. Here, we investigated regional relationships between metabolism, inflammation, and antimicrobial defense in *Salmonella*-infected liver in a mouse typhoid fever model. Using a novel combination of immunostaining and enzyme histochemistry, we demonstrated that granulomatous inflammatory lesions that were formed by infiltrating neutrophils and inflammatory macrophages, had a distinct metabolic pattern with a particularly high capacity to generate NADPH, an essential substrate for generation of reactive nitrogen and oxygen species (RNS, ROS). Interestingly, both neutrophils and macrophages but not resident liver macrophages, had already elevated NADPH production capacities in uninfected control mice suggesting metabolic pre-adaptation. Local NADPH production capability in granulomas coincided with expression of inducible nitric oxide synthase as well as nitrosative and oxidative damage. Many *Salmonella* that resided in these regions were unable to retain internal GFP suggesting *Salmonella* envelope damage and killing. Taken together, these data suggested that partial host control of *Salmonella* infection was supported by a specific local metabolism that provided essential NADPH for generation of bactericidal/bacteriostatic host effector molecules.

Introduction

Salmonella enterica can cause diarrhea or a systemic infection called typhoid/paratyphoid fever (2008). Systemic salmonellosis affects some 18 million patients, and causes 200'000 to 800'000 deaths predominantly in young children each year. Systemic *Salmonella* infection provokes prominent host inflammatory responses that are partially responsible for pathology (Dougan et al., 2011). On the other hand, some of these inflammatory responses are important to control *Salmonella*. Antimicrobial host activities pose large metabolic demands for energy and building blocks such as NADPH for ROS/RNS generation, lipids for membranes involved in phagocytosis, and amino acids for cationic antimicrobial peptides and digestive hydrolases (Wolowczuk et al., 2008). Indeed, systemic inflammation during *Salmonella* infection has a profound impact on liver metabolism (Pastor et al., 1995; Sakaguchi et al., 1980; Spitzer et al., 1988). In addition, crucial cell types for antimicrobial defense such as macrophages can dramatically alter their central carbon metabolism to adapt to specific demands (Mosser and Edwards, 2008; Rodriguez-Prados et al., 2010; Shapiro et al., 2011; Simon et al., 1977). However, most available data for these adaptations were obtained from cell culture experiments with macrophage-like cancer cells, which might not be representative for the behavior of primary cells under relevant conditions in infected tissues.

Here, we analyzed phagocyte metabolism in *Salmonella*-infected liver in a mouse typhoid fever model that closely mimics human disease (Santos et al., 2001). The data suggested that infiltrating neutrophils and inflammatory macrophages possessed intrinsically high hexose monophosphate shunt capacity that provided NAPDH for generation of reactive oxygen species to kill *Salmonella*. In contrast, resident Kupffer cell macrophages had a distinct metabolic profile with limited NADPH production capacity, poor generation of antibacterial effector molecules, and inefficient *Salmonella* control. Together, these findings highlighted the importance of host metabolism for *Salmonella* control, and revealed distinct in vivo metabolism patterns in phagocyte populations with different functions.

Results

Liver metabolism changes during *Salmonella* infection

To determine host metabolic changes during infection, we administered low doses of 1000 CFU *Salmonella enterica* serovar Typhimurium (henceforth, *Salmonella*) to genetically susceptible mice by tail vein injection. *Salmonella* proliferated exponentially in liver and spleen with a concomitant increase in size and weight of these two host organs as observed previously (Maskell et al., 1987).

During infection, liver glycogen content decreased dramatically (Fig. 1A), while liver triglyceride content increased (Fig. 1D) in agreement with previous studies (Sakaguchi et al., 1980). Activities of selected enzymes revealed characteristic rapid changes in glycolysis (increased activity of GAPDH) and TCA cycle (reduced activity of SDH) (Fig. 2A,B) consistent with previous observations in inflamed liver (Hinkelbein et al., 2010; Liu and Zhang, 1985). In addition, G6PDH that catalyzes the first committed step of the hexose monophosphate shunt, showed progressively increasing activity (Fig. 2C).These alterations were largely mediated by host enzymes as *Salmonella* accounted for less than 0.01% of total material in infected liver.

To test the functional relevance of two striking infection-induced changes in liver metabolism, we treated infected mice with C75, an inhibitor of fatty acid synthase (Loftus et al., 2000), or DHEAS, a reversible inhibitor of G6PDH catalyzing the first dedicated step of the hexose monophosphate shunt (Schwartz and Pashko, 2004). C75 treatment abrogated lipid accumulation in liver (Fig. 1F) but had no impact on *Salmonella* growth (SFig. 1). In contrast, DHEAS treatment exacerbated infection (Fig. 2D) suggesting that the hexose monophosphate shunt might support host control of *Salmonella*.

Method for assigning in situ enzyme activities to distinct cell types

Liver is organized in modular structures, so-called lobules, with a clear zonation of metabolic activities (Jungermann and Kietzmann, 1996). *Salmonella* infection distorts this structure by infiltrating inflammatory cells and formation of distinct inflammatory lesions (Richter-Dahlfors et al., 1997). To determine how infection-induced metabolic changes were distributed across this complex tissue structure in the various cell types, we visualized activities of several metabolic enzymes in liver sections. For this purpose, we developed a new method to assign metabolic

activities to specific cell types by combining histochemical enzyme assays with immunohistochemistry using antibodies to cell-type specific markers.

Previous attempts to combine histochemistry and immunohistochemistry using light microscopy had been hampered by interference of staining methods and limited resolution for co-localization of dark precipitates. Only a limited number of publications report on successful combinations of the two methods for single enzymes (Gorza, 1990; Thomas et al., 1982).

We replaced standard light microscopy assays for enzyme histochemistry with fluorescence-based detection. The widely used redox reagent nitrotetrazolium blue chloride (NBT) had previously been shown to yield a formazan with detectable fluorescence in the near infrared (Trinh le et al., 2007). However, NBT also accumulated unspecifically in lipid droplets that were abundantly present in infected liver, and this strong background impairs interpretation (Van Noorden and Butcher, 1984). We therefore replaced NBT with tetranitroblue tetrazolium chloride (TNBT) which also yielded a fluorescent formazan (Fig. 3) but much less background staining compared to NBT (Van Noorden and Butcher, 1984).

Fluorescent histochemical products could enable co-localization with fluorescent antibody staining to assign enzyme activities to specific cell types. Unfortunately, standard histochemistry protocols involving NBT/TNBT damaged various antigens impairing their detection with antibodies, and produced dark precipitates that limited fluorescence emission. However, optimization of reagent concentrations, incubation conditions, and spectral filters for fluorescence microscopy (see Methods) enabled sensitive enzyme activity detection while preserving antigenicity of diverse cell markers for co-localization (Fig. 3).

Local metabolic patterns in granulomas

We used the novel method to analyze activities of seven host enzymes involved in central carbon metabolism (Fig. 4; SFig. 2). The data revealed distinct metabolic patterns in inflammatory foci ranging from neutrophil-rich abscesses to mature granulomas that consisted of Ly-6G^{hi} Ly-6C^{me} neutrophils, Ly-6G^{-}Ly-6C^{hi} inflammatory macrophages (Valdez et al., 2009), CD19^{+} B cells, and likely additional cell types. These inflammatory foci had commonly low activities in fermentation, TCA cycle and respiration, but exceptionally high activities in hexokinase and the key hexose monophosphate shunt enzyme G6PDH compared to surrounding hepatocytes and resident liver macrophages (so-called Kupffer cells). High G6PDH activity was

also evident in individual infiltrating neutrophils and inflammatory macrophages in surrounding tissues.

Endothelial cells in the vicinity of inflammatory foci up-regulated ICAM-1 indicating an inflammatory response of the surrounding liver tissue (Fig.5). On the other hand, hepatocytes around inflammatory foci largely maintained the typical metabolic zonation pattern with opposite pathway activities in periportal vs. perivenous regions (Jungermann and Kietzmann, 1996). This was particularly evident for glucose-6-phosphatase which mobilizes glucose from hepatocytes to plasma (Fig.6). This local resilience of hepatocyte enzyme activities despite clear inflammatory responses of adjacent endothelial cells was somewhat surprising since inflammation can modulate hepatocyte glucose metabolism through induction of insulin resistance (Dhar and Castillo, 2011). On the other hand, hepatocytes immediately adjacent to granuloma frequently showed increased activity of various enzymes suggesting that these cells might actually respond to local inflammatory signals.

Differential regulation of enzyme levels in phagocyte subpopulations

Enzyme histochemistry/immunohistochemistry suggested distinct metabolic activities of G6PDH activity in infiltrating neutrophils and inflammatory macrophages compared to resident Kupffer cells. To confirm these findings with an independent method, we purified the various phagocyte subpopulations from infected liver as well as from tissues of non-infected control mice. Proteome analysis of the various fractions confirmed high levels of G6PDH and other enzymes involved in the hexose monophosphate shunt, but low levels of TCA cycle enzymes in neutrophils and inflammatory macrophages during infection in agreement with our histochemistry data and previous observations for activated macrophages (Garedew and Moncada, 2008; Rodriguez-Prados et al., 2010); (Fig.7A).

Interestingly, these high enzyme levels were already present in such cell types in non-infected mice (Fig. 7B). In general, enzymes associated with central carbon metabolism in all three phagocyte populations remained rather constant during infection which was surprising when compared to cell culture observations (Rodriguez-Prados et al., 2010). Only glycolytic enzymes were up-regulated in inflammatory macrophages during infection as previously observed for activated macrophage-like cancer cells (Cramer et al., 2003). Interestingly, TCA cycle enzymes were slightly up-regulated in neutrophils.

Despite this rather limited regulation of metabolic enzyme abundance, inflammation-associated proteins such as iNOS and metallothioneins changed dramatically in inflammatory macrophages and Kupffer cells during infection demonstrating that these cells actually could respond.

Local antibacterial responses in inflammatory foci

Inflammatory lesions largely consisted of infiltrated neutrophils and inflammatory macrophages that had strong G6PDH activities. This local activity of the first dedicated step in the hexose monophosphate shunt could be relevant for host/*Salmonella* interactions since this pathway is the main source of NADPH for generation of antibacterial reactive oxygen and nitrogen species (ROS/RNS) (Robinson, 2009) as well as for reduced glutathione for preventing collateral damage of host cells (Splettstoesser and Schuff-Werner, 2002). Indeed, staining with an antibody to inducible nitric oxide synthase (iNOS) revealed high local expression in the inflammatory macrophage-rich regions of inflammatory foci as previously observed (Umezawa et al., 1997); (manuscript in preparation), (Fig.8). iNOS produced relevant local amounts of nitric oxide that caused detectable nitrosative damage consistent with previous studies (Umezawa et al., 1997); (manuscript in preparation). In addition, staining with an antibody directed against 4-hydroxynonenal revealed lipid damage by reactive oxygen species in these regions (Fig.8).

ROS and RNS can kill or inhibit growth of microbial pathogens. To determine if local ROS/RNS production in inflammatory foci had an impact on *Salmonella*, we employed a recently developed method for distinguishing life and dead *Salmonella* based on retention of cytosolic GFP (manuscript submitted). Mice were infected with a *Salmonella* strain that expressed GFP from the chromosomal *sifB* promoter that is constitutively active during infection. Tissue sections were stained with an antibody to *Salmonella* lipopolysaccharide and analyzed for co-localization with green GFP fluorescence using confocal microscopy. The data revealed that most *Salmonella* in non-inflamed liver regions retained detectable GFP amounts indicating that they were alive. In contrast, many lipopolysaccharide-positive particles in inflammatory foci lacked any detectable GFP suggesting that they represented killed *Salmonella*. Statistical analysis of six independent samples confirmed that significant more *Salmonella* killing occurred in inflammatory foci as compared to non-inflamed liver regions (Fig.9).

Discussion

Salmonella infection induces inhomogeneous host inflammatory responses that lead to inflammatory foci with high density of infiltrating phagocytes surrounded by non-inflamed regions with few infiltrates (Valdez et al., 2009). We showed here that inflammatory foci had a high capacity to kill *Salmonella* compared to non-inflamed regions. *Salmonella* killing during acute infection was consistent with previous data although these studies did not reveal the regional distribution of life and dead *Salmonella* (Benjamin et al., 1990; Grant et al., 2008; Hormaeche, 1980). Preferential killing of *Salmonella* within established inflammatory foci could explain why *Salmonella* growth occurs mostly by *Salmonella* spreading to new tissue regions with little local growth in already existing infection foci (Sheppard et al., 2003).

The relevance of various antimicrobial effector mechanisms for *Salmonella* control still remains controversial (Fang, 2011; Slauch, 2011). Our data indicated that *Salmonella* killing preferentially occurred in tissue regions that generated substantial amounts of ROS and RNS causing local oxidative and nitrosative damage. These observations were consistent with the essential role of ROS production through NADPH oxidase for at least partial control of *Salmonella* infection (Mastroeni et al., 2000). ROS might kill *Salmonella* directly through oxidative damage, through synergistic effects with other antimicrobial effector mechanisms, or through indirect mechanisms involving ROS as signaling molecule that coordinates host defense (Hattori et al., 2010; Pastor et al., 1995; Slauch, 2011).

Generation of both ROS and RNS requires stoichiometric amounts of NADPH as electron donor (Robinson, 2009). NADPH is also required to maintain normal levels of reduced glutathione for minimizing collateral ROS/RNS-mediated damage of host components (Splettstoesser and Schuff-Werner, 2002). Using an optimized histochemistry/immunohistochemistry method we showed here that inflammatory foci with high ROS/RNS generation had a distinct pattern of central carbon metabolism with high capacity for NADPH production through the hexose monophosphate shunt. Pharmacological inhibition of the key enzyme G6PDH impaired host control of *Salmonella* suggesting that this metabolic pathway might indeed support relevant host antimicrobial effector mechanisms. On the other hand, complete inhibition of the hexose monophosphate shunt would have been impossible due to its essential role in many tissue functions.

Proteome analysis of various ex vivo purified phagocyte populations confirmed that neutrophils and inflammatory macrophages had high levels of hexose monophosphate shunt enzymes. Interestingly, this property was already pre-existing in neutrophils and macrophages in non-infected tissues. This was in contrast with an early study suggesting increasing hexose monophosphate shunt flux in activated macrophages (Costa Rosa et al., 1995). It is important to note that both histochemistry and proteome analysis only provide upper limits for enzyme activities that could be actually lower because of post-translational modifications and allosteric interactions. Resting cells might thus have indeed low metabolic fluxes through the hexose monophosphate shunt despite abundant enzymes (Frederiks et al., 2008). However, the intrinsic high capacity for rapid up-regulation of NADPH production with no need for de novo enzyme synthesis might protect these cells when they suddenly encounter and infiltrate inflamed tissues with high toxic levels of ROS/RNS. In addition, it would provide them with instant metabolic support for their own ROS/RNS production to combat pathogens. In addition to these intrinsic metabolic properties, inflammatory macrophages in infected mice up-regulated glycolytic enzymes for fast energy conversion in agreement with the current paradigm for inflammatory macrophages.

Surprisingly, Kupffer cells that represented the resident liver macrophage pool did not regulate their central carbon metabolism enzyme levels during infection in contrast to the inflammatory macrophages and well-studied macrophage-like cancer cells in cell culture (Rodriguez-Prados et al., 2010). Kupffer cells had a lower intrinsic capacity for NADPH generation through the hexose monophosphate shunt compared to infiltrating neutrophils and inflammatory macrophages. This distinct metabolic pattern could reflect the predominant Kupffer cell role in removal of old erythrocytes and neutrophils and immune surveillance, but not primarily in antimicrobial action on pathogens (Holub et al., 2009). Interestingly, Kupffer cells strongly responded to increased oxidative stress during infection but employed potentially NADPH-unrelated mechanisms for redox protection. Some of these properties might contribute to the permissiveness of Kupffer cells for *Salmonella* survival and growth (Mastroeni and Grant, 2011).

Conclusion

This study revealed highly heterogeneous host defense patterns in *Salmonella*-infected tissues. *Salmonella* killing occurred mostly in inflammatory foci with high local ROS/RNS production. ROS/RNS generation was supported by particularly high hexose monophosphate shunt capacity of infiltrating phagocytes. In vivo analysis of various phagocyte populations revealed distinct metabolic patterns that may correlate with differential phagocyte functions. Some of these metabolic patterns differed markedly from paradigms that were discovered in macrophage cell cultures. This may suggest a need for in situ enzyme analysis in suitable in vivo models to obtain a more comprehensive understanding of the metabolic basis for diverse macrophage functions.

Methods

Mouse infections

Susceptible female Balb/c mice, 7-15 weeks of age, were infected intravenously with 1000 CFU *Salmonella enterica* serovar typhimurium strain SL1344 or SL1344 sifB::gfp from late log phase LB cultures.

Pharmacological treatment of *Salmonella typhimurium* infected mice

Mice were pre-treated with the fatty acid synthase inhibitor C75 (CAS-Nr. 218137-86-1) for 7 days prior to infection. 22 mg/kg C75 were injected i.p. in a volume of 0.2 ml PBS, 5% DMSO, every third day. Pre-treated mice were infected as described and application of C75 continued throughout the infection.

The G6PDH inhibitor DHEAS (CAS-Nr. 78590-17-7) was applied as a fine emulsion at a concentration of 800 mg/kg in 0.2 ml 0.9% NaCl, 5% Tween-80, twice daily. Application was done i.p. and started with after infection and continued throughout. Mice were checked daily for changes in behavior, food intake and weight. Vehicle-treated mice served as control.

Sample processing

2-5 days after infection, liver was prepared. For embedding of unfixed tissue, the liver was cut in small pieces, washed with PBS and covered with Tissue-Tek O.C.T. and frozen at -80°C. Pieces of liver for homogenate enzyme assays were cut and immediately frozen at -80°C. For isolation of host cells, tissue was minced into small pieces and gently forced through a 200 µm pore size steel mesh on ice; cells were subsequently collected in HBSS, 10% FCS.

For plating of bacteria, pieces were homogenized in 20% PBS/0.3% Triton with a syringe plunger and dilution series were plated out on LB plates containing adequate antibiotics.

Tissue processing

Blocks were cut on a Cryocut 1800 cryostat (Leica), using High Profile Microtome Blades (Leica 818). Fatty liver was routinely cut at -13°C. Section thickness varied between 6 µm to 10 µm. Sections were mounted on glass slides (SuperFrost Plus, Thermo Scientific). Alternatively, sections were mounted on pre-coated coverslips (Poly-D-Lysine Cell Ware,BD). Sections were

dried at RT for 30-60 min in a desiccator. For enzyme assays, sections were dried only several minutes to maximally preserve enzyme activity and were directly used.

Biochemistry

For measurement of whole liver glucokinase enzyme activity, a frozen tissue aliquot was homogenized in lysis buffer containing 0.1% Triton, 0.1x PBS and 10 mM EDTA, pH 7.4. For each 100 mg, 300 µl of buffer was added. For measurement of all other enzyme activities, the tissue was homogenized in 0.25 M sucrose, 1mM EDTA. For each 100 mg, 600 µl buffer was added.

For measurement of enzyme activities in cell preparations, cells were centrifuged and pellets stored at -80°C. A minimum of $5x10^5$ cells was used in each assay reaction and resuspended in 0.3% Triton, 20% PBS.

Glucokinase activity was measured measured according to Pakoskey et al. (Pakoskey et al., 1965) in the presence of 50 mM Tris-HCl, pH 7.4, 10 mM $MgSO_4$, 1mM glucose, 1mM ATP, 0.5 mM $NADP^+$ and 6U G6PDH as an auxiliary enzyme at 37°C. The increase of absorbance at 340 nm was monitored for at least 2 min.

G6PDH activity was measured in the presence of 33 mM Tris-HCl, pH 7.5, 1.6 mM glucose-6-phosphate, 0.13 mM $NADP^+$ and 6.67 mM $MgCl_2$ at 30°C. The increase of absorbance at 340 nm monitored for 3-5 min. Deoxycholate was added 1:10 to the samples prior to measurement of **glucose-6-phosphatase activity.** 20 mM sodium-D-glucose-6-phosphate was dephosphorylated in the presence of 50 mM PIPES/NaOH with 10 mg/ml BSA, pH 6.5. The reaction was incubated at 30°C for 5 or 10 min.

The inorganic phosphate was colorimetrically determined by the method of Taussky and Shorr (Taussky and Shorr, 1953). The absorbance at 700 nm was read immediately at RT and the amount of inorganic phosphate determined by comparison with a standard.

GAPDH activity was measured in the presence of 0.013 sodium pyrophosphate buffer, pH 8.5 containing 0.026 M sodium arsenate, 0.25 mM NAD^+, 0.5 mM DL-glyceraldehyde-3-phosphate and 3.3 mM dithiothreitol at 25°C. The increase of absorbance at 340 nm monitored. ΔA_{340}/min was determined from the initial linear portion of the curve.

LDH activity was measured according to Bergmeyer (Bergmeyer et al., 1983) in the presence of 80 mM Tris, 200 mM NaCl, 0.2 mM NADH and 1.6 mM pyruvate at 30°C. The decrease of absorbance at 340 nm was monitored for at least 2 min.

MDH ($NADP^+$) activity was measured in the presence of 66.67 mM Triethanolamine HCl buffer, pH 7.4, 3.3 mM L-malic acid, 0.33 mM $NADP^+$ and 5 mM $MnCl_2$ at 25°C. The increase of absorbance at 340 nm was monitored for approximately 5-10 min.

PGDH activity was measured according to De Silva and Fraenkel (de Silva and Fraenkel, 1979) in the presence of 50 mM Tris-HCl, pH 7.5, 1 mM phosphogluconate, 0.2 mM $NADP^+$ and 10 mM $MgCl_2$ at 30°C. The increase of absorbance at 340 nm was monitored for approximately 5 min.

SDH activity was measured in the presence of 20 mM potassium phosphate, 0.1% Triton-X 100, pH 7.5, 5 mM sodium azide, 0.025 mM dichlorophenol indophenol and 0.01 M sodium succinate. Samples were measured against sample containing 0.01 M sodium malonate, a specific inhibitor of SDH. The photometer was adjusted to 23°C and the decrease of absorbance at 600 nm was monitored for at least 2 min.

Samples were always measured against a blank without sample (or containing specific inhibitor of the tested enzyme, *see SDH*). Enzyme activities of liver homogenate were expressed as U/g liver wet weight. Enzyme activities of cell suspensions were expressed as U/l per 10^3 cells. One Unit represented 1 µmol min^{-1}.

Triglycerides and glycogen

For determination of lipid content of infected and uninfected livers, the Triglyceride Quantification Kit (BioVision) was used. For determination of glycogen, the EnzyChromGlycogenassay kit (BioAssay Systems) was used. Tissue homogenization and measurements were conducted according to manufacturer's recommendations.

Histochemistry and immunofluorescence

Glycogen was detected in tissue sections according to Yataghanas et al. (Yataghanas et al., 1969) following a conventional Periodic acid Schiff staining protocol, but instead of Schiff´s reagent a 2,5-Bis-(4-aminophenyl)-1,3,4-oxadiazole (BAO) and metabisulfite solution was used. An additional step of 6 min incubation with sulfurous acid after BAO was included in the protocol. Fluorescent BAO (ex 365 nm/ em 450 nm) was detected using a conventional UV filter set.

Nile Red was used to detect **lipids**. A 0.05% (w/v) stock solution of Nile Red in acetone was diluted 1:1000 in glycerol:water (75:25). This solution was directly applied to frozen sections and incubated for 7 min in the dark. Sections were washed three times in 1xTBS, containing 0.05%

Tween-20, pH 7.4 (TBST). Neutral lipids were detected with a FITC filter set, phospholipids and membrane proteins were detected with a rhodamine filter set.

Free cholesterol was demonstrated with filipin. Sections were incubated for 30 min with a 1:100 dilution of a filipin stock solution (50 mg/ml in DMSO) in TBS. During incubation, no Tween-20 was present in the buffer, because filipin permeabilizes cells and too much permeabilization should be prevented.

For detection of **esterified cholesterol,** native unesterified cholesterol was extracted with 70% ethanol. Esterified cholesterol was enzymatically converted to unesterified cholesterol and then stained with filipin according to Kruth (Kruth, 1984).

Combination of immunostaining and enzyme histochemistry

Enzyme histochemistry

6 µm sections were cut freshly. For staining of enzymes unfixed frozen sections were used as fixation significantly reduced enzyme activities. Incubations were conducted at 37°C in a dark and within a moist chamber. Enzyme incubations were kept rather short (1-5 min) and sections washed several times in 1xTBST for 60 min before antibody staining.

Glucose-6-phosphatase was demonstrated with a cerium salt capture method according to Jonges et al. (Jonges et al., 1990).

Lactate dehydrogenase , 3-hydroxybutyrate dehydrogenase, malate dehydrogenase (NAD^+ dependent), malate dehydrogenase ($NADP^+$ dependent), isocitrate dehydrogenase (NAD^+ dependent), isocitrate dehydrogenase ($NADP^+$ dependent), phosphogluconate dehydrogenase, succinate dehydrogenase, glucokinase, glucose-6-phosphate dehydrogenase and glucose-6-phosphate isomerase were demonstrated according to TNBT tetrazolium salt methods of Van Noorden and Frederiks (Noorden and Frederiks, 1992). A substrate concentration of 25 mM glucose-6-phosphate was used for glucose-6-phosphate dehydrogenase.

Glyceraldehyde-3-phosphate dehydrogenase was demonstrated according to Henderson (Henderson, 1976), adapted to the standard protocol provided by Van Noorden and Frederiks (Noorden and Frederiks, 1992). Aldolase was applied as an auxiliary enzyme onto slides prior to mounting of the sections.

Preparation of polyvinyl alcohol (PVA) containing buffers

Depending on the solubility of the enzyme of interest, the concentration and average molecular weight of PVA was varied. Low viscosity medium consisted of 18% Mowiol 4-88 and was used for staining of SDH activity. High viscosity medium was prepared with PVA (average molecular weight 85.000-124.000) and was used for staining of malate dehydrogenases and isocitrate dehydrogenases. Medium viscosity was generated by a 50:50 mixture of Mowiol 4-88 and PVA (average molecular weight 85.000-124.000) and used in all other enzyme assays.

Immunostaining

Following enzyme histochemistry, sections were washed for 60 min in TBST and subsequently blocked for 1 h in 2% mouse serum (Invitrogen), 1% blocking reagent (Invitrogen). Primary antibodies used were: rat anti-mouse Ly6C (clone AL-21, BD), rat anti-mouse Ly6G (clone 1A8, BD), rat anti-mouse CD19 (clone 1D3, BD), hamster anti-mouse ICAM-1 (clone 3E2, BD), rabbit anti-mouse iNOS (Acris), rat anti-mouse F4/80 (clone A3-1, Serotec), rabbit anti-mouse CPS-1 (abcam), rat anti-mouse CD45 (clone 30-F11, antibodies online), rabbit anti-*Salmonella* LPS (Sifin), goat anti-4-hydroxynonenal (alpha diagnostics) and goat anti-nitrotyrosine (alpha diagnostics).

Primary antibodies were used in a 1:100 dilution in TBST 1% blocking reagent and sections were incubated for 60 min. Sections were washed three times for 5 min in TBST and incubated for 30 min with a secondary antibody directed against the host species or label of the primary antibody. Again, sections were washed three times in TBST. When needed, cell nuclei were stained with Hoechst 33342 (Invitrogen) for 5 min and sections rinsed in TBST.

Depending on the labeling of primary and secondary antibodies and different detection systems, several modifications to the standard protocol were used:

Biotin labeled antibodies

To prevent detection of endogenous biotin which is especially abundant in liver tissue, the Streptavidin/Biotin Blocking Kit (Vector Laboratories) was used according to manufacturer´s recommendations. For the detection of biotin labeled antibodies, Streptavidin conjugates labeled with Alexa dyes were used (Invitrogen).

Horseradish peroxidase labeled antibodies / Tyramide amplification

To prevent detection of endogenous peroxidases which are especially abundant in activated immune cells, sections were blocked with a solution of 0.05% diaminobenzidine 0.003% H_2O_2 in TBST before the normal blocking step. Incubation was for 30 min or until sections appeared pale brown. Sections were washed for 5 min in TBST and blocking proceeded according to the standard protocol.

Fluorescent tyramide conjugates were used as substrates for horseradish peroxidase. The application was done according to the manufacturer´s protocol (Invitrogen).

Mounting

To preserve sections after staining procedures, aqueous mounting medium (Sigma) was used and sections protected with coverslips (Roth). For high-resolution images and fluorescence quantification, glycerol was used on sections that were mounted on coverslips. Coverslips were sealed on object holders using nail polish or RotiHistoKitt (Roth).

Microscopy and image analysis

For light microscopy, the Olympus CKX41 microscope was used.

For fluorescence microscopy, the DMIRE II system (Leica) with the default filter blocks A4, GFP, N2.1, and Y5 was used in combination with a Hamamatsu CCD camera.The fluorescent signal of TNBT was detected with a custom filter cube (excitation filter BP 620/660, dichromatic mirror LP 660, suppression filter LP 720, AHF Analysentechnik).

Confocal images were obtained with the SP5 system (Leica) and the TNBT signal detected with a 633 laser excitation and 750-800 detection range.

Images were processed with ImageJ and PhotoShop PS3. Quantification of images was conducted with ImageJ software.

Flow cytometry

Isolation of Kupffer cells

For the isolation of Kupffer cells, a two-step collagenase perfusion was performed. Mice were sacrificed and the abdomen was opened. In situ, a syringe with a 25G microlance gauge was injected directly at the entry site of the hepatic vein into the liver. 50 ml of Ca^{2+}- free HBSS were

slowly pressed through the liver so that the tissue appeared pale and swollen. The liver was dissected and cut into small pieces using a razor blade. It was then transferred to icecold 10 ml HBSS, containing 0.25% collagenase. Digestion with collagenase was performed in a petri dish at 37°C in a slowly shaking incubator (55 rpm). Completion of collagenase digestion was checked after 30 min and then every 5 min to prevent over-digestion. After assessment of sufficient softness of the tissue with two pipette tips, the tissue was filtered through a 200 µm stainless steel mesh. All further steps were proceeded on ice. All centrifugations were carried out in a swing-out rotor.

The cells were initially centrifuged at 60xg for 1 min with low-brake setting. The supernatant was then centrifuged at 480xg for 8 min. The pellet was resuspended in 2 ml erythrocyte lysing buffer (Red Blood Cell Lysing Buffer, Sigma) and incubated for 5 min at 4°C. Then the solution was supplemented with 1 ml FCS and again centrifuged at 480xg for 8 min.

Isolation of infiltrates

Mice were sacrificed and the liver dissected. The tissue was pressed through a 200 µm stainless steel mesh. One liver was suspended in a volume of 2x12.5 ml icecold HBSS 2% FCS, containing 40U/ml benzonase. All further steps were done on ice. The cells were initially centrifuged at 60xg for 1 min with low-brake setting. The supernatant was then centrifuged at 480xg for 8 min. The pellet was resuspended in 2 ml erythrocyte lysing buffer and incubated for 5 min at 4°C. Then the solution was supplemented with 1 ml FCS and centrifuged at 480xg for 8 min. Final cell pellets were resuspended in icecold HBSS, 2% FCS, 2% mouse serum for subsequent antibody staining.

Assessment of cell number and viability

Cells were diluted 1:1 in trypan blue and counted using a Neubauer counting chamber.

Antibody staining and gating strategy

Usually, one pellet corresponding to 50% of the whole liver was resuspended in icecold HBSS 2% FCS 2% mouse serum. All further steps were done on ice. Primary antibodies used were: rat anti-mouse Ly6C (clone AL-21, BD), rat anti-mouse Ly6G (clone 1A8, BD), rat anti-mouse CD11b (clone M1/70, BD) and rat anti-mouse F4/80 (clone A3-1, Serotec). Primary antibodies were diluted in the suspension to yield a concentration of 2-5 µg/ml. The optimal concentration was

titrated for each antibody and was 5 µg/ml for the anti-Ly6C and anti-Ly6G antibodies and 2 µg/ml for the anti-CD11b and anti-F4/80 antibodies, respectively. Primary antibody incubation was done for 20 min. After incubation, the suspension was centrifuged at 200xg for 5 min. The pellet was resuspended in HBSS 2% FCS 2% mouse serum and secondary antibodies added. Incubation was done for 10 min. Afterwards, the suspension was centrifuged as before and the pellet reconstituted in 5 ml HBSS 2% FCS. The cells were filtered through a MACS pre-separation filter (MiltenyiBiotec).

FACS analysis and sorting of cells

For FACS analysis a FACS Canto (BD) was used. $CD11b^+$ cells were gated and then back-gating on bigger cells in the side scatter (SSC) was done. $Ly6G^+$ and $Ly6C^+$ cells were gated and events recorded.

Sorting was conducted with a FACS Aria (BD) using a 100 µm nozzle. For live/dead gating, cells were stained with DAPI. Cells were sorted at 4°C into 1 ml HBSS 10% FCS.

After sorting, cells were counted in a Neubauer counting chamber to assess sorting efficiency. To verify cell purity and identity, cells before and after the sort were routinely analyzed by fluorescence microscopy.

The volume corresponding to 10^5 cells was filled into low-binding tubes (Eppendorf) and centrifuged at 300xg for 5 min at 4°C in a table-top centrifuge. After removal of the supernatant, the tubes were centrifuged again for 3 min. The remaining liquid was removed and the tubes stored at -80°C.

Proteomics

Sample preparation for proteomics

For cell lysis, the pellet was dissolved in 8 M urea, 0.1 M ammonium bicarbonate 0.1 % rapigest in a volume two times bigger than the pellet. Vortexing for 10 sec was followed by spinning down. Samples were sonicated 2 x 10 sec.

Proteins werereduced with 0.2 M TCEP, 0.1 M Tris solution pH 8.5, added 1:40 to the sample, followed by a 1 h incubation at 37°C in an Eppendorf shaker at 1000 rpm. The sample was alkylated with 0.4M iodoacetamide, added at 1:40. Incubation was carried out in the dark at 25°C for 30 min in an Eppendorf shaker at 500 rpm. 0.5 M N-acetylcysteine, 0.1 M Tris, pH 8.5 were added 1:40 and the solution incubated at RT for 10 min in an Eppendorf shaker at 500 rpm.

The endoproteinase Lys-C was added to a final enzyme/protein ratio of 1:100 and digestion followed for 3.5 h at 37°C in an Eppendorf shaker at 500 rpm. Subsequently, the sample was diluted 1:5 with 0.1 M ammonium bicarbonate. Trypsin was added to a final enzyme/protein ratio of 1:50. Incubation was carried out over night at 37°C in an Eppendorf shaker at 500 rpm.
5% trifluoroacetic acid was added 1:10 and 2 M HCl 1:40 to inactivate rapigest and trypsin. Incubation followed at 37°C for 45 min. The peptides were cleaned up by C18 reversed-phase spin columns according to the manufacturer's instructions (Harvard Apparatus). Peptides were dried and pellets stored at -80°C before analysis.

Analysis by mass spectrometry

The dried peptides were resuspended in 5% acetonitrile/95% water/0.15% formic acid to yield a concentration of 0.5 µg/µl, ultrasonicated 2x10 sec and incubated for 5 min at 1400 rpm at 37°C in an Eppendorf shaker. Samples were then analyzed by directed LC-MS/MS using an LTQ-Orbitrap-Velos instrument (Thermo Fischer Scientific). Protein abundance was normalized using the Proteomics Dynamic Range Standard (Sigma). Peptides were searched against all mouse entries from SwissProt (Version 57.12) and all sequences in reversed order (total 42502 entries) using the Mascot search algorithm. The false discovery rate was set to 1% for protein and peptide identifications.

Visualization of proteome data

Metabolic networks were reconstructed using the Omix software (Droste et al., 2011).

Figures

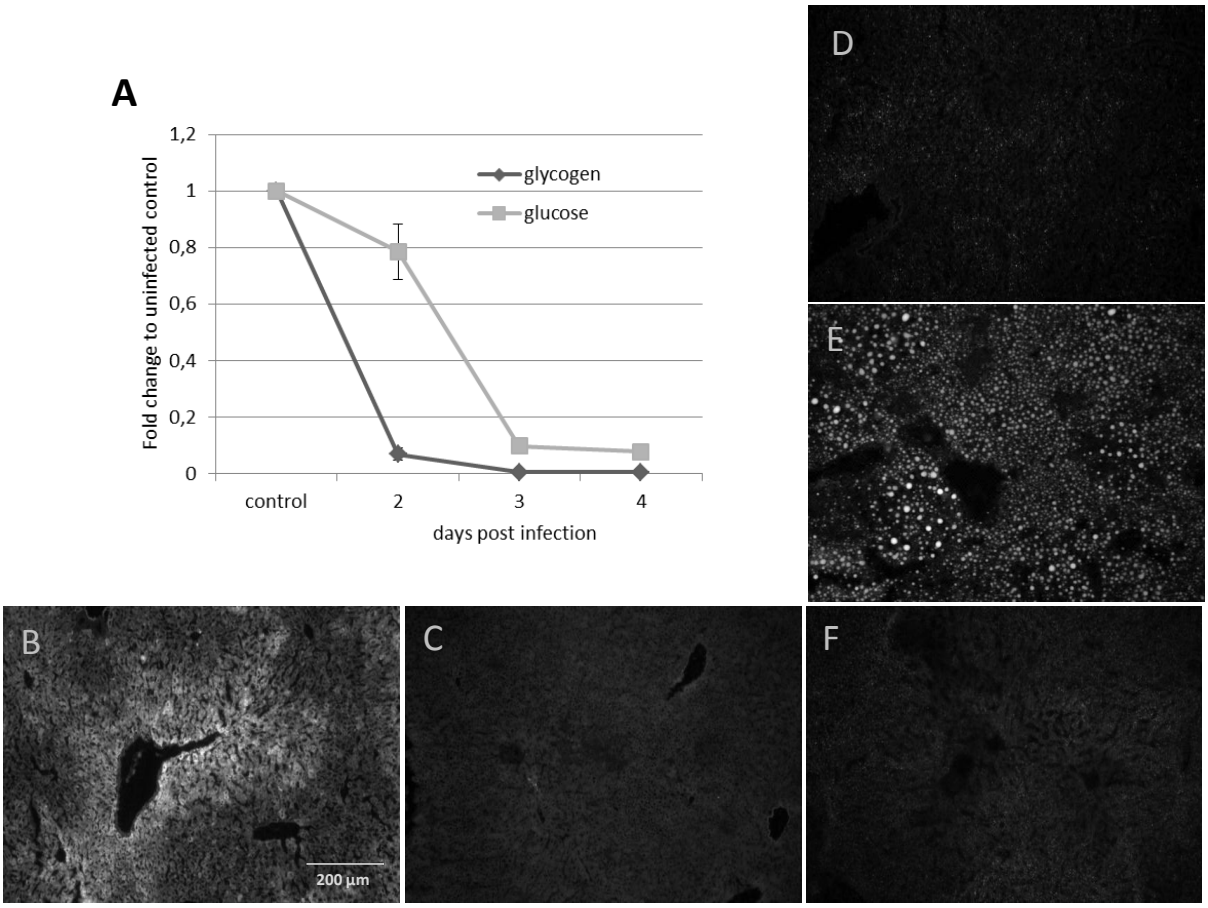

Figure 1: Abundance of lipids and carbohydrates. A) Glycogen and glucose levels in liver during early *Salmonella* infection. Means ± SD for groups of three mice are shown**. B) and C):** Histochemical glycogen staining of liver sections. Glycogen was stained with BAO. **B)** Uninfected, **C)** liver obtained at day 4 after *Salmonella* infection. The scale bar in B) represents 200 µm. **D)-F):** Histochemical lipid staining of liver sections. Lipids were stained with Nile Red. **D)** Uninfected**, E)** liver obtained at day 4 after *Salmonella* infection, **F)** liver obtained at day 4 after *Salmonella* infected from a mouse treated with the fatty acid synthase inhibitor C75. Similar observations were made for groups of three independently infected mice.

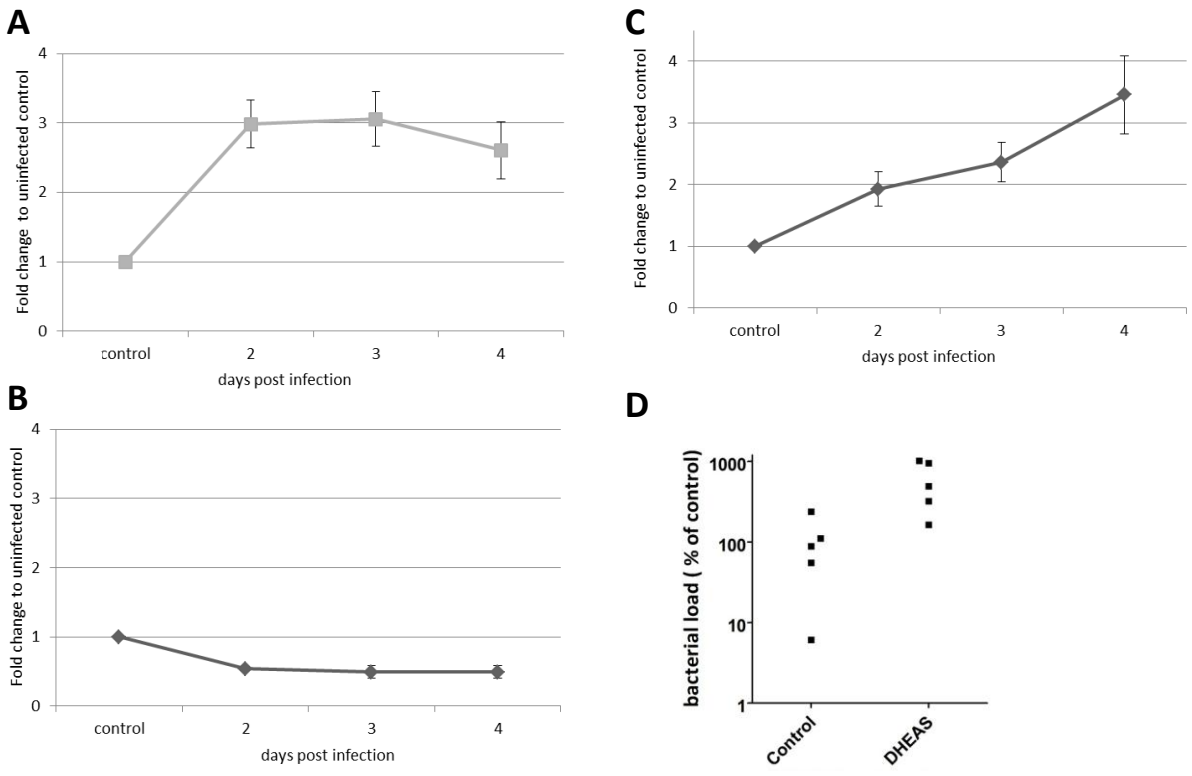

Figure 2: Enzyme activities in infected liver homogenates. Panels A to C show mean values ± SD for groups of three mice for Glyceraldehyde-3-phosphate dehydrogenase (GAPDH) (**A**), Succinate dehydrogenase (SDH) (**B**), and Glucose-6-phosphate dehydrogenase (G6PDH) (**C**). The change of enzyme activities over time is compared to enzyme activities in a group of three uninfected mice. **D**) Impact of treatment with G6PDH inhibitor DHEAS on *Salmonella* colonization levels in liver at day 4 post infection. Data points represent individual control-treated or DHEAS-treated mice.

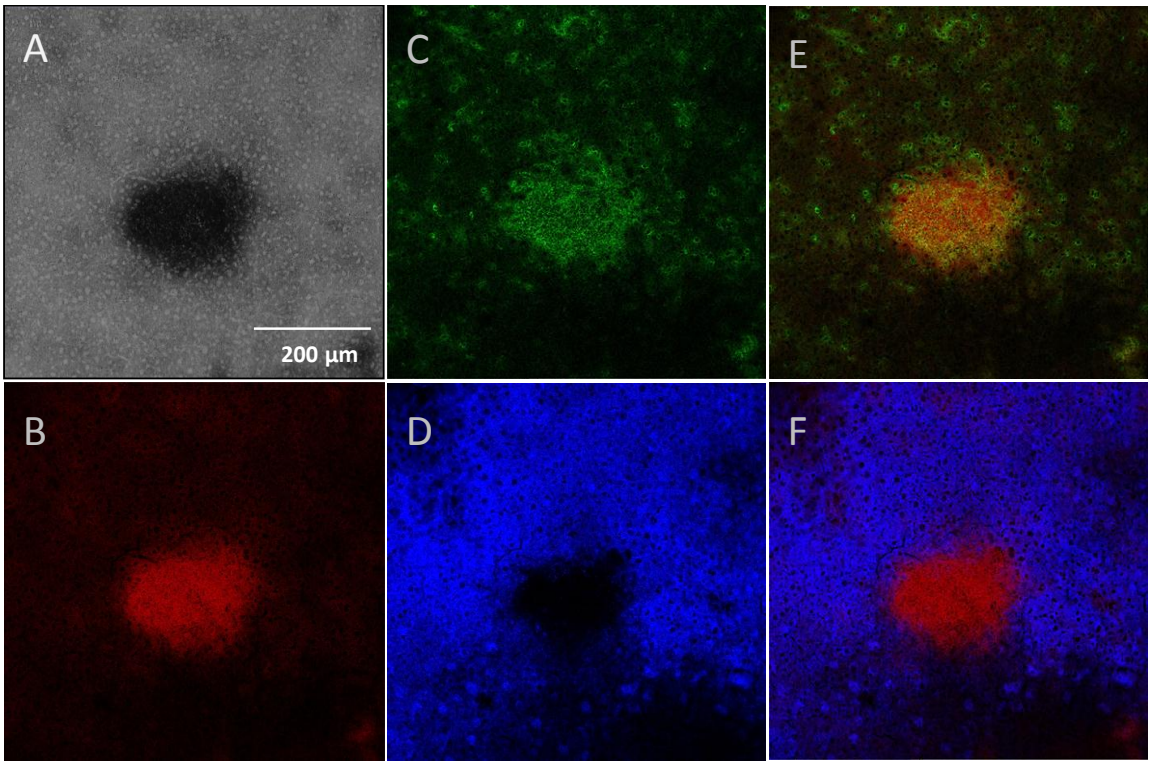

Figure 3: TNBT fluorescence and combined immunostaining. A) Shows a light microscopy picture of TNBT staining (black). In **B)**, the fluorescent TNBT signal was detected with a confocal system, using 633 laser excitation and far-red emission settings. **C)** and **D)**: Fluorescent immunostaining in the same tissue sections. **C)** Staining of leukocytes, using a pan-leukocyte marker (CD45), or a hepatocyte-marker (CPS-1) **(D)**. **E) and F):** Overlays of antibody staining and enzyme histochemistry. Leukocyte accumulations that characterize granulomas colocalize with the enzyme staining (G6PDH); **(E)**. CPS-1 staining in **F)** excludes hepatocytes as cell types contributing to the enzyme staining observed. The scale bar in A) represents 200 µm.

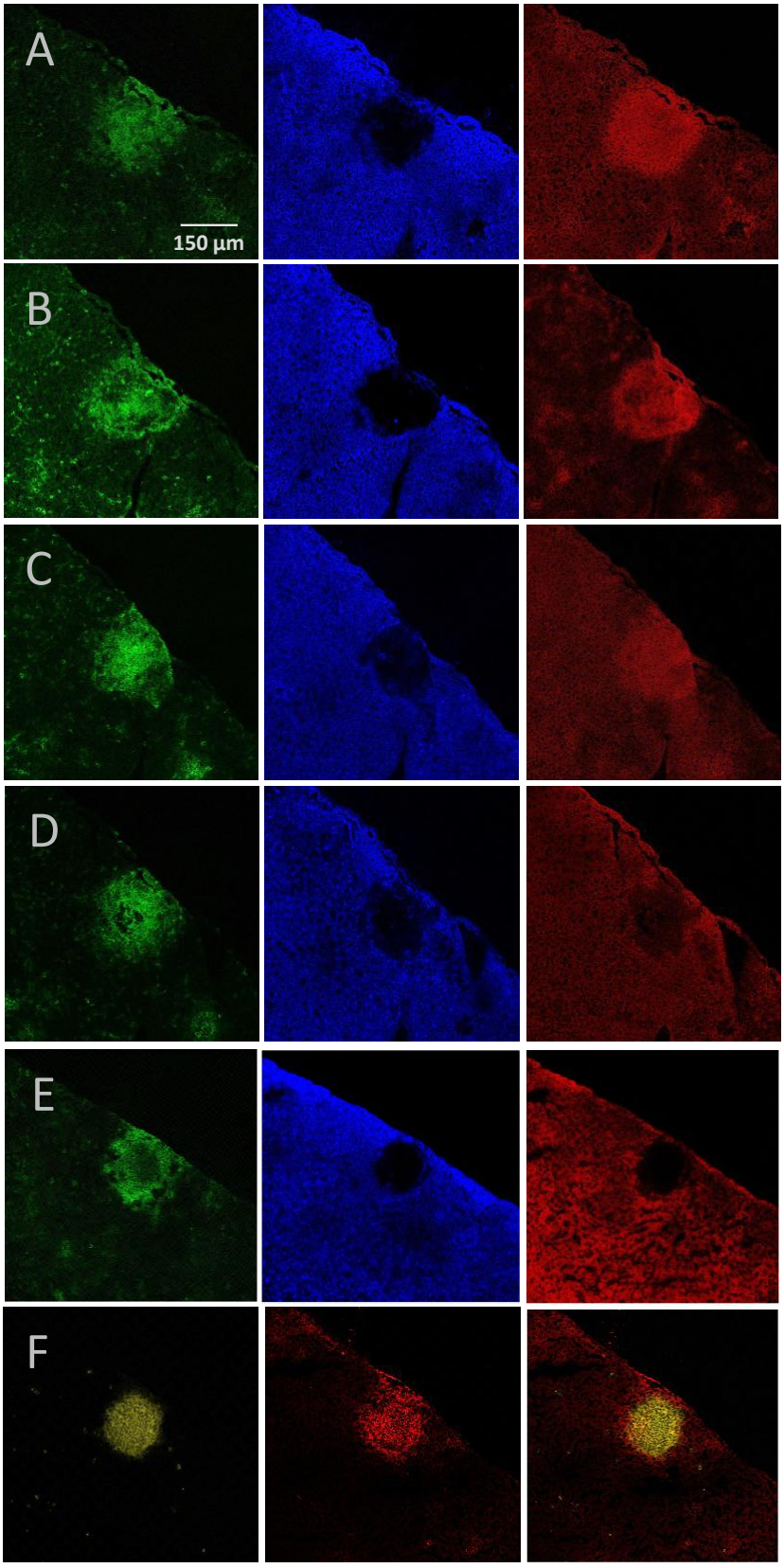
A
150 µm
B
C
D
E
F

Figure 4 A: Metabolism of granulomatous lesions in liver tissue. Staining of leukocytes with the pan-leukocyte marker CD45 is shown in green. Hepatocytes, stained with an antibody against CPS-1, are depicted in blue. Corresponding enzyme stainings are shown in red. The following enzyme activities are shown: **A)** Glucokinase, **B)** G6PDH, **C)** PGDH, **D)** GAPDH, **E)** SDH. **F)** Identifies these distinct tissue areas as granulomas by staining of neutrophils with an anti-Ly6G antibody (yellow, first picture) and macrophages and neutrophils with an anti-Ly6C antibody (red, second picture). The third picture shows an overlay. Panels A)-F) represent neighbouring sections. Similar observations were made in at least three different mice for each enzyme. The scale bar in B) represents 150 µm.

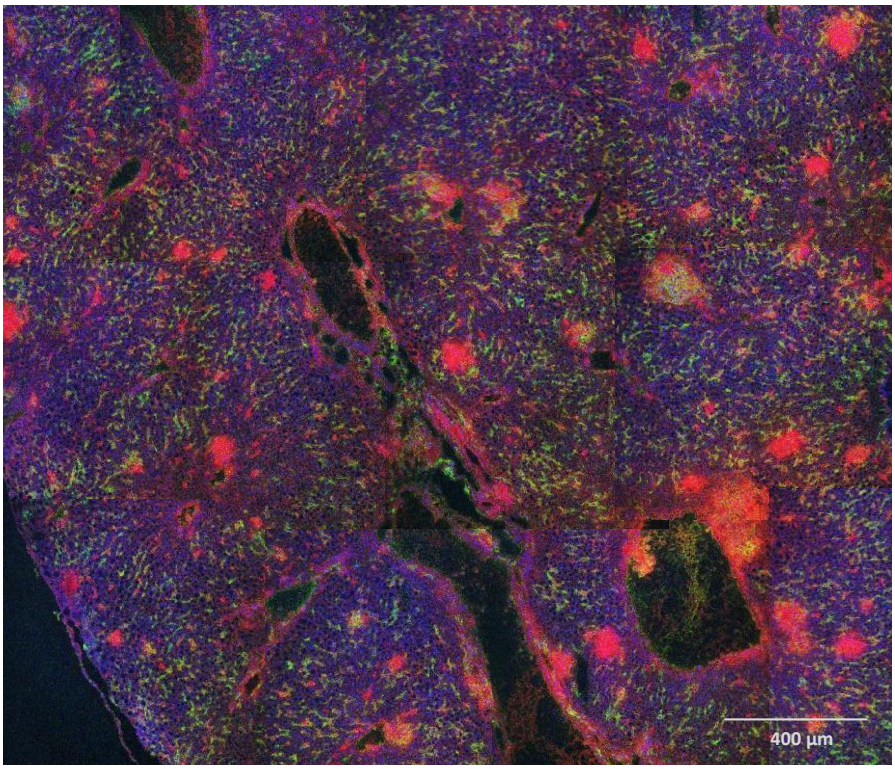

Figure 4 B: Metabolism of granulomatous lesions in liver tissue (overview). This picture shows the spatial distribution of G6PDH activity in infected liver tissue. Macrophages were stained using an antibody against F4/80 (pan macrophage marker), shown in green. Enzyme staining is shown in red. Cell nuclei were stained with Hoechst 33342 (blue). Stitched overview. The scale bar represents 400 µm.

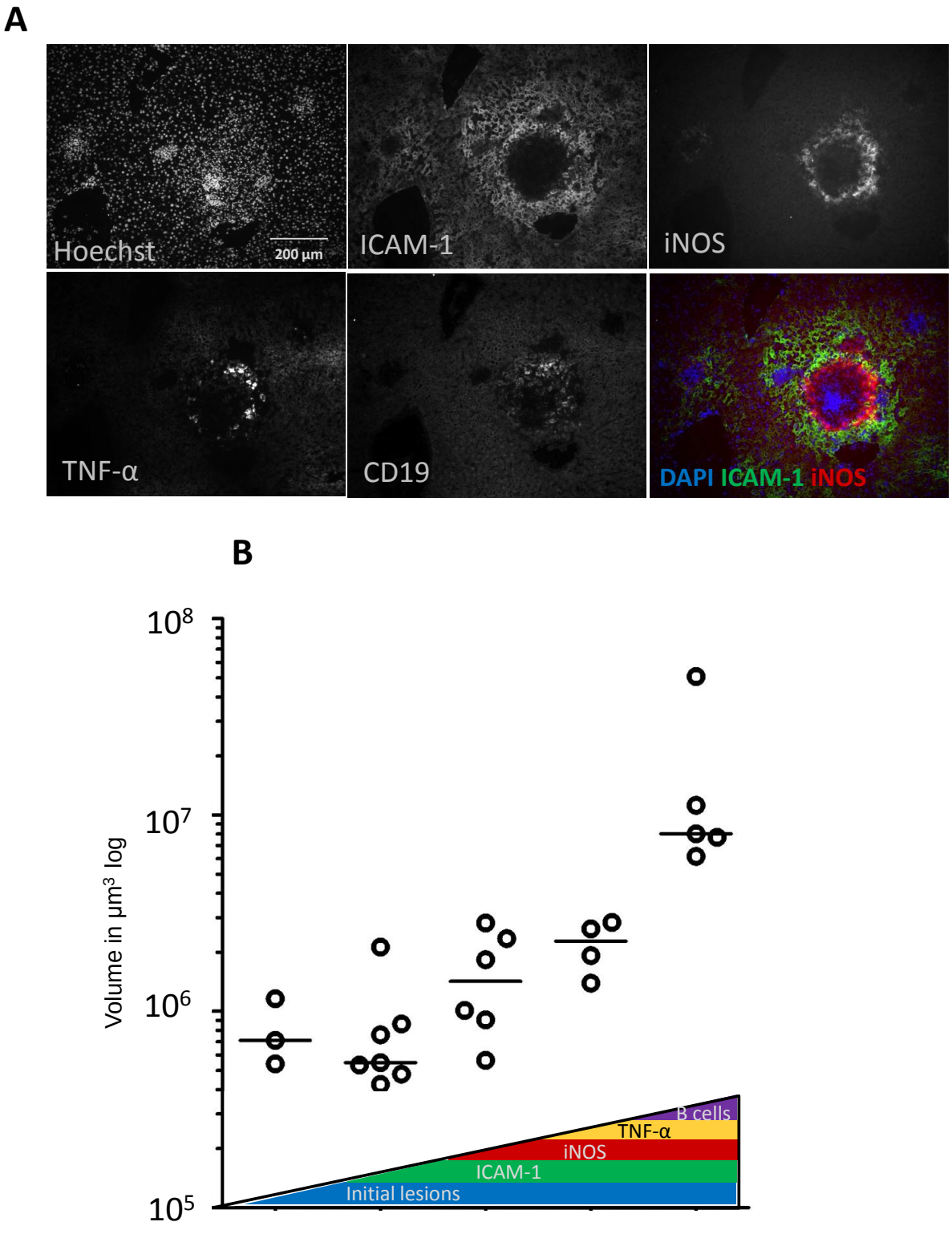

Figure 5: Progression of inflammatory lesions. A) Tissue sections were stained with Hoechst 33342 and antibodies against ICAM-1, iNOS, TNF-α and CD19 in 12 alternating neighbouring

sections. The diameter of 25 granulomatous lesions was determined following these lesions through the sections and the volume calculated, assuming globular shape (which was independently verified). The scale bar in A) represents 200 µm. **B)** Expression patterns become more complex with size of the lesions. Each data point represents one granuloma.

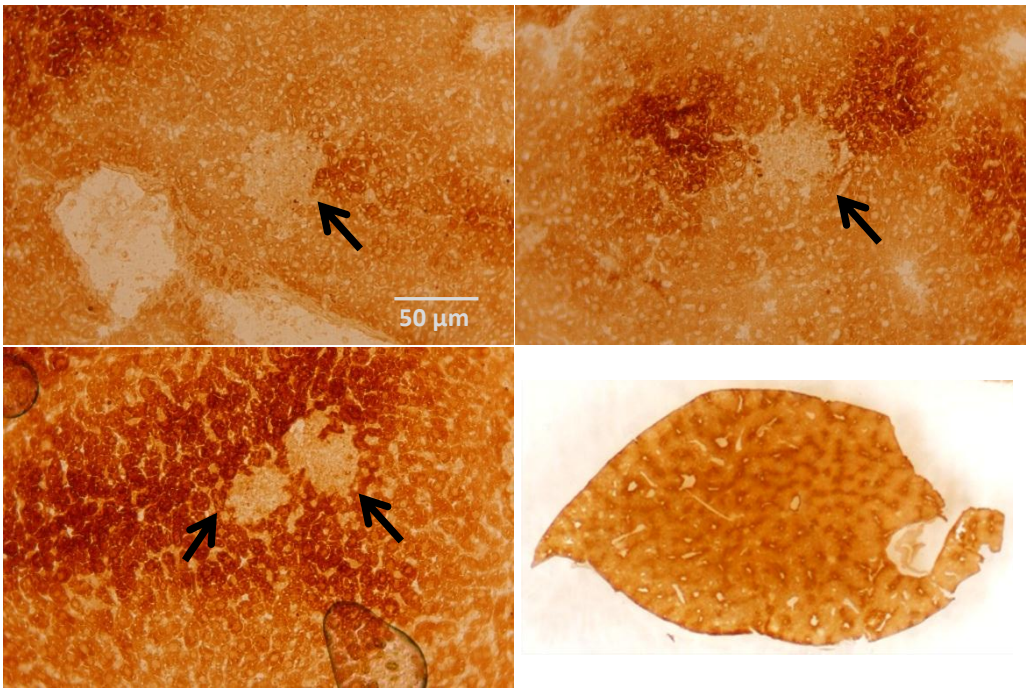

Figure 6: Local inflammation does not disturb metabolic zonation in the liver. All pictures show Glucose-6-phosphatase (G6Pase) activity in the infected liver. The enzyme was stained using a Cerium-diaminobenzidine method. Brown: Glucose-6-phosphatase activity. Black arrows indicate granulomatous lesions. Down right: overview of a liver section (right lobe), showing the pattern of metabolic zonation. Glucose-6-phosphatase is active in a pattern corresponding to metabolic zonation. No local disturbance of metabolic pattern could be observed during infection. The scale bar represents 50 µm.

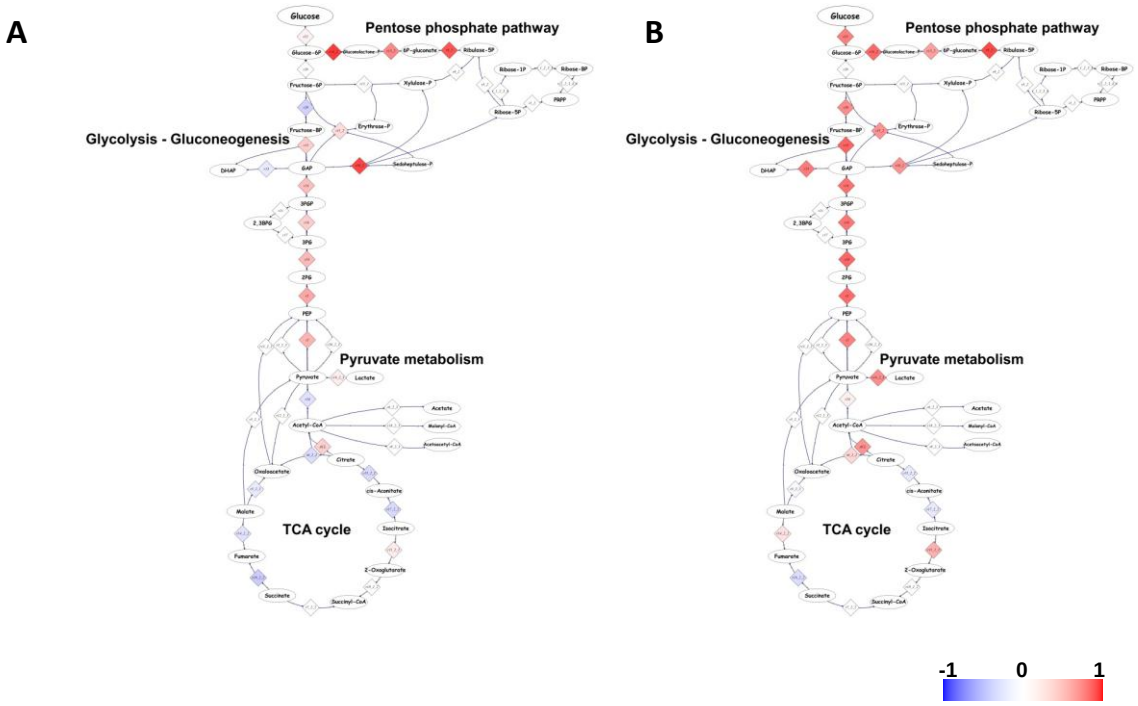

Figure 7 A: Central carbon metabolic enzyme abundances. Comparison of infiltrates and resident tissue macrophages in infected liver tissue. Blue: lower protein abundance, red: higher protein abundance. Values represent log10 of fold abundances. **A)** Compares the neutrophil proteome to the Kupffer cell proteome. HMP shunt enzymes are significantly more abundant; glycolysis enzymes are slightly more abundant. In contrast, Kupffer cells have higher capacity for TCA cycle. **B)** Compares the inflammatory macrophage proteome to the Kupffer cell proteome. HMP shunt enzymes and glycolysis enzymes are more abundant. Data were obtained from technical replicates.

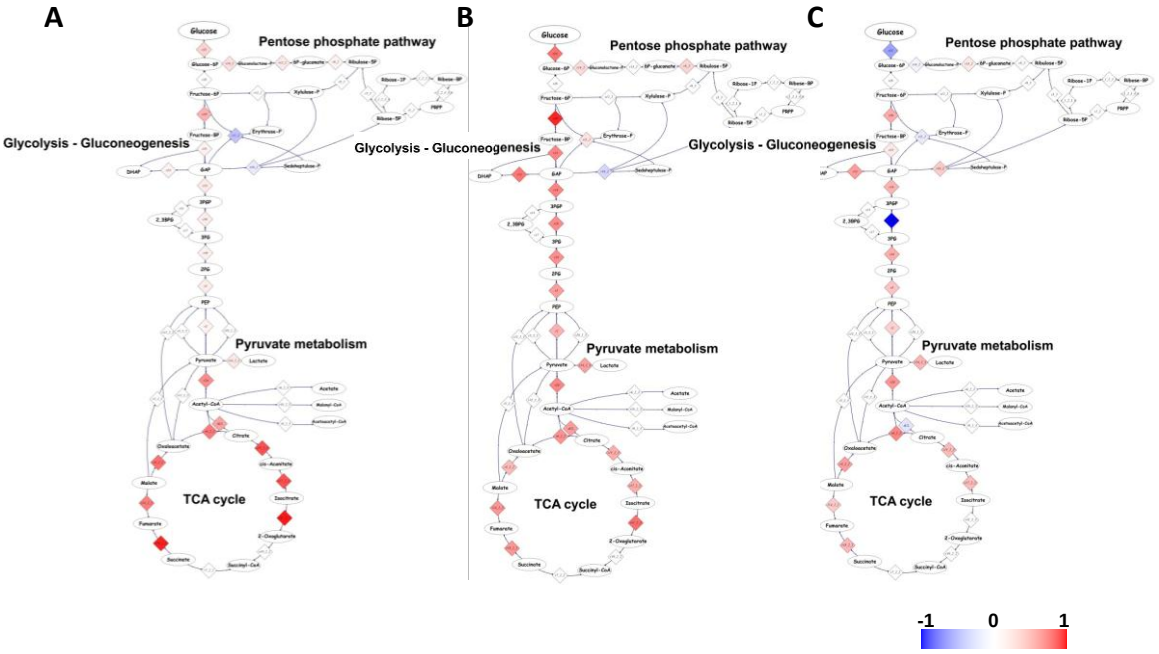

Figure 7 B: Central carbon metabolic enzyme abundances. Comparison of phagocytes from *Salmonella*- infected liver to cells from naïve liver. Blue: lower protein abundance, red: higher protein abundance. Values represent log10 of fold abundances. **A)** Comparison of neutrophils from infected vs. uninfected tissue*. Interestingly, TCA cycle enzyme abundance was higher in cells from infected tissue, but other pathways were similar. **B)** Comparison of inflammatory macrophages from infected vs. uninfected tissue. Enzyme abundance of glycolysis and TCA cycle increased in cells from infected tissue, HMP shunt enzyme abundance was similar. **C)** Comparison of Kupffer cells from infected vs. uninfected tissue. Enzyme abundance of glycolysis and TCA cycle was slightly higher in cells from infected liver. HMP shunt enzyme abundance was similar in both cell populations. Data were obtained from technical replicates. *: Uninfected tissue was spleen.

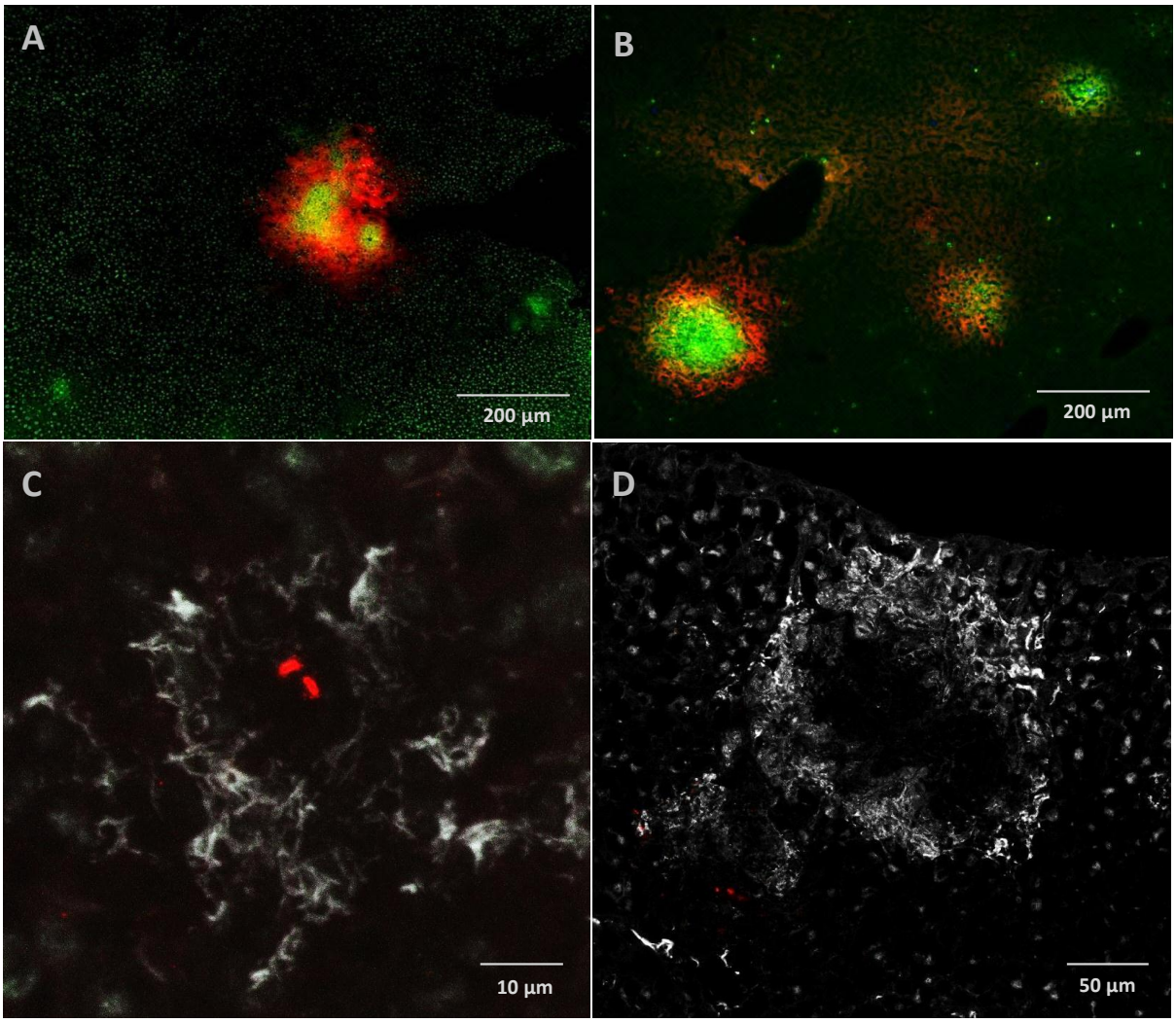

Figure 8: Oxidative and nitrosative stress in inflammatory foci and *Salmonella* co-localization. In **A),** G6PDH activity (green) was stained and an antibody staining against iNOS performed (red). The picture shows peripheral iNOS expression and G6PDH inside two granulomas. In **B),** the granuloma neutrophil core was stained using an anti-Ly6G^{+} antibody (green) and co-stained using an anti-iNOS antibody (red). iNOS expression does not colocalize with the neutrophil core. **C)** Shows the nitrosative tissue damage, stained with an anti-nitrotyrosine antibody (grey) and *Salmonella*, stained with an antibody against Salmonella-LPS (red). Nitrosative damage is often concentrated at the granuloma periphery. The oxidative damage in a mature granuloma, stained with an antibody against 4-HNE (grey), is shown in panel **D).** Both nitrosative and oxidative damage seldom colocalize with intact bacteria. The same observations were made in liver and

spleen sections of three mice sacrificed 4 days post infection. The scale bars in A) and B) represent 200 µm, the scale bar in C) represents 10 µm, in D) 50 µm.

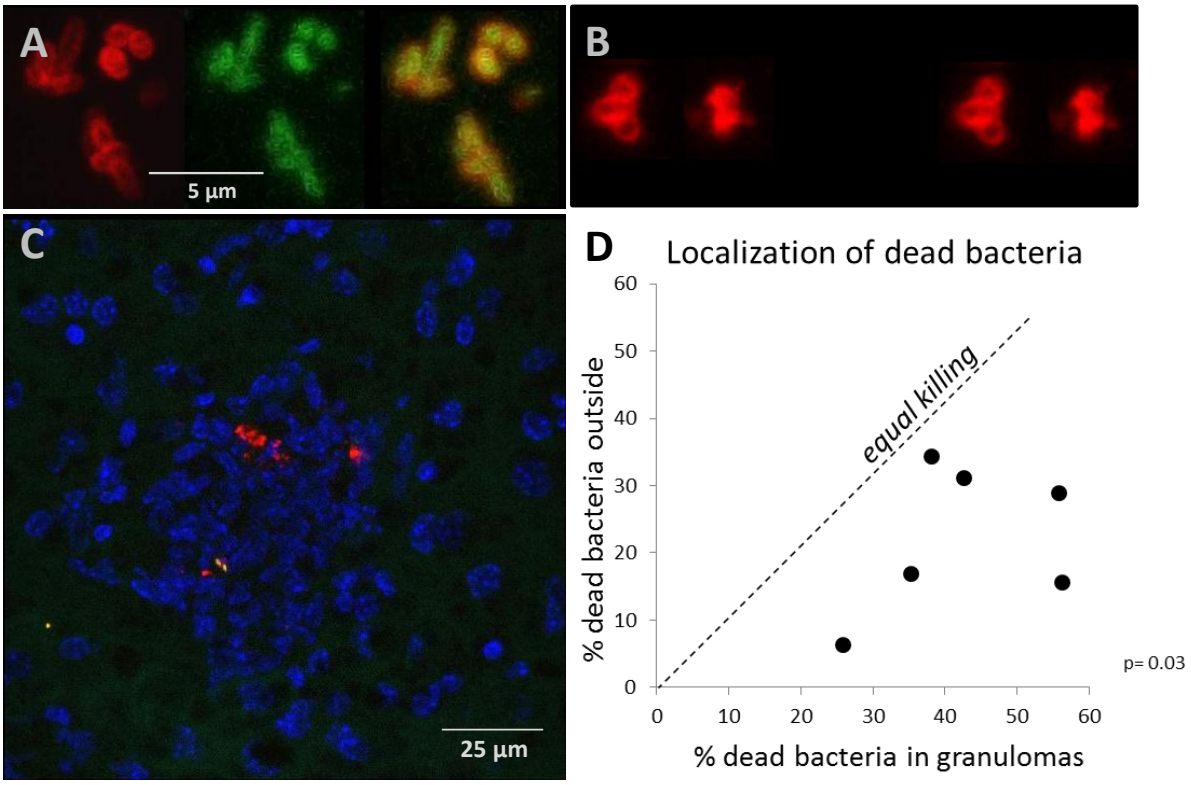

Figure 9: Killing of *Salmonella* inside inflammatory foci. Cytosolic GFP was used as a marker for *Salmonella* viability in tissue sections. Panel **A)** shows *Salmonella,* stained with an anti-*Salmonella* LPS antibody that makes the cell envelope visible (red). Cytosolic GFP is shown in green, followed by an overlay of both stainings. GFP positive bacteria are assumed to be alive. Panel **B)** shows the same stainings as in A), but the GFP signal is negative. Therefore, these bacteria are thought to be dead. The diffuse LPS-staining suggests a loss of cell integrity and thus loss of cytosolic GFP. In **C),** an inflammatory focus is identified by Hoechst 33342 staining (blue), which shows the dense accumulation of small leukocyte nuclei. Live and dead bacteria can be identified based on red or mixed green and red fluorescence. In **D)**, dead bacteria were quantified inside and outside inflammatory foci/granulomas. Each data point represents one full liver section. Sections from three different mice were quantified.

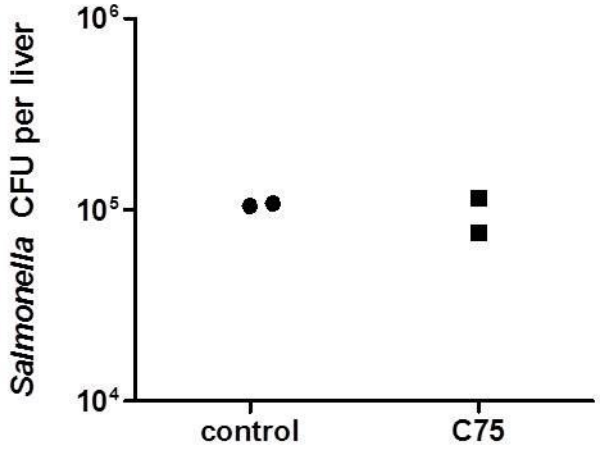

Supplemental figure 1: Effect of treatment with fatty acid synthase inhibitor C75 on *Salmonella* colonization levels in liver at day 3 post infection. Data points represent individual control-treated or C75-treated mice.

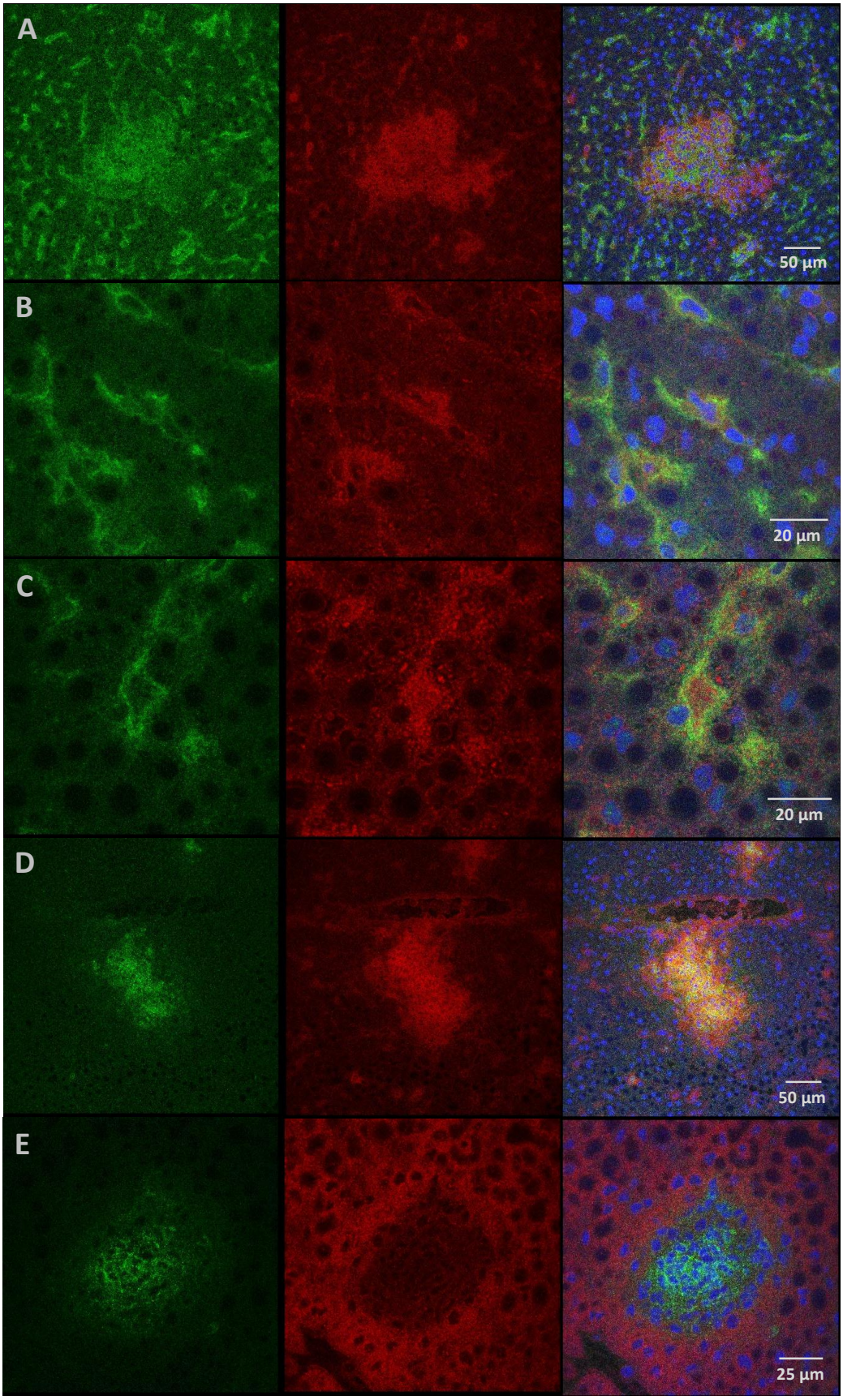
A
50 µm
B
20 µm
C
20 µm
D
50 µm
E
25 µm

Supplemental figure 2: Metabolism of granulomatous lesions *(continued from figure 4).* The first column (green) shows antibody stainings. The second row shows the corresponding enzyme stainings (red) and the third column an overlay of the pictures, together with a Hoechst 33342 staining for cell nuclei (blue). Panels **A)** to **C)** show G6PDH enzyme activity and macrophage-colocalization, stained by an anti-F4/80 antibody (green). Panel **D)** shows G6PDH activity and colocalization with neutrophils, stained with an anti-Ly6G antibody. **E)** Shows LDH activity and neutrophil colocalization. The picture suggests a higher LDH activity in hepatocytes, compared to granulomas. The scale bars represent 50 µm in A), 20 µm in B) and C), 50 µm in D) and 25 µm in E).

Supplemental table 1: Antibodies used.

Ly6C-biotin	BD 557359	rat	clone AL-21
Ly6G-FITC	BD 551460	rat	clone 1A8
CD-19-biotin	BD 553784	rat	clone 1D3
ICAM-1-biotin	BD 553251	armenian hamster	clone 3E2
iNOS	Acris iNOS-A	rabbit	polyclonal
F4/80-FITC	Serotec MCA497F	rat	clone A3-1
CPS-1	Abcam ab3682	rabbit	polyclonal
CD45-FITC	antibodies online ABIN161559	rat	clone 30-F11
4-HNE	alpha diagnostics HNE12-S	goat	ubiquitous
Nitrotyrosine	alpha diagnostics NITT13-S	goat	ubiquitous
Salmonella-LPS	Sifin REF TS 1624	rabbit	polyclonal
CD11b-PE	BD 557397	rat	clone M1/70

Acknowledgments

We thank Beatrice Claudi and Alain Mazé for technical help with in vivo experiments and Janine Zankl for excellent assistance in cell sorting. We are grateful to Julien Limenitakis for visualization of the proteome data.

References

2008. Typhoid vaccines: WHO position paper. *Wkly Epidemiol Rec*. 83:49-59.

Benjamin, W.H., Jr., P. Hall, S.J. Roberts, and D.E. Briles. 1990. The primary effect of the Ity locus is on the rate of growth of Salmonella typhimurium that are relatively protected from killing. *J Immunol*. 144:3143-3151.

Bergmeyer, H.U., J. Bergmeyer, and M. Grassl. 1983. Methods of enzymatic analysis. Verlag Chemie, Weinheim Germany ; Deerfield Beach, Fla.

Costa Rosa, L.F., R. Curi, C. Murphy, and P. Newsholme. 1995. Effect of adrenaline and phorbol myristate acetate or bacterial lipopolysaccharide on stimulation of pathways of macrophage glucose, glutamine and O2 metabolism. Evidence for cyclic AMP-dependent protein kinase mediated inhibition of glucose-6-phosphate dehydrogenase and activation of NADP+-dependent 'malic' enzyme. *Biochem J*. 310 (Pt 2):709-714.

Cramer, T., Y. Yamanishi, B.E. Clausen, I. Forster, R. Pawlinski, N. Mackman, V.H. Haase, R. Jaenisch, M. Corr, V. Nizet, G.S. Firestein, H.P. Gerber, N. Ferrara, and R.S. Johnson. 2003. HIF-1alpha is essential for myeloid cell-mediated inflammation. *Cell*. 112:645-657.

de Silva, A.O., and D.G. Fraenkel. 1979. The 6-phosphogluconate dehydrogenase reaction in Escherichia coli. *J Biol Chem*. 254:10237-10242.

Dhar, A., and L. Castillo. 2011. Insulin resistance in critical illness. *Curr Opin Pediatr*. 23:269-274.

Dougan, G., V. John, S. Palmer, and P. Mastroeni. 2011. Immunity to salmonellosis. *Immunol Rev*. 240:196-210.

Droste, P., S. Miebach, S. Niedenfuhr, W. Wiechert, and K. Noh. 2011. Visualizing multi-omics data in metabolic networks with the software Omix: a case study. *Biosystems*. 105:154-161.

Fang, F.C. 2011. Antimicrobial actions of reactive oxygen species. *MBio*. 2.

Frederiks, W.M., P. Vizan, K.S. Bosch, H. Vreeling-Sindelarova, J. Boren, and M. Cascante. 2008. Elevated activity of the oxidative and non-oxidative pentose phosphate pathway in (pre)neoplastic lesions in rat liver. *Int J Exp Pathol*. 89:232-240.

Garedew, A., and S. Moncada. 2008. Mitochondrial dysfunction and HIF1alpha stabilization in inflammation. *J Cell Sci*. 121:3468-3475.

Gorza, L. 1990. Identification of a novel type 2 fiber population in mammalian skeletal muscle by combined use of histochemical myosin ATPase and anti-myosin monoclonal antibodies. *J Histochem Cytochem*. 38:257-265.

Grant, A.J., O. Restif, T.J. McKinley, M. Sheppard, D.J. Maskell, and P. Mastroeni. 2008. Modelling within-host spatiotemporal dynamics of invasive bacterial disease. *PLoS biology*. 6:e74.

Hattori, H., K.K. Subramanian, J. Sakai, Y. Jia, Y. Li, T.F. Porter, F. Loison, B. Sarraj, A. Kasorn, H. Jo, C. Blanchard, D. Zirkle, D. McDonald, S.Y. Pai, C.N. Serhan, and H.R. Luo. 2010. Small-molecule screen identifies reactive oxygen species as key regulators of neutrophil chemotaxis. *Proc Natl Acad Sci U S A*. 107:3546-3551.

Henderson B. 1976. Quantitative cytochemical measurement of glyceraldehyde 3-phosphate dehydrogenase activity. *Histochemistry.* 48:191-204.

Hinkelbein, J., A. Kalenka, C. Schubert, A. Peterka, and R.E. Feldmann, Jr. 2010. Proteome and metabolome alterations in heart and liver indicate compromised energy production during sepsis. *Protein Pept Lett*. 17:18-31.

Holub, M., C.W. Cheng, S. Mott, P. Wintermeyer, N. van Rooijen, and S.H. Gregory. 2009. Neutrophils sequestered in the liver suppress the proinflammatory response of Kupffer cells to systemic bacterial infection. *J Immunol*. 183:3309-3316.

Hormaeche, C.E. 1980. The in vivo division and death rates of Salmonella typhimurium in the spleens of naturally resistant and susceptible mice measured by the superinfecting phage technique of Meynell. *Immunology*. 41:973-979.

Jonges, G.N., C.J. Van Noorden, and R. Gossrau. 1990. Quantitative histochemical analysis of glucose-6-phosphatase activity in rat liver using an optimized cerium-diaminobenzidine method. *J Histochem Cytochem*. 38:1413-1419.

Jungermann, K., and T. Kietzmann. 1996. Zonation of parenchymal and nonparenchymal metabolism in liver. *Annu Rev Nutr*. 16:179-203.

Kruth, H.S. 1984. Histochemical detection of esterified cholesterol within human atherosclerotic lesions using the fluorescent probe filipin. *Atherosclerosis*. 51:281-292.

Liu, M.S., and J.N. Zhang. 1985. Glycolytic and tricarboxylic acid cycle intermediates in dog livers during endotoxic shock. *Biochem Med*. 34:335-343.

Loftus, T.M., D.E. Jaworsky, G.L. Frehywot, C.A. Townsend, G.V. Ronnett, M.D. Lane, and F.P. Kuhajda. 2000. Reduced food intake and body weight in mice treated with fatty acid synthase inhibitors. *Science*. 288:2379-2381.

Maskell, D.J., C.E. Hormaeche, K.A. Harrington, H.S. Joysey, and F.Y. Liew. 1987. The initial suppression of bacterial growth in a salmonella infection is mediated by a localized rather than a systemic response. *Microb Pathog*. 2:295-305.

Mastroeni, P., and A.J. Grant. 2011. Spread of Salmonella enterica in the body during systemic infection: unravelling host and pathogen determinants. *Expert Rev Mol Med*. 13:e12.

Mastroeni, P., A. Vazquez-Torres, F.C. Fang, Y. Xu, S. Khan, C.E. Hormaeche, and G. Dougan. 2000. Antimicrobial actions of the NADPH phagocyte oxidase and inducible nitric oxide synthase in experimental salmonellosis. II. Effects on microbial proliferation and host survival in vivo. *J Exp Med*. 192:237-248.

Mosser, D.M., and J.P. Edwards. 2008. Exploring the full spectrum of macrophage activation. *Nat Rev Immunol*. 8:958-969.

Noorden, C.J.F.v., and W.M. Frederiks. 1992. Enzyme histochemistry : a laboratory manual of current methods. Oxford University Press,Royal Microscopical Society, Oxford ; New York, Oxford. vi, 116 p. pp.

Pakoskey, A.M., E.C. Lesher, and D.B. Scott. 1965. Hexokinase of Escherichia Coli. Assay of Enzyme Activity and Adaptation to Growth in Various Media. *J Gen Microbiol*. 38:73-80.

Pastor, C.M., T.R. Billiar, M.R. Losser, and D.M. Payen. 1995. Liver injury during sepsis. *J Crit Care*. 10:183-197.

Richter-Dahlfors, A., A.M. Buchan, and B.B. Finlay. 1997. Murine salmonellosis studied by confocal microscopy: Salmonella typhimurium resides intracellularly inside macrophages and exerts a cytotoxic effect on phagocytes in vivo. *J Exp Med*. 186:569-580.

Robinson, J.M. 2009. Phagocytic leukocytes and reactive oxygen species. *Histochem Cell Biol*. 131:465-469.

Rodriguez-Prados, J.C., P.G. Traves, J. Cuenca, D. Rico, J. Aragones, P. Martin-Sanz, M. Cascante, and L. Bosca. 2010. Substrate fate in activated macrophages: a comparison between innate, classic, and alternative activation. *J Immunol*. 185:605-614.

Sakaguchi, O., C.C. Hsu, and S. Sakaguchi. 1980. Metabolic aspects in mice administered live Salmonella typhimurium. *Microbiol Immunol*. 24:789-802.

Santos, R.L., S. Zhang, R.M. Tsolis, R.A. Kingsley, L.G. Adams, and A.J. Baumler. 2001. Animal models of Salmonella infections: enteritis versus typhoid fever. *Microbes Infect*. 3:1335-1344.

Schwartz, A.G., and L.L. Pashko. 2004. Dehydroepiandrosterone, glucose-6-phosphate dehydrogenase, and longevity. *Ageing Res Rev*. 3:171-187.

Shapiro, H., A. Lutaty, and A. Ariel. 2011. Macrophages, meta-inflammation, and immuno-metabolism. *ScientificWorldJournal*. 11:2509-2529.

Sheppard, M., C. Webb, F. Heath, V. Mallows, R. Emilianus, D. Maskell, and P. Mastroeni. 2003. Dynamics of bacterial growth and distribution within the liver during Salmonella infection. *Cell Microbiol*. 5:593-600.

Simon, L.M., E.D. Robin, J.R. Phillips, J. Acevedo, S.G. Axline, and J. Theodore. 1977. Enzymatic basis for bioenergetic differences of alveolar versus peritoneal macrophages and enzyme regulation by molecular O2. *J Clin Invest*. 59:443-448.

Slauch, J.M. 2011. How does the oxidative burst of macrophages kill bacteria? Still an open question. *Mol Microbiol*. 80:580-583.

Spitzer, J.J., G.J. Bagby, K. Meszaros, and C.H. Lang. 1988. Alterations in lipid and carbohydrate metabolism in sepsis. *JPEN J Parenter Enteral Nutr*. 12:53S-58S.

Splettstoesser, W.D., and P. Schuff-Werner. 2002. Oxidative stress in phagocytes--"the enemy within". *Microsc Res Tech*. 57:441-455.

Taussky, H.H., and E. Shorr. 1953. A microcolorimetric method for the determination of inorganic phosphorus. *J Biol Chem*. 202:675-685.

Thomas, J.A., G. Janossy, M. Chilosi, J. Pritchard, and J.R. Pincott. 1982. Combined immunological and histochemical analysis of skin and lymph node lesions in histiocytosis X. *J Clin Pathol*. 35:327-337.

Trinh le, A., M.D. McCutchen, M. Bonner-Fraser, S.E. Fraser, L.A. Bumm, and D.W. McCauley. 2007. Fluorescent in situ hybridization employing the conventional NBT/BCIP chromogenic stain. *Biotechniques*. 42:756-759.

Umezawa, K., T. Akaike, S. Fujii, M. Suga, K. Setoguchi, A. Ozawa, and H. Maeda. 1997. Induction of nitric oxide synthesis and xanthine oxidase and their roles in the antimicrobial mechanism against Salmonella typhimurium infection in mice. *Infect Immun*. 65:2932-2940.

Valdez, Y., R.B. Ferreira, and B.B. Finlay. 2009. Molecular mechanisms of Salmonella virulence and host resistance. *Curr Top Microbiol Immunol*. 337:93-127.

Van Noorden, C.J., and R.G. Butcher. 1984. Histochemical localization of NADP-dependent dehydrogenase activity with four different tetrazolium salts. *J Histochem Cytochem*. 32:998-1004.

Wolowczuk, I., C. Verwaerde, O. Viltart, A. Delanoye, M. Delacre, B. Pot, and C. Grangette. 2008. Feeding our immune system: impact on metabolism. *Clin Dev Immunol*. 2008:639803.

Yataghanas, X., G. Gahrton, and B. Thorell. 1969. Microspectrofluorometry of a periodic acid-schiff reaction in blood cells. *Exp Cell Res*. 56:59-68.

2.3 Immunity to *Salmonella* depends on surface-associated antigens

Barat S, Willer Y, Rizos K, Schemmer AK, Kirchhoff D, Burton N, Schmidt A, Bumann D

(Submitted)

Summary:

Vaccines against human *Salmonella* infections are still suboptimal. Neither do they cover the full range of *Salmonella* serovars, nor do they confer full protective immunity. The development of new vaccines is therefore required.

The goal of this study was to determine antigen properties that lead to enhanced immune recognition and to identify promising candidates for vaccine development.

The study identified several novel protective antigens which confer partial protection. While internal as well as surface-expressed antigens could induce immune responses, all identified protective antigens were exclusively associated with *Salmonella* surface, suggesting accessibility of antigens is crucial to T cell mediated immunity to live *Salmonella*.

We could show that live bacteria localize to different areas than dead bacteria *in vivo*.

Our data support a model in which internal antigens are only accessible, if the bacterium is dead, while in live bacteria they are shielded from the immune system. Therefore, internal antigens do not confer immunity, as they target T cells to sites in the tissue that harbor dead bacteria.

These findings might serve as a basis for future vaccine development.

Statement of my work:

I contributed to this publication by data that distinguished live and dead *Salmonella* in tissue sections using GFP and lipopolysaccharide co-staining. By confocal microscopy I could show that bacteria mostly located within host phagocytes, but did not reside extracellularly within tissues. Most infected host cells contained either exclusively dead or live bacteria. Furthermore, I could demonstrate that dead bacteria are already present during early stages of the infection.

These data were crucial for building a model to explain fundamentally different immune responses to internal versus surface-associated antigens.

Immunity to intracellular *Salmonella* depends on surface-associated antigens

Somedutta Barat[1†], Yvonne Willer[2†], Konstantin Rizos[3†], Anne K. Schemmer[1], Denis Kirchhoff[4], Neil Burton[1], Dirk Bumann[1,2,3]*

[1]Focal Area Infection Biology, Biozentrum, University of Basel, CH-4056 Basel, Switzerland; [2]Junior Group "Mucosal Infections", Hannover Medical School, D-30625 Hannover, Germany; [3]Dept. Molecular Biology, Max-Planck-Institute for Infection Biology, D-10117 Berlin, Germany; [4]Immunomodulation Group, Deutsches Rheuma-Forschungszentrum Berlin, 10117 Berlin, Germany

[†]equal contribution

Corresponding author:

Dirk Bumann

Biozentrum
Klingelbergstr. 50/70
CH-4056 Basel
Switzerland
Phone: +41 61 267 2382

E-mail: dirk.bumann@unibas.ch

Abstract

Invasive *Salmonella* infection is an important health problem that is worsening because of rising antimicrobial resistance and changing *Salmonella* serovar spectrum. Novel vaccines with broad serovar coverage are needed, but suitable protective antigens remain largely unknown. Here, we tested 37 broadly conserved *Salmonella* antigens in a mouse typhoid fever model, and identified several antigens that conferred partial protection against lethal disease. Antigen properties such as high in vivo abundance or immunodominance in convalescent individuals did not correlate with protectivity, but all protective antigens were associated with the *Salmonella* surface. Surprisingly, this was not due to superior immunogenicity of surface antigens compared to internal antigens as had been suggested by previous studies and novel findings for CD4 T cell responses to model antigens. Confocal microscopy of infected tissues revealed that many live *Salmonella* resided alone in infected host macrophages with no damaged *Salmonella* releasing internal antigens in their vicinity. In the absence of accessible internal antigens, detection of these infected cells might require CD4 T cell recognition of *Salmonella* surface-associated antigens that could be processed and presented even from intact *Salmonella*. In conclusion, our findings might pave the way for development of an efficacious *Salmonella* vaccine with broad serovar coverage, and suggest a similar crucial role of surface antigens for immunity to both extracellular and intracellular pathogens.

Introduction

Enteric fever caused by systemic *Salmonella* infection causes tremendous morbidity and mortality worldwide (1). Current control strategies become increasingly inefficient as a result of increasing antimicrobial resistance (2, 3) and emergence of *Salmonella* serovars that are not covered by currently available safe vaccines (4, 5). This situation generates an urgent medical need for novel *Salmonella* vaccines with broad serovar coverage.

Early killed whole-cell vaccines containing mixtures of different serovars provide broad protection, but cause unacceptable adverse reactions (1). As an alternative to whole-cell vaccines, subunit vaccines containing a few defined *Salmonella* components could minimize adverse reactions. Indeed, vaccines containing the capsular polysaccharide Vi antigen provide moderate protection and excellent safety (1). On the other hand, serovars Paratyphi A and non-typhoidal *Salmonella* (NTS) that cause an increasing number of invasive salmonelloses (6), lack the Vi antigen and are therefore not covered by Vi vaccines (5). Apart from Vi, few *Salmonella* antigens have been identified, and all of these provide at best moderate levels of protection against challenge infection with virulent *Salmonella* strains in the commonly used mouse typhoid fever model. Moreover, antigens such as flagellin (7) and OmpD (8) are poorly conserved among relevant serovars.

For extracellular pathogens with antibody-mediated immunity, protective antigens must be surface-exposed (9), and this enables an effective strategy for priorization of antigen candidates (9). Humoral response to surface antigens can also contribute to immunity to intracellular pathogens such as invasive *Salmonella* (10). Indeed, Vi which induces protective antibody responses in human vaccinees, forms an extracellular capsule around *Salmonella* Typhi (11). Two additional antigens that confer partial immunity in the mouse typhoid fever model, flagellin (7) and SseB (12), are also part of *Salmonella* surface structures (flagella, needle complex of a type III secretion system). Furthermore, outer membrane preparations (but not the outer membrane component lipopolysaccharide) have been suggested to mediate protective humoral immune responses against extracellular *Salmonella* bacteremia (13) and attenuated *Salmonella* strains in the mouse model (8, 14). A number of porins such as OmpC, OmpD, and OmpF are highly abundant in such outer membrane preparations suggesting that they might represent protective antigens (8, 14, 15).

However, immunity to *Salmonella* critically depends also on CD4 T cells (10). Unfortunately, protective T cell antigens seem to be rare, and priorization of candidates is difficult since relevant antigen properties for CD4 T cell responses remain unclear (9, 16, 17). One key precondition for protective responses is expression of the respective *Salmonella* antigen during infection (18), and some data suggest that highly abundant antigens might be particularly well recognized by CD4 T cells (12, 19). Antigen in vivo expression can be deduced from various complementary approaches including screening of promoter trap libraries (20, 21), proteomics (22), serum antibody response (23-25), as well as mutant virulence phenotypes.

In addition to antigen expression, antigen immunogenicity could play a major role. Antigen detection by cognate CD4 T cells requires antigen processing and presentation of the resulting small peptides by major histocompatibility (MHC) class II molecules. Peptide sequence properties that are characteristic for well recognized epitopes, can be used for genome-wide prediction of promising antigens (26). However, a large number of non-protective antigens contain putative high-score epitopes (16, 18) which could compromise the discriminatory power of this approach.

Experimental detection of immune responses to an antigen in convalescent individuals that have survived infection, demonstrates that this antigen was expressed in vivo and could be recognized by the immune system (23-25). Indeed, this approach has been recently shown to facilitate identification of protective *Chlamydia* antigens (27). On the other hand, many immunodominant antigens in convalescent individuals lack protective efficacy, while a number of protective antigens may induce immune responses below the detection threshold during natural infection (17).

Another antigen property that can affect CD4 T cell responses is antigen localization. In particular, secreted or surface-associated antigens might induce particularly strong cellular immune responses because of superior processing, kinetic advantages compared to internal antigens, and/or physical association with pathogen-associated molecular patterns (PAMP) such as lipopolysaccharide that provide potent stimuli for innate and adaptive immunity (14, 28-34). Indeed, secretion/surface localization has been widely used to prioritize candidates for antigen identification. However, antigens with likely internal localization can also induce specific CD4 T cell responses that mediate protection against various intracellular pathogens (35, 36).

Taken together, relevant antigen properties for CD4 T cell mediated immunity to intracellular pathogens remain poorly characterized, and this impairs antigen priorization for vaccine development. To address this issue, we compared here 37 diverse *Salmonella* antigens in a mouse model that closely mimics human typhoid fever (37). The results suggested that recognition of surface-associated antigens might be necessary to detect and combat live intracellular *Salmonella,* whereas recognition of internal antigens would only mediate futile non-protective attack of already dead *Salmonella*. In conclusion, we propose a similar crucial role of surface-associated antigens for immunity to both extracellular and intracellular pathogens.

Results

Immune responses to *Salmonella* antigens in convalescent individuals

To determine immune responses to *Salmonella* antigens, we selected 21 broadly conserved *Salmonella* proteins. We focused on proteins that *Salmonella* expressed during systemic infection in a mouse typhoid fever model based on ex vivo proteome data (22) (and manuscript in preparation), mutant phenotype data, and/or previous immunization experiments (Tab. 1). To investigate the impact of antigen localization, we selected proteins localized in *Salmonella* cytosol, inner membrane, periplasm, and outer membrane/surface. To determine potential cross-protection between different serovars, we cloned the corresponding genes from *Salmonella enterica* serovar Typhi (except for OmpD which was obtained from serovar Typhimurium). We expressed the proteins as C-terminal His_6-fusions in *E. coli* followed by Ni-affinity chromatography purification. We purified the control antigen GFP-His_6 using the same protocol.

We determined immune responses to these antigens in genetically resistant, convalescent mice that had survived infection with *Salmonella enterica* serovar Typhimurium. We detected antigen-specific CD4 T cells in spleen using a sensitive CD154 assay (38) and measured serum IgG antibody responses using ELISA. All tested antigens were recognized by CD4 T cells (Fig. 1A; Tab. 1), many of which secreted IFNγ or IL-17 upon stimulation. Both cytokines play crucial roles in immunity to *Salmonella* (10). Frequencies of responsive CD4 T cells were in the same range as for flagellin, which has been considered an immunodominant antigen (39). These data suggested that *Salmonella* infection elicited a broad cellular immune response against a large number of in vivo expressed antigens from all *Salmonella* compartments in agreement with data observed for *S*. Typhi infected human patients (40). There was no correlation between in vivo antigen abundance as determined by proteome analysis of ex vivo purified *Salmonella*, and CD4 T cell frequency or cytokine profile (Tab. 1).

Serum antibody responses revealed similar broad recognition of antigens from several *Salmonella* compartments (Fig. 1B) in agreement with previous data for human typhoid fever patients (24, 25, 41). Interestingly, the three immunodominant humoral antigens T2461, PhoN, and PdgL were all highly expressed in vivo (Tab. 1) suggesting a potential impact of antigen dose

on antibody responses to *Salmonella*, although responses among minor antigens did not correlate with antigen abundance.

Immunization and challenge infection

Many of the tested *Salmonella* antigens were capable to induce cellular and humoral immune responses. To test if these responses could confer protective immunity, we tested the 21 recombinant *Salmonella* antigens in immunization/challenge infection experiments in genetically susceptible BALB/c mice. Based on the results, we selected 16 additional *Salmonella* antigens primarily from the outer membrane, and tested them using the same experimental approach. For simplicity, we discuss results for both antigen sets together.

Out of 37 tested antigens, only a small minority including previously identified SseB enabled prolonged survival after oral challenge infection with virulent *Salmonella* at a 100fold LD_{50} dose. Antigen protectivity did not correlate with CD4 T cell responses (Fig. 2A) or serum antibody levels (Fig. 2B) during natural infection of resistant mice. This could in part reflect differences in MHC class II haplotypes ($H2^{d}$ in BALB/c vs. $H2^{bc}$ in 129/Sv (42)), although T cell epitope predictions revealed epitopes with high scores for $I\text{-}A^{d}$ and/or $I\text{-}E^{d}$ in all tested antigens (data not shown). Interestingly, in vivo expression levels also did not correlate with protectivity (Fig. 3A). In fact, the two antigens that enabled the longest survival, IroN and CirA, had in vivo expression levels that were too low for quantification. By comparison, antigens T2461 and PhoN were highly expressed in vivo and induced potent CD4 T cell and humoral responses in convalescent individuals, yet completely failed to protect.

In contrast to immunogenicity and in vivo abundance, antigen localization seemed to be crucial (Fig. 3B). In fact, protective antigens were exclusively associated with the *Salmonella* surface, either as experimentally validated outer membrane-associated lipoproteins (43), as outer membrane proteins, or as the needle complex of the type III secretion system encoded by *Salmonella* pathogenicity island two (SPI-2) (Tab. 1). These data suggested distinct immune responses to *Salmonella* outer membrane/surface antigens that fundamentally differ from those to internal antigens.

On the other hand, surface localization alone was not sufficient for protectivity. As examples, two outer membrane proteins, PgtE and PagC, were highly expressed in vivo and elicited potent CD4 T cell responses in convalescent individuals (Fig. 1A). PagC is also well recognized by antibodies and CD4 T cells of human typhoid fever patients (24). However, both PagC and PgtE failed to protect. Interestingly, structural models revealed that these proteins were largely buried in the outer membrane bilayer (Fig. 4), and their extracellular loops contained only one predicted CD4 T cell epitope each, and no or two linear antibody epitopes, respectively. Importantly, key amino acids in exposed T cell epitopes differed among *Salmonella* serovars which might have impaired cross-protectivity of serovar Typhi antigens against serovar Typhimurium challenge infection. In contrast to these non-protective antigens, antigens IroN and CirA that enabled extended survival after challenge infection, had extracellular loops with several highly conserved T and B cell epitopes. Further studies with larger data sets will be required to validate the relevance of these structural properties for protectivity.

Impact of *Salmonella* antigen localization in an ovalbumin model

The strong bias for surface-associated *Salmonella* antigens might have been expected based on previous data for model antigens suggesting superior immunogenicity of surface antigens compared to internal antigens (28, 44-48). However, these model antigen data were in striking contrast to results from us and others demonstrating comparable immune responses to autologous *Salmonella* antigens from all *Salmonella* compartments (Fig. 1A,B). Furthermore, there was no obvious correlation between immunogenicity and protectivity (Fig. 2A,B).

To better understand these discrepancies between model antigens and autologous *Salmonella* antigens, we re-visited the impact of antigen localization using a well-characterized, sensitive model system in which a MHC II-restricted T cell epitope from ovalbumin comprising amino acids 319 to 343 (OVA) is recognized by adoptively transferred cognate T cell receptor transgenic CD4 T cells (49, 50). We targeted the OVA epitope to different *Salmonella* compartments by fusing it to various proteins with known localization: GFP_OVA (cytosol (51)), OVA_MglB (periplasm (52)), Lpp_OVA (inner leaflet of the outer membrane (53)), and OVA_AIDA (outer leaflet of the outer membrane (54)) (Fig. 5A). To modulate expression levels, we used ribosome binding sites with differential translation initiation efficiency (12). We

expressed these fusion proteins from an in vivo inducible promoter (55) in an attenuated *Salmonella enterica* serovar Typhimurium *aroA* strain (56). Antigen localization was validated in in vitro cultures using cell fractionation followed by western blotting, trypsin treatment, and antibody binding (data not shown). Interestingly, small fractions of both outer membrane antigens LPP_OVA and partially processed OVA_AIDA were released to the extracellular surroundings when expressed at high levels (Supplemental Fig. 1 online) in agreement with previous findings for similar proteins (57-59).

We infected BALB/c mice with *Salmonella* strains by intragastric gavage of 10^{10} CFU. All *Salmonella* strains colonized intestinal Peyer's patches with peak tissue loads of 3 x 10^4 to 1.5 x 10^5 CFU at day seven post infection as observed before for attenuated *Salmonella aroA* (60). All constructs stably maintained their respective ovalbumin-expression plasmids (> 80% at 7 days post infection). To determine antigen-specific CD4 T cell induction, we adoptively transferred OVA-specific TCR-transgenic CD4 T cells one day prior to *Salmonella* infection. OVA-specific T cells upregulated the early activation marker CD69 and formed blasts in mice infected with *Salmonella* expressing ovalbumin model antigens, but not in mice infected with control *Salmonella* (Supplemental Fig. 2A) as observed previously (51). CD4 T cell induction kinetics were similar for all constructs and consistent with our previous observations (51) suggesting a response to *Salmonella* in situ antigen expression, but not to the inoculum (55, 61).

To compare T cell responses against the various *Salmonella* constructs, we measured T cell blast formation at peak *Salmonella* colonization at day seven post infection. *Salmonella* tissue loads varied somewhat between individual mice but for each construct, there was a linear relationship between the number of ovalbumin-specific DO11.10 blasts and *Salmonella* loads (Supplemental Fig. 2B) in agreement with our earlier observations (55). To determine the specific immunogenicity of each *Salmonella* strain, we calculated the average ratio of DO11.10 CD4 T cell blasts per viable *Salmonella* (i.e., the slopes in Supplemental Fig. 2B) (55). The data revealed comparable immunogenicity of model antigens GFP_OVA and OVA_MglB (Fig. 5B). In contrast, high-level expression of surface-associated LPP_OVA and OVA_AIDA induced superior responses that clearly surpassed responses even to saturating amounts (12) of internal GFP_OVA.

The OVA_AIDA fusion protein contained a fragment of the virulence factor AIDA from enteropathogenic *E. coli* and a cystein-deficient variant of the cholera toxin B subunit from *Vibrio cholerae* (62). Both components might have stimulatory effects (63, 64) that could potentiate ovalbumin immunogenicity. To test this potentially confounding factor, we compared *Salmonella* expressing a suboptimal level of cytosolic GFP_OVA (12) (some 54.000 copies per *Salmonella* cell) to *Salmonella* expressing the same amount of GFP_OVA together with AIDA and cholera toxin B. Both strains induced DO11.10 T cell blasts with similar efficacy (Fig. 5B) suggesting that AIDA and cholera toxin B expression had no impact on the immunogenicity of *Salmonella*-encoded OVA.

Taken together, these findings suggested that antigens from all *Salmonella* compartments could induce specific CD4 T cell responses, but highly expressed outer membrane-associated antigens were clearly superior in agreement with previous observations in other model systems. However, these data were in striking contrast to responses to autologous *Salmonella* antigens (see discussion).

Distribution of intact and damaged *Salmonella* in infected tissues

The fundamentally superior protectivity of surface-associated *Salmonella* antigens might reflect their unique accessibility to antigen processing and presentation in infected host cells (Fig. 7) in contrast to internal *Salmonella* antigens that are shielded by the *Salmonella* envelope und thus remain invisible for the host immune system until *Salmonella* is damaged and the bacterial cell breaks open. To detect intact and damaged *Salmonella* in infected tissues, we used cytosolic GFP as a marker for internal antigens.

Salmonella expressing GFP from the chromosomal in vivo induced locus *sifB* were readily detected in infected tissue homogenates using flow cytometry (12) (Fig. 6A). Flow cytometric GFP^+ *Salmonella* counts closely correlated with viable *Salmonella* counts as determined by plating (Fig. 6A, inset) suggesting that detectable GFP levels were present in all live intact *Salmonella*.

Confocal microscopy of infected spleen and liver sections revealed many particles that were stained by a polyclonal antibody to *Salmonella* lipopolysaccharide, had typical *Salmonella*

size and morphology, and contained GFP (Fig. 6B) as previously observed (51) suggesting that these particles represented live intact *Salmonella*. In addition, we also detected numerous lipopolysaccharide-positive particles with distorted shapes that lacked detectable GFP (Fig. 6C), and likely represented killed and partially degraded *Salmonella*. Such particles were absent in non-infected control sections. Some *Salmonella* killing during acute infections had previously been proposed (65-67). We observed some infected cells containing both intact and damaged *Salmonella*, but a large number of live *Salmonella* resided alone (or together with other live *Salmonella*) in infected cells with no detectable dead *Salmonella*. In such infected cells, internal *Salmonella* antigens were thus shielded and inaccessible for immune recognition.

Discussion

There is an urgent medical need for an efficacious *Salmonella* vaccine with broad coverage of invasive serovars. One important bottleneck in the development of such a vaccine is the identification of suitable protective antigens. In this study, we identified novel broadly conserved *S*. Typhi antigen candidates that protected against *S*. Typhimurium challenge infection in the mouse typhoid fever model. Two siderophore receptors (IroN, CirA) enabled the longest survival (Tab. 1) consistent with previous studies that revealed siderophore receptors including IroN as promising vaccine antigens in other models (68-70). Interestingly, siderophore receptors are induced by iron starvation and/or activation of the PhoPQ two component sensory system (71). IroN and CirA induction could thus contribute to increased protective efficacy of membrane preparations from iron-starved *Salmonella* (72), or live attenuated *Salmonella phoQ*^{24} with constitutive hyperactivation of the PhoP response regulator (73).

On the other hand, all identified antigens still provided only partial protection against challenge infection with virulent *Salmonella* suggesting a need for additional antigens. Unfortunately, protective *Salmonella* antigens might be rather rare as even among the 37 tested in vivo expressed antigens that were all highly immunogenic during infection, only a small minority enabled prolonged survival. OmpC, OmpD, and OmpF were previously proposed as potential protective antigens based on data obtained for enriched *Salmonella* membrane preparations. However, all three antigens failed to protect in our model. This could reflect higher stringency of our model (challenge infection with virulent *Salmonella* vs. highly attenuated mutant *Salmonella*), denatured three-dimensional structures of our recombinant antigen preparations vs. native antigens, and/or presence of undetected minor protective antigens (such as IroN and CirA) besides OmpC, OmpD, and OmpF in the previously used outer membrane antigen preparations.

Additional protective *Salmonella* antigens could be identified by comprehensive immunization/challenge experiments, but this would require extensive animal experimentation. Antigen priorization using relevant antigen properties could help to narrow down the number of antigen candidates to more practical numbers. Unfortunately, some previously proposed antigen properties seemed to have limited relevance for protectivity in our model. This included *Salmonella* in vivo expression levels, sequence-based antigenicity predictions, and

immunodominance in convalescent individuals. Poor correlation of antigen immunodominance with protective efficacy has been also observed in tuberculosis (17). On the other hand, immune recognition in convalescent individuals can still provide valuable information about antigen expression during at least some stage of infection that might be difficult to obtain otherwise (23, 27).

In contrast to these non-predictive antigen properties, surface-association appeared to be an essential prerequisite for protection. Surprisingly, protective surface-associated proteins also included lipoproteins which were likely to reside in the inner leaflet of the outer membrane facing the internal periplasmic space with no exposure to the outside. It is possible that some lipoproteins might flip across the outer membrane as observed for other Gram-negative bacteria (74). Moreover, some lipoprotein fraction is constantly released to the outside through outer membrane vesicle shedding (57, 58).

Several mechanisms could contribute to the striking superiority of surface-associated antigens. Antibody responses are important for full protection against virulent *Salmonella* (10), and protective antibody responses must be directed against surface antigens (9). On the other hand, CD4 T cells are even more important for immunity to *Salmonella* at least in the mouse typhoid fever model (10), and it is unclear why CD4 T cells should respond to surface-associated antigens in a fundamentally different way compared to the much larger number of internal antigens.

In fact, early cell culture experiments suggested no impact of *Salmonella* antigen localization on CD4 T cell recognition of infected cells (75). However, in this study a large amount of antigen was already present in the inoculum, and rapid killing of the majority of phagocytosed *Salmonella* (76) would have released this antigen from all *Salmonella* compartments. Several subsequent in vivo studies suggested that surface-associated model antigens might have intrinsically higher immunogenicity compared to internal model antigens (28, 44-48). However, the various model antigen targeting constructs could have differed in antigen in vivo expression levels, antigen stability, and epitope processing. Fusion partners could also have direct immunomodulatory effects. We therefore re-visited this issue and tried to control some of these factors. Our results clearly supported the previous finding of superior immunogenicity of highly expressed surface-associated model antigens in *Salmonella*.

In surprising contrast to these data from model antigens, however, humoral and cellular immune responses in *Salmonella*-infected convalescent mice did not show any bias for surface-associated autologous *Salmonella* antigens. Broad recognition of antigens from all pathogens compartments has also been observed in *Salmonella* Typhi-infected or *Chlamydia*-infected human patients (24, 25, 27, 40, 41). Model antigens and autologous antigens were also discordant with respect to the impact of antigen abundance. Specifically, our data for ovalbumin model antigens in this and a previous study (12), as well as similar findings for *Mycobacterium bovis* BCG overexpressing Ag85b (19), suggested that high in vivo expression levels enhance antigen immunogenicity. However, for autologous *Salmonella* antigens in vivo expression levels did not correlate with immunogenicity or protectivity. Striking discrepancies between results for model antigens vs. autologous antigens have also been observed in other pathogens (36).

Some of the discrepancies could reflect technical issues. In particular, strong expression of foreign surface model antigens might induce subtle alteration in *Salmonella* in vivo properties such as increasing outer membrane vesicle shedding or alterations in protein secretion that could affect antigen presentation and immune recognition. Furthermore, model antigens might not be representative of autologous antigens that may have been shaped by host/pathogen co-evolution selecting for weak immunogenicity. Regardless of the actual causes of these discrepancies, our data indicated that in contrast to evidence from model antigens, protective *Salmonella* surface-associated antigens were not more immunogenic compared to internal antigens.

As an alternative explanation, surface-associated antigens might become more rapidly available for immune recognition compared to internal antigens that are only released after some pathogen damage. This could be relevant since early immune responses might facilitate infection control (30). In the mouse typhoid fever model, however, a detectable fraction of *Salmonella* is rapidly killed early during infection as observed in this and previous studies (65, 67) similar to events during *Mycobacterium* infection (77). Consistent with these observations, CD4 T cell induction kinetics in the ovalbumin model system were similar for *Salmonella* strains with internal or surface-associated OVA-expression.

Instead, we propose an alternative explanation based on the observation that many live *Salmonella* resided alone, or together with other live *Salmonella*, in infected host cells with no

dead *Salmonella* releasing their internal antigens. As a consequence, internal antigens remained inaccessible for antigen processing and presentation in these cells. In contrast, surface-exposed *Salmonella* antigens, or antigens released by outer membrane vesicle shedding, could be accessible for processing and presentation to cognate CD4 T cells for initiation of protective anti-*Salmonella* effector mechanisms (Fig. 7). In comparison, CD4 T cells recognizing internal *Salmonella* antigens would have limited impact on infection control because they miss many cells containing live *Salmonella* and instead direct their responses to host cells containing already dead *Salmonella*. According to this model, surface-associated antigens thus differ fundamentally from internal antigens because they are uniquely accessible in host cells containing only live *Salmonella*.

Surface-associated/secreted antigens have been shown to be crucial for CD8 T cell-dependent immunity to *Listeria* infection (29, 31). Our data suggested that such antigens might also be crucial for CD4 T cell mediated immunity to *Salmonella* and potentially other intracellular pathogens. Interestingly, some internal antigens have been shown to confer partial protection in infectious diseases caused by intracellular pathogens such as *Leishmania* (36) and *Mycobacterium* (35). In these infections live and dead pathogens often co-occur in the same host microenvironments (78, 79) suggesting that both internal and surface-associated antigens might be available for T cell recognition and initiation of antimicrobial immune effector mechanisms targeting both live and already dead pathogens (80). We speculate that full protection might still require detection of all live pathogens including those that reside in microenvironments with yet no accessible internal antigens from dead pathogens. Further studies are required to test this hypothesis.

Conclusion

This study identified novel *Salmonella* antigens that conferred partial protection against virulent *Salmonella* in a stringent typhoid fever model. High sequence conservation among relevant *Salmonella* serovars and cross-protection of serovar Typhi antigens against serovar Typhimurium challenge infection, suggested that these antigens might help to pave the way for a broadly protective vaccine against systemic *Salmonella* infection. In addition, our findings suggested that surface-associated antigens might represent particular promising antigens for both humoral and cellular immunity to *Salmonella*, since recognition of surface antigens uniquely enables detection and destruction of live *Salmonella* in relevant host microenvironments. This crucial importance of antigen localization could facilitate discovery of additional protective antigens for *Salmonella* and potentially other intracellular pathogens.

Material and Methods

Cloning, expression, and purification of *Salmonella* antigens. Antigens were PCR-amplified from *Salmonella enterica* serovar Typhi Ty2 (or *Salmonella enterica* serovar Typhimurium SL1344 (56) for *ompD*), cloned as His_6-fusions by conventional ligation into pET22b, or by Enzyme Free Cloning into plasmid pLICHIS (81), and overexpressed in *E. coli* BL21. GFP_His_6 was cloned as control antigen. Antigens were purified from washed inclusion bodies using immobilized metal ion affinity chromatography (Protino Ni TED 1000, Macherey Nagel) followed by ion exchange chromatography (Ion exchange spin columns, Pierce Thermo Scientific, cationic or anionic resins depending on antigen isoelectric point).

Construction of ovalbumin-expressing *Salmonella*. Translational fusions of the ovalbumin peptide containing amino acids 319 to 343 to various proteins with differential targeting in the *Salmonella* cell were constructed by PCR cloning. To generate *ova_aida*, coding sequence for the ovalbumin peptide (*ova*) was inserted between the signal peptide derived from cholera toxin B and the HA tag in plasmid pLAT260 (82). A control plasmid coding for CTB_AIDA and GFP_OVA was also constructed. To generate *lpp_ova*, *lpp* without the C-terminal lysine codon that can cross-link to peptidoglycan (83), was amplified from *E. coli* DH5α and fused with *ova*. To generate *ova_mglB*, *mglB* gene without the signal peptide sequence was amplified from *E. coli* DH5α and fused with a *ctB* signal sequence followed by *ova*. The construction of *gfp_ova* has been described (84). All fusion genes were cloned into a pBR322-derived plasmid backbone downstream of a *Salmonella* genome fragment containing the in vivo inducible *pagC* promoter (55) and ribosomal binding sites with differential translation initiation efficiencies (12). The various plasmids were transformed into attenuated *Salmonella enterica* serovar Typhimurium aroA SL3261 (56).

Biochemical analysis. Ovalbumin expression was assessed by western blotting with a polyclonal antibody to ovalbumin (Sigma) that recognizes the OVA peptide comprising amino acids 319 to 343 (51). *Salmonella* outer membranes were prepared by extraction with L-lauryl sarcosinate as described (82). Periplasm was prepared by chloroform extraction as described (85). Culture supernatants were sterile filtered (0,2 µm pore size) and subjected to TCA precipitation (86), or ultracentrifugation (100.000 x g, 1h, 4°C). To assess ovalbumin surface accessibility, intact or lysed *Salmonella* cells were treated with 50 µg ml^{-1} trypsin at 37°C for 10 min.

Immune responses in convalescent mice. Female 8 to 12 weeks old 129/Sv mice were obtained from Charles River. Mice were orally infected with 10^9 CFU *Salmonella enterica* serovar Typhimurium SL1344 (56) from late log cultures using a round-tip stainless steel needle. Control mice were sham-infected. Mice were sacrificed 6 months after infection. Splenocytes were isolated and tested for antigen-specific CD4 T cell responses as described (38). Plasma was tested for antigen-specific IgG responses using ELISA with an IgG calibration curve for absolute quantification.

Immunization and challenge experiments. Female, 8 to 12 weeks old BALB/c mice were obtained from Charles River. Groups of 5 mice were immunized subcutaneously with 10 µg antigen emulsified in complete Freund's adjuvant followed by a second immunization with incomplete Freund's adjuvant four weeks later. After additional four weeks, mice were orally infected with 6 x 10^5 CFU *Salmonella enterica* serovar Typhimurium SL1344 (56) from late log cultures using a round-tip stainless steel needle. Infected BALB/c were monitored twice daily and sacrificed when moribund.

Ovalbumin-specific CD4 T cell responses. BALB/c and DO11.10 mice (49) were bred in the Bundesamt für gesundheitlichen Verbraucherschutz und Veterinärmedizin (Berlin, Germany) under specific-pathogen free conditions. Adoptive transfer of 4 x 10^6 DO11.10 T cells into syngenic age- and sex-matched BALB/c mice was performed one day before infection as described (51). For infection, attenuated *Salmonella* strains carrying expression cassettes for various ovalbumin fusion proteins were grown to late log phase and harvested. Bacteria were washed twice and resuspended in LB containing 3% sodium bicarbonate. Doses containing ca. 10^{10} cfu in 100 µl were administered intragastrically to chimeric mice with a round-tip stainless steel needle. At various time points post infection, mice were anesthetized and sacrificed. DO11.10 T cell blast formation was determined by flow cytometry as described (51). Aliquots of the same Peyer's patch preparations were treated with 0.1% Triton x-100 to release intracellular *Salmonella* for CFU determination by plating, and for quantitation of GFP_OVA *in vivo* expression levels by two-color flow cytometry as described (84).

Detection of intact *Salmonella* in infected tissues. BALB/c mice with *Salmonella* loads of 10^6 to 10^7 in spleen and liver were sacrificed. 10 µm cryosections were stained with polyclonal rabbit antibodies to *Salmonella* lipopolysaccharide (SIFIN) and anti-CD68 (abcam) followed by Alexa

546-conjugated goat anti-rabbit and Alexa 647-conjugated goat anti-rat antibodies (Invitrogen). Sections were examined by confocal microscopy (Leica, SP5).

Structural models and epitope prediction. Structural models for selected *Salmonella* outer membrane antigens based on solved structures of homologues were obtained from SWISS-MODEL (87) available at http://swissmodel.expasy.org. Linear B-cell epitopes were predicted using FBCPred (88) available at http://ailab.cs.iastate.edu/bcpreds/predict.html using an epitope length of 14 and 90% specificity. Peptides that bind to MHC II I-A^d and/or I-E^d were predicted using RANKPEP (89) available at http://bio.dfci.harvard.edu/Tools/rankpep.html.

Acknowledgements

We thank Claus Lattemann, Thomas Meyer, and Reinhold Förster for helpful discussions and generous support. D.B. and co-workers are funded by the Swiss National Science Foundation (31003A-121834), SystemsX (RTD project BattleX) and Deutsche Forschungsgemeinschaft (SFB641-A9, SPP1316 Bu971/6).

References

1. Anonymous (2008) Typhoid vaccines: WHO position paper. *Wkly Epidemiol Rec* 83:49-59.
2. Alcaine SD, Warnick LD, & Wiedmann M (2007) Antimicrobial resistance in nontyphoidal *Salmonella*. *J Food Prot* 70:780-790.
3. Ahmed D, D'Costa LT, Alam K, Nair GB, & Hossain MA (2006) Multidrug-resistant *Salmonella* enterica serovar typhi isolates with high-level resistance to ciprofloxacin in Dhaka, Bangladesh. *Antimicrob Agents Chemother* 50:3516-3517.
4. Graham SM (2010) Nontyphoidal salmonellosis in Africa. *Curr Opin Infect Dis* 23:409-414.
5. Podda A*, et al.* (2010) Conjugate vaccines for enteric fever: proceedings of a meeting organized in New Delhi, India in 2009. *J Infect Dev Ctries* 4:404-411.
6. Crump JA & Mintz ED (2010) Global trends in typhoid and paratyphoid Fever. *Clin Infect Dis* 50:241-246.
7. McSorley SJ, Cookson BT, & Jenkins MK (2000) Characterization of CD4+ T Cell Responses During Natural Infection with *Salmonella* typhimurium. *J Immunol.2000.Jan.15.;164.(2.):986.-993.* 164:986-993.
8. Gil-Cruz C*, et al.* (2009) The porin OmpD from nontyphoidal *Salmonella* is a key target for a protective B1b cell antibody response. *Proc Natl Acad Sci U S A* 106:9803-9808.
9. Sette A & Rappuoli R (2010) Reverse vaccinology: developing vaccines in the era of genomics. *Immunity* 33:530-541.
10. Dougan G, John V, Palmer S, & Mastroeni P (2011) Immunity to salmonellosis. *Immunol Rev* 240:196-210.
11. Khan MI, Ochiai RL, & Clemens JD (2010) Population impact of Vi capsular polysaccharide vaccine. *Expert Rev Vaccines* 9:485-496.
12. Rollenhagen C, Sorensen M, Rizos K, Hurvitz R, & Bumann D (2004) Antigen selection based on expression levels during infection facilitates vaccine development for an intracellular pathogen. *Proc.Natl.Acad.Sci.U.S.A* 101:8739-8744.
13. Gondwe EN*, et al.* (2010) Importance of antibody and complement for oxidative burst and killing of invasive nontyphoidal *Salmonella* by blood cells in Africans. *Proc Natl Acad Sci U S A* 107:3070-3075.

14. Alaniz RC, Deatherage BL, Lara JC, & Cookson BT (2007) Membrane vesicles are immunogenic facsimiles of *Salmonella* typhimurium that potently activate dendritic cells, prime B and T cell responses, and stimulate protective immunity in vivo. *J Immunol* 179:7692-7701.
15. MacLennan CA*, et al.* (2010) Dysregulated humoral immunity to nontyphoidal *Salmonella* in HIV-infected African adults. *Science* 328:508-512.
16. Stober CB*, et al.* (2006) From genome to vaccines for leishmaniasis: screening 100 novel vaccine candidates against murine Leishmania major infection. *Vaccine* 24:2602-2616.
17. Sable SB, Plikaytis BB, & Shinnick TM (2007) Tuberculosis subunit vaccine development: impact of physicochemical properties of mycobacterial test antigens. *Vaccine* 25:1553-1566.
18. Lee SJ*, et al.* (2012) Temporal expression of bacterial proteins instructs host CD4 T cell expansion and th17 development. *PLoS Pathog* 8:e1002499.
19. Egen JG*, et al.* (2011) Intravital imaging reveals limited antigen presentation and T cell effector function in mycobacterial granulomas. *Immunity* 34:807-819.
20. Heithoff DM*, et al.* (1997) Bacterial infection as assessed by in vivo gene expression. *Proc.Natl.Acad.Sci.U.S.A* 94:934-939.
21. Bumann D & Valdivia RH (2007) Identification of host-induced pathogen genes by differential fluorescence induction reporter systems. *Nat Protoc* 2:770-777.
22. Becker D*, et al.* (2006) Robust *Salmonella* metabolism limits possibilities for new antimicrobials. *Nature.* 440:303-307.
23. Rollins SM*, et al.* (2005) In vivo induced antigen technology (IVIAT). *Cell Microbiol.* 7:1-9.
24. Harris JB*, et al.* (2006) Identification of in vivo-induced bacterial protein antigens during human infection with *Salmonella* enterica serovar Typhi. *Infect Immun* 74:5161-5168.
25. Hu Y*, et al.* (2009) Identification of in vivo induced protein antigens of *Salmonella* enterica serovar Typhi during human infection. *Sci China C Life Sci* 52:942-948.
26. Lundegaard C, Hoof I, Lund O, & Nielsen M (2010) State of the art and challenges in sequence based T-cell epitope prediction. *Immunome Res* 6 Suppl 2:S3.
27. Finco O*, et al.* (2011) Approach to discover T- and B-cell antigens of intracellular pathogens applied to the design of Chlamydia trachomatis vaccines. *Proc Natl Acad Sci U S A* 108:9969-9974.

28. Hess J*, et al.* (1996) Superior efficacy of secreted over somatic antigen display in recombinant *Salmonella* vaccine induced protection against listeriosis. *Proc.Natl.Acad.Sci.U.S.A* 93:1458-1463.

29. Shen H*, et al.* (1998) Compartmentalization of bacterial antigens: differential effects on priming of CD8 T cells and protective immunity. *Cell* 92:535-545.

30. Kaufmann SH & Hess J (1999) Impact of intracellular location of and antigen display by intracellular bacteria: implications for vaccine development. *Immunol.Lett.* 65:81-84.

31. Zenewicz LA, Foulds KE, Jiang J, Fan X, & Shen H (2002) Nonsecreted bacterial proteins induce recall CD8 T cell responses but do not serve as protective antigens. *J.Immunol.* 169:5805-5812.

32. Pepper M, Dzierszinski F, Crawford A, Hunter CA, & Roos D (2004) Development of a system to study CD4+-T-cell responses to transgenic ovalbumin-expressing Toxoplasma gondii during toxoplasmosis. *Infect Immun* 72:7240-7246.

33. Bergman MA*, et al.* (2005) CD4+ T cells and toll-like receptors recognize *Salmonella* antigens expressed in bacterial surface organelles. *Infect.Immun.* 73:1350-1356.

34. Prickett S*, et al.* (2006) In vivo recognition of ovalbumin expressed by transgenic Leishmania is determined by its subcellular localization. *J.Immunol.* 176:4826-4833.

35. Andersen P & Doherty TM (2005) TB subunit vaccines--putting the pieces together. *Microbes Infect* 7:911-921.

36. Goldszmid RS & Sher A (2010) Processing and presentation of antigens derived from intracellular protozoan parasites. *Curr Opin Immunol* 22:118-123.

37. Tsolis RM, Xavier MN, Santos RL, & Baumler AJ (2011) How to become a top model: The impact of animal experimentation on human *Salmonella* disease research. *Infect Immun* 79:1806-1814.

38. Kirchhoff D*, et al.* (2007) Identification and isolation of murine antigen-reactive T cells according to CD154 expression. *Eur J Immunol* 37:2370-2377.

39. Cookson BT & Bevan MJ (1997) Identification of a natural T cell epitope presented by *Salmonella*- infected macrophages and recognized by T cells from orally immunized mice. *J Immunol.* 158:4310-4319.

40. Sheikh A*, et al.* (2011) Interferon-gamma and proliferation responses to *Salmonella* enterica Serotype Typhi proteins in patients with S. Typhi Bacteremia in Dhaka, Bangladesh. *PLoS Negl Trop Dis* 5:e1193.

41. Charles RC*, et al.* (2010) Characterization of anti-*Salmonella* enterica serotype Typhi antibody responses in bacteremic Bangladeshi patients by an immunoaffinity proteomics-based technology. *Clin Vaccine Immunol* 17:1188-1195.

42. Kumanovics A*, et al.* (2002) QUOD ERAT FACIENDUM: sequence analysis of the H2-D and H2-Q regions of 129/SvJ mice. *Immunogenetics* 54:479-489.

43. Chooneea D*, et al.* (2010) Elucidation of the outer membrane proteome of *Salmonella* enterica serovar Typhimurium utilising a lipid-based protein immobilization technique. *BMC Microbiol* 10:44.

44. Lee JS, Shin KS, Pan JG, & Kim CJ (2000) Surface-displayed viral antigens on *Salmonella* carrier vaccine. *Nat.Biotechnol.* 18:645-648.

45. Kang HY & Curtiss R, 3rd (2003) Immune responses dependent on antigen location in recombinant attenuated *Salmonella* typhimurium vaccines following oral immunization. *FEMS Immunol Med Microbiol* 37:99-104.

46. Rizos K, Lattemann CT, Bumann D, Meyer TF, & Aebischer T (2003) Autodisplay: Efficacious Surface Exposure of Antigenic UreA Fragments from Helicobacter pylori in *Salmonella* Vaccine Strains. *Infect.Immun.* 71:6320-6328.

47. Galen JE*, et al.* (2004) Adaptation of the endogenous *Salmonella* enterica serovar Typhi clyA-encoded hemolysin for antigen export enhances the immunogenicity of anthrax protective antigen domain 4 expressed by the attenuated live-vector vaccine strain CVD 908-htrA. *Infect Immun* 72:7096-7106.

48. Panthel K*, et al.* (2005) *Salmonella* pathogenicity island 2-mediated overexpression of chimeric SspH2 proteins for simultaneous induction of antigen-specific CD4 and CD8 T cells. *Infect.Immun.* 73:334-341.

49. Murphy KM, Heimberger AB, & Loh DY (1990) Induction by antigen of intrathymic apoptosis of CD4+CD8+TCRlo thymocytes in vivo. *Science* 250:1720-1723.

50. Pape KA*, et al.* (1997) Use of adoptive transfer of T-cell-antigen-receptor-transgenic T cell for the study of T-cell activation in vivo. *Immunol Rev* 156:67-78.

51. Bumann D (2001) In vivo visualization of bacterial colonization, antigen expression, and specific T-cell induction following oral administration of live recombinant *Salmonella* enterica serovar Typhimurium. *Infect.Immun.* 69:4618-4626.

52. Scholle A*, et al.* (1987) Sequence of the mglB gene from Escherichia coli K12: comparison of wild-type and mutant galactose chemoreceptors. *Mol.Gen.Genet.* 208:247-253.

53. Braun V (1975) Covalent lipoprotein from the outer membrane of Escherichia coli. *Biochim.Biophys.Acta* 415:335-377.

54. Benz I & Schmidt MA (1989) Cloning and expression of an adhesin (AIDA-I) involved in diffuse adherence of enteropathogenic Escherichia coli. *Infect.Immun.* 57:1506-1511.

55. Bumann D (2001) Regulated Antigen Expression in Live Recombinant *Salmonella* enterica Serovar Typhimurium Strongly Affects Colonization Capabilities and Specific CD4(+)-T-Cell Responses. *Infect.Immun.* 69:7493-7500.

56. Hoiseth SK & Stocker BA (1981) Aromatic-dependent *Salmonella* typhimurium are non-virulent and effective as live vaccines. *Nature* 291:238-239.

57. Zhang X, Kelly SM, Bollen WS, & Curtiss R (1997) Characterization and immunogenicity of *Salmonella* typhimurium SL1344 and UK-1 delta crp and delta cdt deletion mutants. *Infect.Immun.* 65:5381-5387.

58. Aliprantis AO*, et al.* (1999) Cell activation and apoptosis by bacterial lipoproteins through toll-like receptor-2. *Science* 285:736-739.

59. Ruiz-Olvera P*, et al.* (2003) Display and release of the Plasmodium falciparum circumsporozoite protein using the autotransporter MisL of *Salmonella* enterica. *Plasmid* 50:12-27.

60. Dunstan SJ, Simmons CP, & Strugnell RA (1998) Comparison of the abilities of different attenuated *Salmonella* typhimurium strains to elicit humoral immune responses against a heterologous antigen. *Infect.Immun.* 66:732-740.

61. Bumann D (2003) T cell receptor-transgenic mouse models for studying cellular immune responses to *Salmonella* in vivo. *FEMS Immunol.Med.Microbiol.* 37:105-109.

62. Maurer J, Jose J, & Meyer TF (1997) Autodisplay: one-component system for efficient surface display and release of soluble recombinant proteins from Escherichia coli. *J.Bacteriol.* 179:794-804.

63. Eriksson K & Holmgren J (2002) Recent advances in mucosal vaccines and adjuvants. *Curr.Opin.Immunol.* 14:666-672.

64. Shreedhar VK, Kelsall BL, & Neutra MR (2003) Cholera Toxin Induces Migration of Dendritic Cells from the Subepithelial Dome Region to T- and B-Cell Areas of Peyer's Patches. *Infect.Immun.* 71:504-509.

65. Hormaeche CE (1980) The in vivo division and death rates of *Salmonella* typhimurium in the spleens of naturally resistant and susceptible mice measured by the superinfecting phage technique of Meynell. *Immunology* 41:973-979.

66. Benjamin WH, Jr., Hall P, Roberts SJ, & Briles DE (1990) The primary effect of the Ity locus is on the rate of growth of *Salmonella* typhimurium that are relatively protected from killing. *J Immunol.* 144:3143-3151.

67. Grant AJ*, et al.* (2008) Modelling within-host spatiotemporal dynamics of invasive bacterial disease. *PLoS Biol* 6:e74.

68. Kaneshige T, Yaguchi K, & Ohgitani T (2009) Siderophore receptor IroN is an important protective antigen against *Salmonella* infection in chickens. *Avian Dis* 53:563-567.

69. Baghal SM, Gargari SL, & Rasooli I (2010) Production and immunogenicity of recombinant ferric enterobactin protein (FepA). *Int J Infect Dis* 14 Suppl 3:e166-170.

70. Skaar EP (2010) The battle for iron between bacterial pathogens and their vertebrate hosts. *PLoS Pathog* 6:e1000949.

71. Yu JL & Guo L (2011) Quantitative proteomic analysis of *Salmonella* enterica serovar Typhimurium under PhoP/PhoQ activation conditions. *J Proteome Res* 10:2992-3002.

72. Sood S, Rishi P, Dhawan V, Sharma S, & Ganguly NK (2005) Protection mediated by antibodies to iron-regulated outer-membrane proteins of S. typhi in a mouse peritonitis model. *Mol Cell Biochem* 273:69-78.

73. Miller SI & Mekalanos JJ (1990) Constitutive expression of the phoP regulon attenuates *Salmonella* virulence and survival within macrophages. *J.Bacteriol.* 172:2485-2490.

74. Martens EC, Koropatkin NM, Smith TJ, & Gordon JI (2009) Complex glycan catabolism by the human gut microbiota: the Bacteroidetes Sus-like paradigm. *J Biol Chem* 284:24673-24677.

75. Wick MJ, Harding CV, Normark SJ, & Pfeifer JD (1994) Parameters that influence the efficiency of processing antigenic epitopes expressed in *Salmonella* typhimurium. *Infect.Immun.* 62:4542-4548.

76. Buchmeier NA & Libby SJ (1997) Dynamics of growth and death within a *Salmonella* typhimurium population during infection of macrophages. *Can.J Microbiol* 43:29-34.

77. Gill WP*, et al.* (2009) A replication clock for Mycobacterium tuberculosis. *Nat Med* 15:211-214.

78. Ridley MJ & Wells CW (1986) Macrophage-parasite interaction in the lesions of cutaneous leishmaniasis. An ultrastructural study. *Am J Pathol* 123:79-85.

79. Hoff DR*, et al.* (2011) Location of intra- and extracellular M. tuberculosis populations in lungs of mice and guinea pigs during disease progression and after drug treatment. *PLoS One* 6:e17550.

80. Filipe-Santos O*, et al.* (2009) A dynamic map of antigen recognition by CD4 T cells at the site of Leishmania major infection. *Cell Host Microbe* 6:23-33.

81. de Jong RN, Daniels MA, Kaptein R, & Folkers GE (2006) Enzyme free cloning for high throughput gene cloning and expression. *J Struct Funct Genomics* 7:109-118.

82. Kramer U, Rizos K, Apfel H, Autenrieth IB, & Lattemann CT (2003) Autodisplay: development of an efficacious system for surface display of antigenic determinants in *Salmonella* vaccine strains. *Infect.Immun.* 71:1944-1952.

83. Zhang WY & Wu HC (1992) Alterations of the carboxyl-terminal amino acid residues of Escherichia coli lipoprotein affect the formation of murein-bound lipoprotein. *J.Biol.Chem.* 267:19560-19564.

84. Bumann D (2002) Examination of *Salmonella* gene expression in an infected mammalian host using the green fluorescent protein and two-colour flow cytometry. *Mol.Microbiol.* 43:1269-1283.

85. Ames GF, Prody C, & Kustu S (1984) Simple, rapid, and quantitative release of periplasmic proteins by chloroform. *J.Bacteriol.* 160:1181-1183.

86. Komoriya K*, et al.* (1999) Flagellar proteins and type III-exported virulence factors are the predominant proteins secreted into the culture media of *Salmonella* typhimurium. *Mol Microbiol* 34:767-779.

87. Kiefer F, Arnold K, Kunzli M, Bordoli L, & Schwede T (2009) The SWISS-MODEL Repository and associated resources. *Nucleic Acids Res* 37:D387-392.

88. El-Manzalawy Y & Honavar V (2010) Recent advances in B-cell epitope prediction methods. *Immunome Res* 6 Suppl 2:S2.

89. Reche PA, Glutting JP, Zhang H, & Reinherz EL (2004) Enhancement to the RANKPEP resource for the prediction of peptide binding to MHC molecules using profiles. *Immunogenetics* 56:405-419.

90. Ferguson AD*, et al.* (2000) A conserved structural motif for lipopolysaccharide recognition by procaryotic and eucaryotic proteins. *Structure* 8:585-592.

Figures

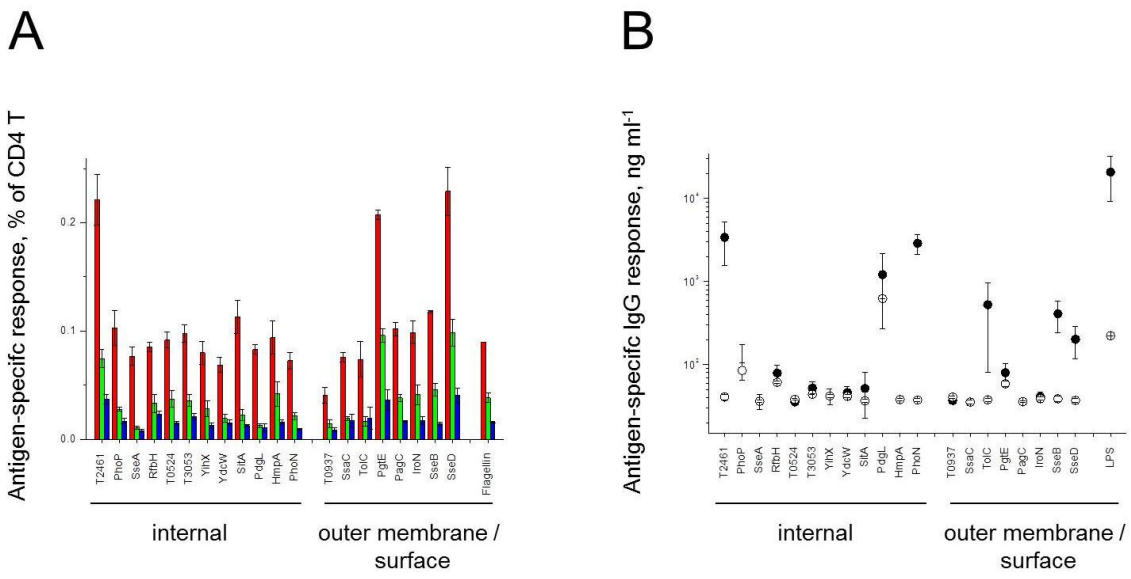

Figure 1: Cellular and humoral immune responses of convalescent *Salmonella*-infected mice to recombinant *Salmonella* antigens. **A**) Antigen-specific CD4 T cell frequencies as detected by CD154 upregulation (red) and IFNγ (green) or IL-17 (blue) secretion. The data represent means ± SE of three mice. Low background responses to an unrelated antigen, HP0231 from *Helicobacter pylori*, and responses to *Salmonella* antigens in non-infected control mice were subtracted. **B**) Serum antibody responses to *Salmonella* antigens. The data represent means ± SE of 11 convalescent mice (filled circles) and means ± SE for ten non-infected control mice (open circles).

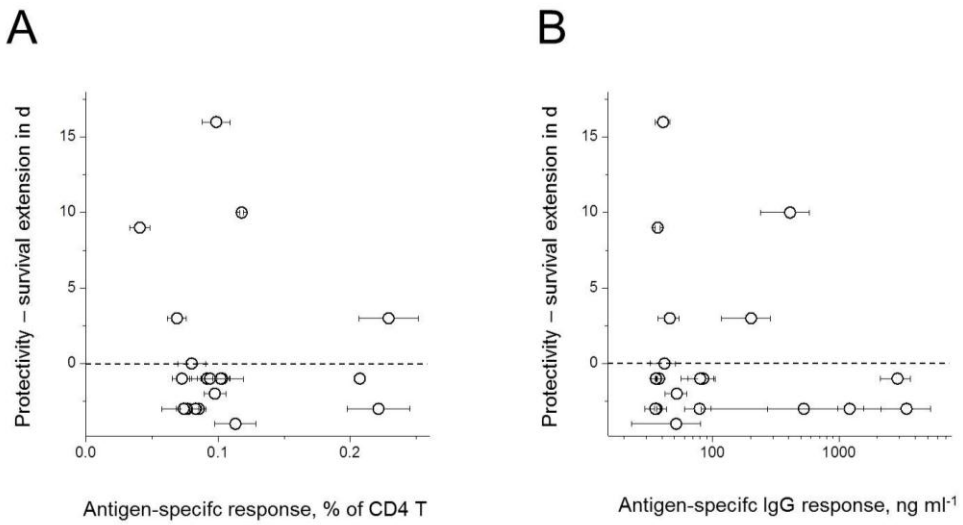

Figure 2: *Salmonella* antigen protectivity against primary infection does not correlate to immunogenicity in convalescent mice. **A**) Relationship between antigen protectivity against primary infection and cognate CD4 T cell responses in convalescent mice (same data as Fig. 1A). Protectivity is expressed as "survival time extension", which is the difference in median survival time of a group of five immunized mice compared to a control group of five mice that were immunized with GFP. **B**) Relationship between antigen protectivity and serum antibody responses in convalescent mice (same data as Fig. 1B).

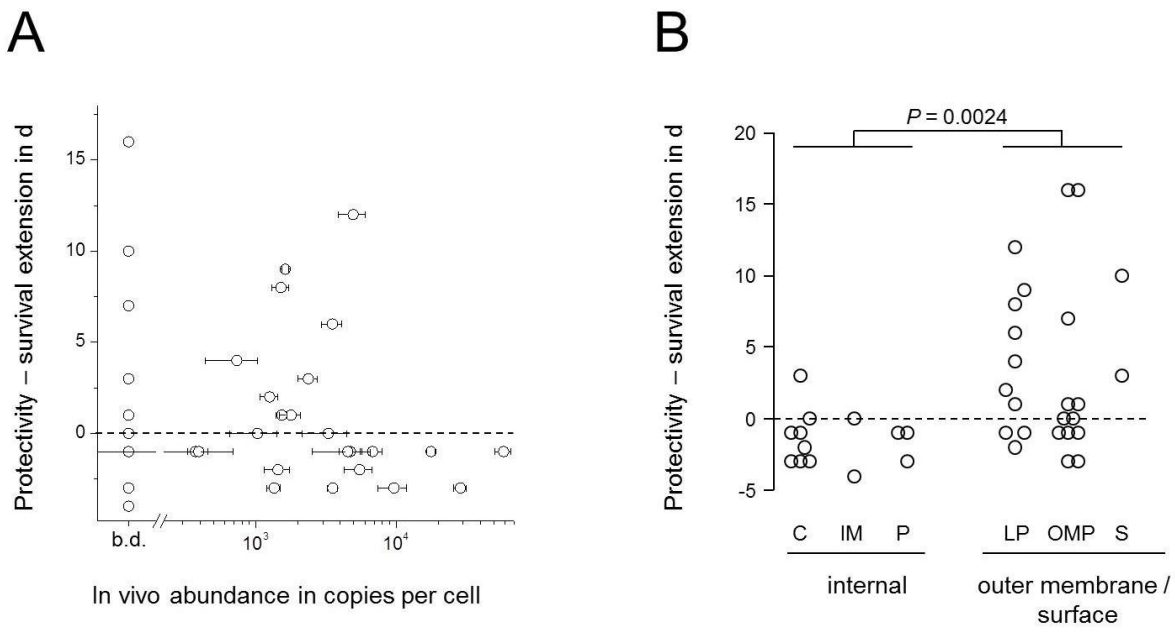

Figure 3: *Salmonella* antigen protectivity does not correlate with in vivo antigen abundance but depends on antigen localization within the *Salmonella* cell. **A**) Relationship between antigen protectivity and in vivo abundance as determined by quantitative proteome analysis of ex vivo purified *Salmonella* (means ± SD for three independently infected mice). **B**) Relationship between antigen protectivity and antigen localization within *Salmonella* (C, cytosol; IM, inner membrane; P, periplasm; LP, outer-membrane associated lipoprotein; OMP, outer membrane protein; S, surface). Statistical significance of differences between internal and outer membrane/surface antigens was tested using the non-parametric Mann-Whitney U test.

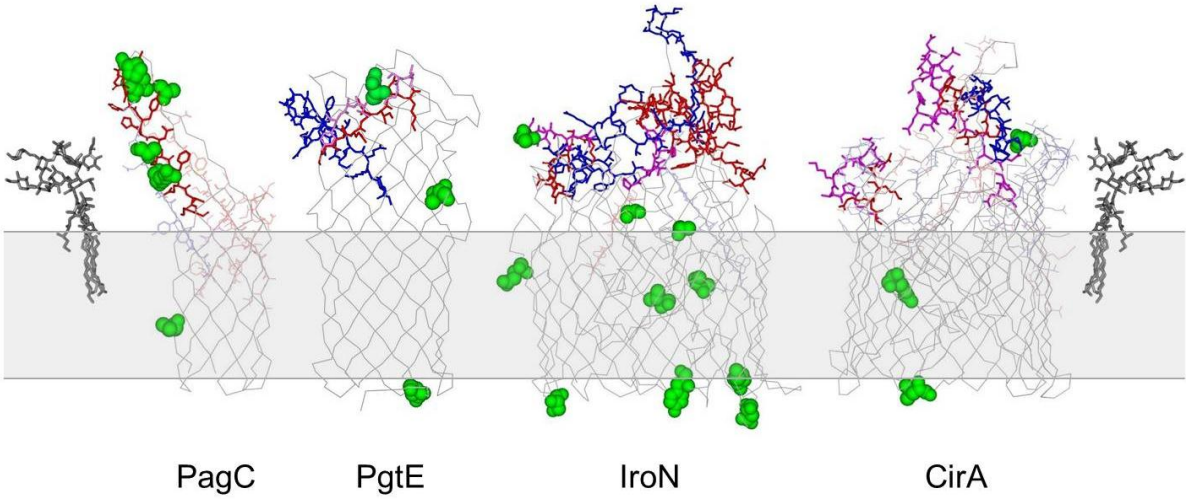

Figure 4: Structural models and exposed immune epitopes of various *Salmonella* outer membrane proteins. The outer membrane is shown as a grey area, predicted T cell epitopes in exposed loops are shown in red, potential antibody binding sites are shown in blue, and overlapping T and B cell epitopes are shown in magenta. Partially exposed epitopes are shown in pale colors. Amino acid residues that differ between *Salmonella enterica* serovars Typhimurium and Typhi are shown in green. LPS structures as observed in FhuA-LPS crystals (90) are also shown.

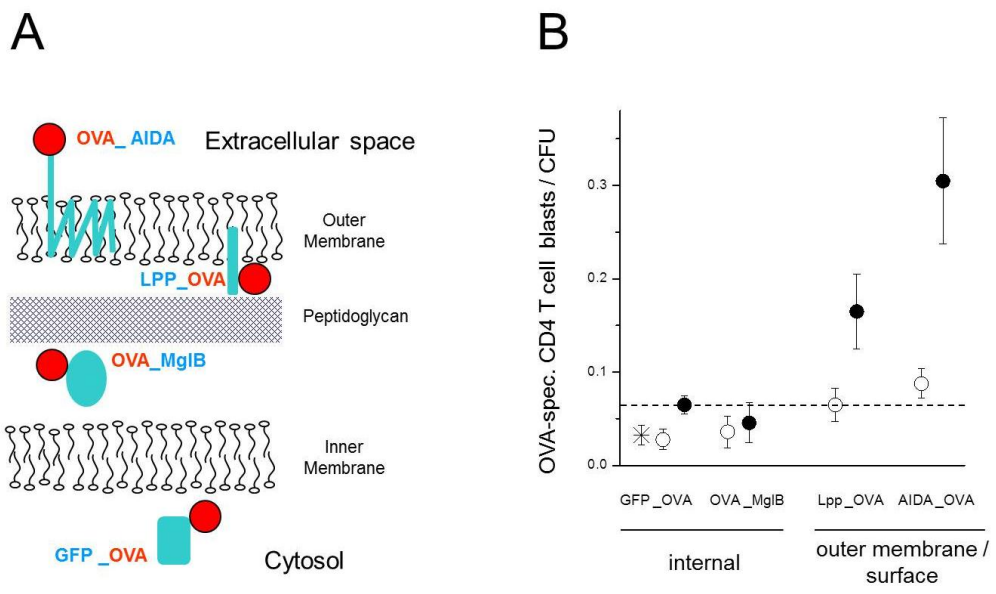

Figure 5: CD4 T cell responses in mice infected with *Salmonella* expressing an ovalbumin model antigen. **A**) Schematic overview of fusion proteins that target an immunodominant ovalbumin epitope (OVA) to various *Salmonella* cell compartments. **B**) OVA-specific CD4 T cell induction in mice infected with *Salmonella* expressing OVA at various levels (open circles, low abundance; filled circles, high abundance) in four different compartments. The dashed line represents CD4 T cell responses to saturating levels of cytosolic OVA. The star represents data for *Salmonella* expressing moderate levels of cytosolic OVA together with cholera toxin B and AIDA. Data represent means ± SE for groups of ten to twenty mice. Statistical significance of differences to *Salmonella* expressing saturating levels of cytosolic OVA were tested using Mann-Whitney U test (*, $P< 0.05$; **, $P< 0.01$).

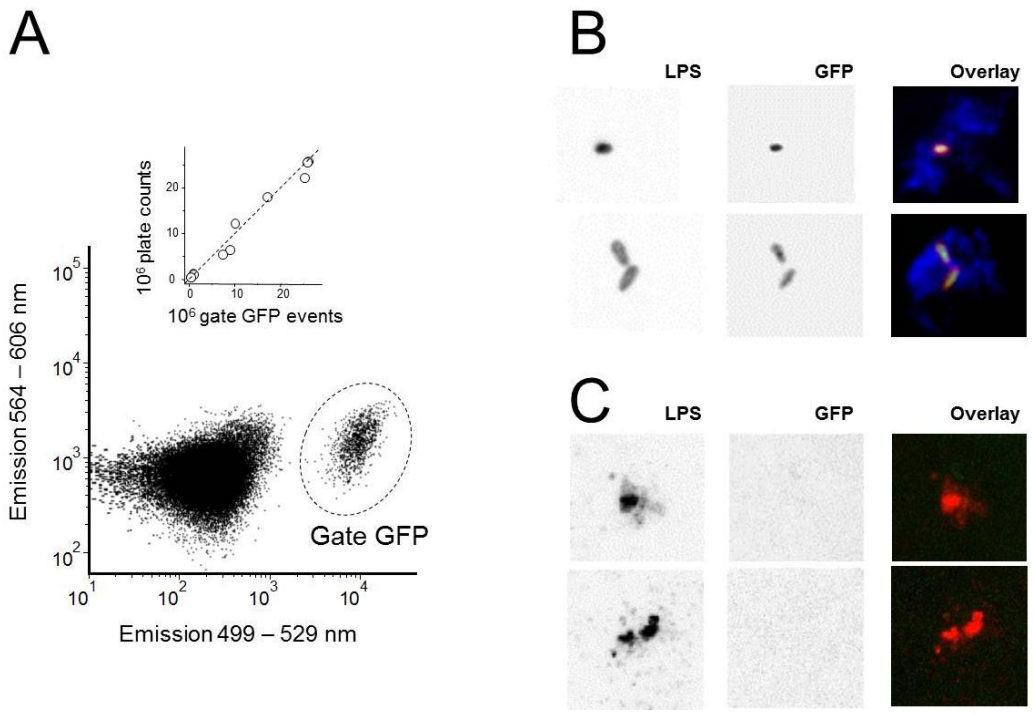

Figure 6: Detection of intact and damaged *Salmonella* cells in infected mouse tissues. **A**) Flow cytometry of a spleen homogenate infected with *Salmonella sifB::gfp* using 488 nm excitation. Gate 1 contains GFP-positive *Salmonella* (84). The inset shows the relationship between flow cytometry data and plate counts for individual mice, the dashed line represents a 1:1 ratio. **B**) Confocal micrographs of liver cryosections infected with *Salmonella sifB::gfp* that were stained with antibodies to *Salmonella* lipopolysaccharide (red) and macrophage marker CD68 (blue). Individual color channels are shown with inverted grey scale for better visualization of weak staining. Micrographs represent typical observations for for four independently infected mice. **C**) Confocal micrographs of lipopolysaccharide-positive particles that lack detectable GFP (even when contrast was increased compared to B). Such particles were absent in non-infected control sections.

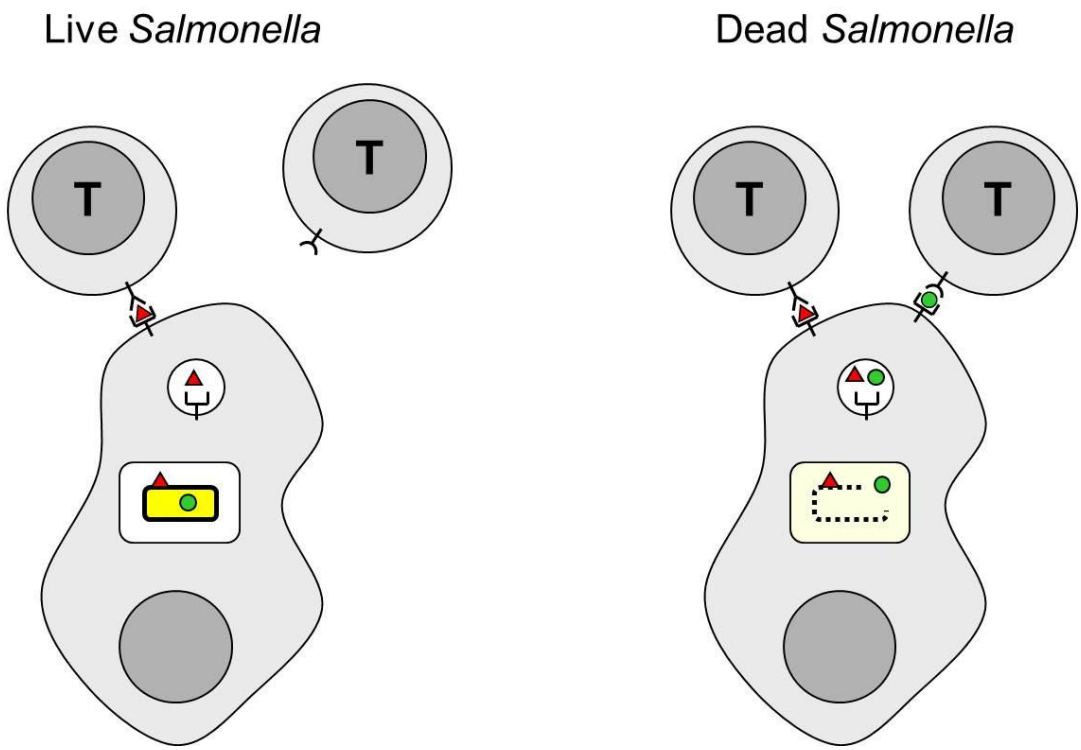

Figure 7: Schematic model for cellular immunity to *Salmonella*. *Salmonella* (yellow) reside in intracellular vacuoles in infected host cells. *Salmonella* possesses internal (green) and surface-associated (red) antigens. **Left**) Live *Salmonella* shield internal antigens, but some of their surface-associated antigens are accessible for processing and presentation. As a consequence, T cells specific for *Salmonella* surface antigens can recognize these infected cells and initiate antibacterial immune effector mechanisms. In contrast, T cells specific for internal *Salmonella* antigens fail to detect host cells that contain exclusively intact *Salmonella*. **Right**) Dead *Salmonella* release internal antigens. As a consequence, both surface-exposed and internal antigens can be processed, presented, and recognized by cognate T cells. However, this recognition is unproductive for infection control since it targets *Salmonella* that are already dead.

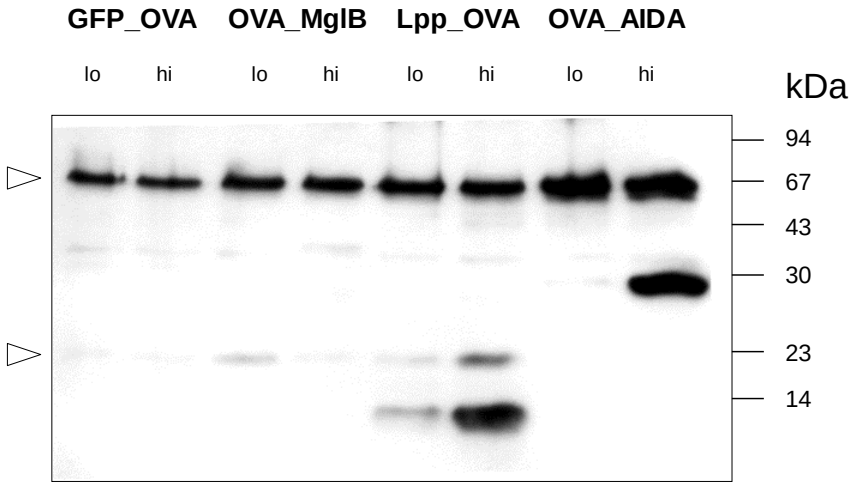

Supporting Figure 1: Release of the ovalbumin epitope OVA by *Salmonella* strains expressing low ("lo") or high ("hi") amounts of various OVA fusion proteins. In vitro culture supernatants of 4.5 x 10^{11} CFU were precipitated with TCA and analyzed by Western Blotting with a polyclonal antibody to ovalbumin. This antibody recognized the OVA epitope but cross-reacted also with endogenous *Salmonella* proteins with apparent molecular weights of ca. 23 and 67 kDa, respectively (arrowheads) that were also detected even in supernatants of plasmid-free strains.

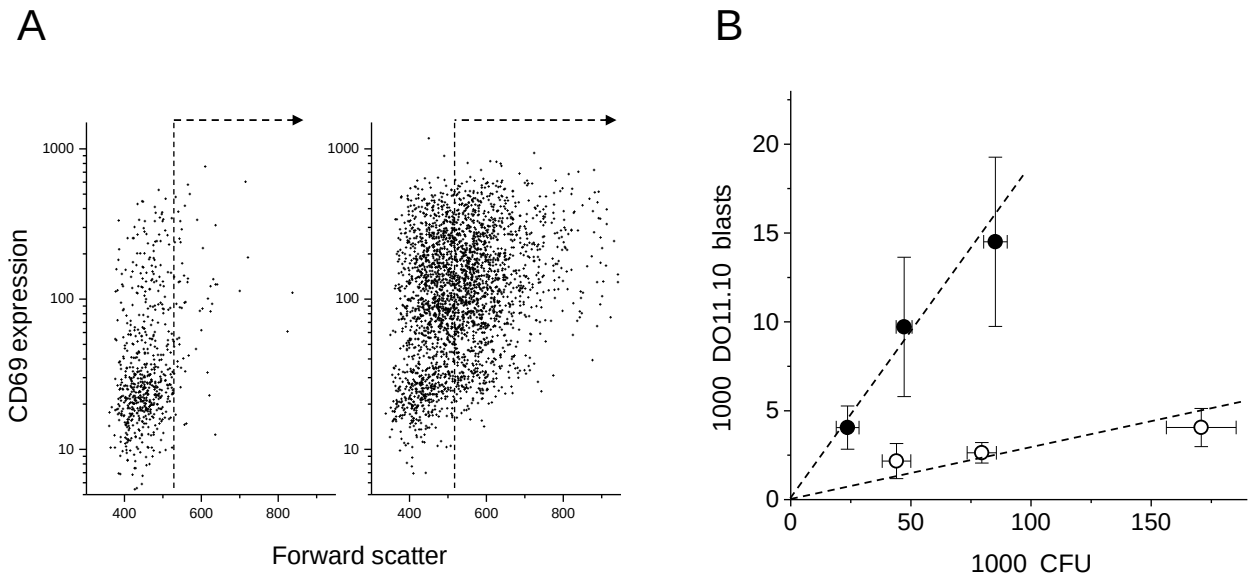

Supporting Figure 2: Induction of OVA-specific transgenic CD4 T cells in mice infected with *Salmonella* expressing OVA. **A**) Flow cytometric analysis of size measured as forward scatter vs. expression of the early activation marker CD69. Mice were infected with control *Salmonella* expressing GFP (left) or *Salmonella* expressing LPP_OVA (right). The dashed line was used to count CD4 T cell blasts. Similar observations were made for more than hundred mice in several independent experiments. **B**) Relationship between *Salmonella* Peyer's patches colonization and OVA_specific CD4 T cell induction in mice infected with *Salmonella* expressing high levels of LPP_OVA (filled circles) or low levels of GFP_OVA (open circles). Data represent means ± SEM's for groups of five to six animals from three independent experiments.

3. Discussion

Systemic infection leads to severe inflammation and metabolic changes of infected host tissues. These host responses to infection have been extensively studied, but most studies employed blood and tissue homogenates. However, information about the spatial distribution of inflammation and metabolism in tissues are lost when analyzing homogenates. Tissues have a complex architecture, are comprised of different cell types and are therefore intrinsically heterogeneous. During infection, this heterogeneity can even increase due to the formation of inflammatory focal lesions and localized tissue damage.
Limited data that have been mostly obtained for tuberculosis models suggested that such heterogeneity might have an impact on disease mechanism, pathology and infection control. However, integrated data unraveling underlying molecular mechanisms and the impact on pathogen biology in complex tissue structures are lacking even for those models.

In this work, we employed a model of murine typhoid fever to study host heterogeneity in liver and spleen tissues. We found important implications of heterogeneity for the infection, which will be discussed below.

3.1 Metabolic heterogeneity of infected host tissues

Metabolic responses to systemic infections, which mainly encompass a shift towards enhanced glucose and lipid supply, are well understood (Spitzer et al., 1988; Trager et al., 2003). Our own results from liver homogenates of *Salmonella*-infected mice confirmed the metabolic profile obtained with other models. However, information about the spatial distribution of metabolism in the infected liver during *Salmonella* infection was lacking.
Here, we investigated host metabolism in liver tissue *in situ* using a newly developed method which combines enzyme histochemistry and immunohistochemistry. It allowed the demonstration of central carbon metabolic enzyme activities, assignment of these activities to different cell types in the same tissue sections, and sensitive detection by fluorescence microscopy. Enzyme histochemistry is superior to homogenate enzyme assays as it shows the *in situ* activity of an enzyme in its natural tissue context (Van Noorden, 2010). In contrast to enzyme expression data obtained with *in situ* mRNA hybridization or antibody staining, histochemistry might reveal enzyme regulation by post-translational modifications. On the other

hand, enzyme histochemistry assays are usually performed using saturating substrate concentrations, thus showing the maximum activity of the respective enzyme, which does not necessarily reflect its true flux *in vivo.* Hence, the method reveals the maximum metabolic capacity as an upper limit for the actual *in vivo* activity.

Application of this method to *Salmonella*-infected liver revealed that inflammatory lesions consisting of neutrophils and macrophages, hereinafter called granulomas, had a strikingly different metabolism compared to the surrounding tissue, including resident tissue macrophages (Kupffer cells). Specifically, we observed high glucose phosphorylation and NADPH production via the HMP shunt but low TCA cycle and lactate dehydrogenase activities in these lesions. We could independently confirm these relative metabolic profiles by homogenate assays and proteomics of *ex vivo* sorted inflammatory macrophages, neutrophils and Kupffer cells.

In tuberculosis, granulomas have previously been shown to have generally high metabolic activity including glucose uptake, HMP shunt, glycolysis, TCA cycle, and other pathways. However, this pattern differed from the striking dominance that we observed during *Salmonella* infection (Davis et al., 2009; Somashekar et al., 2011), probably due to different cell type composition and differentiation of cells.

Taken together, our data revealed striking metabolic heterogeneity in liver tissue and demonstrated a high capacity for NADPH production in granulomas.

3.2 Host inflammatory response

Infections can lead to severe systemic inflammatory responses. Inflammation during systemic salmonellosis has been extensively studied (Dougan et al., 2011). Host organs such as liver and spleen, which are infected by *Salmonella*, show a granulomatous response, involving the recruitment of circulating neutrophils in a first wave and inflammatory macrophages in a second wave (Richter-Dahlfors et al., 1997). Early granulomatous lesions therefore often consist of a core of neutrophils and an outer ring of macrophages, while at later stages of the infection; neutrophils are entirely replaced by macrophages (Hsu, 1989; Richter-Dahlfors et al., 1997). Classically activated macrophages secrete inflammatory mediators such as TNF-α which are essential for granuloma integrity. They also express NADPH oxidase and inducible nitric oxide

synthase (iNOS) which consume NADPH and produce superoxide and nitric oxide, respectively. A colocalization of iNOS expression and granulomas has been consistently demonstrated in *Salmonella*-infected tissue (Umezawa et al., 1997). NADPH oxidase and iNOS are important for early and late control of *Salmonella* infection as demonstrated by phenotypes of respective knockout mice models (Mastroeni et al., 2000).

To analyze potential connections between local metabolism and inflammation, we determined the distribution of antibacterial effector mechanisms in infected tissues.

We found iNOS expression to be highly localized to an outer ring of macrophages in bigger granulomatous lesions, implying heterogeneity within granulomas during the early stage of the disease. We could also detect lipid and protein modifications indicative of oxidative and nitrosative damage inside granulomas in agreement with earlier studies (Alam et al., 2002). Nitrosative stress was frequently localized to the periphery of granulomas, roughly colocalizing with iNOS expression. The production of reactive oxygen species (ROS) and reactive nitrogen species (RNS) by iNOS and NADPH oxidase in granulomas indicated highly heterogeneous antibacterial activities within the tissue.

Importantly, the highest activities occurred in tissue regions that had high capacity of NADPH production. One key substrate for both ROS and RNS generation, as well as for protection against collateral damage of host tissue was locally produced where needed.

These data revealed highly heterogeneous inflammation that correlated with the local metabolic profile.

3.3 Effects of host heterogeneity on *Salmonella*

Salmonella organ colonization has been extensively studied. In the model employed in our study, *Salmonella* directly enters the systemic circulation by intravenous injection. Shortly afterwards, the bacterium is mainly found within Kupffer cells of the liver (Mastroeni, 2002). Population dynamics data obtained using methods of fluorescence, plasmid or phage dilution, revealed bacterial growth rates, but also killing of a substantial part of the entire *Salmonella* population (Benjamin et al., 1990; Helaine et al., 2010; Hormaeche, 1980; Watson and Holden, 2010). However, these methods did not reveal where *Salmonella* growth and killing occurred. A study conducted by Grant et al. visualized the spatial segregation of tagged *Salmonella*

populations within the infected tissue (Grant et al., 2008), but did not include information about adaptation or killing of bacteria. ROS and RNS formation by NADPH oxidase and iNOS has been correlated with infection control (Mastroeni et al., 2000), but it is also known from *in vitro* experiments that *Salmonella* is capable of adapting to these stresses. For example, *Salmonella* up-regulates the expression of the superoxide dismutase SodCI to cope with superoxide or HmpA to detoxify nitric oxide (NO) (Aussel et al., 2011; Henard and Vazquez-Torres, 2011). It is therefore unclear, to what extent *Salmonella* is killed by or adapts to host induced stresses and if adaptation or killing are heterogeneous across tissues. Granulomas have been proposed to mediate pathogen killing but conclusive evidence is lacking.

To address this question, we localized *Salmonella* using an antibody against lipopolysaccharide (LPS).

To analyze the distribution of bacterial killing in the tissue, we used a *Salmonella* strain that constitutively expresses GFP and counterstained with an antibody directed against *Salmonella*-LPS. In this approach, viable *Salmonella* are positive for both GFP and LPS, while dead bacteria loose GFP fluorescence and remain only LPS-positive. This simple method has been previously employed to detect bacterial viability *in vitro* (Grossart et al., 2010). In contrast to other methods that assess population dynamics *in vivo*, this method does not provide temporal resolution of the killing process. In particular, the preservation of bacterial envelopes over time is not known, although our results indicate different stages of 'decay' in the tissue. Completely degraded dead *Salmonella* would be undetectable by LPS-staining. As a consequence, our method underestimates the total amount of killed bacteria. On the other hand, it enables localization at least of recent killing.

Our results revealed enhanced bacterial killing inside granulomas, indicating that *Salmonella* localization across heterogeneous host structures was of fundamental importance. Furthermore, we observed that live bacteria segregated away from dead bacteria, indicating that live and dead bacteria mostly localize to different tissue areas.

The data revealed that part of the *Salmonella* were covered by granulomas, indicating that the bacteria resided in fundamentally different host environments.

To analyze adaptation of surviving bacteria to local host responses we constructed *Salmonella* biosensors, which translate stress responses into a visible GFP signal. FACS analysis of tissue homogenates showed a broad distribution of GFP fluorescence in a *Salmonella* biosensor responsive to NO stress, indicating differential adaptation of the bacteria. Interestingly, NO-

responsive *Salmonella* localized to iNOS-rich tissue regions supporting heterogeneous local host/pathogen interactions.

Together, these data revealed that highly heterogeneous host environments had a striking impact on *Salmonella* infection biology, ranging from localized survival/killing and regionally adapting *Salmonella* subpopulations. It is likely that additional host-*Salmonella* interactions are also heterogeneously distributed and this could be an exciting subject for further analysis. As an example, liver has a clear zonation with differential oxygen concentrations and distinct metabolic host activities (Jungermann and Kietzmann, 1996). *Salmonella* uses aerobic respiration for *in vivo* growth (Becker et al., 2006) and thus might adapt to host oxygen tension.

As a practical aspect of this work, the distribution of live and dead bacteria in the tissue may have important implications for T cell mediated immunity. T cells recognize antigens, which can be either internal or surface-exposed. In a recent vaccine study conducted in our laboratory, surface-exposed antigens were shown to be protective, in contrast to internal antigens. We deduced that only those T cells confer immunity, which effectively recognize antigens from live bacteria. Only cells containing dead bacteria present internal antigens, therefore targeting internal-antigen recognizing T cells to irrelevant sites, while host cells containing live bacteria remain undetected.

Another important implication is the treatment of the infection with antibiotics. Bryk et al. have reported on a therapy involving a synergistic effect of a class of antibiotics and host-derived NO in tuberculosis (Bryk et al., 2008). Taking our result into account that not all bacteria may be exposed to the same level of NO stress, the suitability of such an approach is doubtful in a model of typhoid fever.

Although killing of bacteria inside granulomas has been suggested for other infectious diseases, such as tuberculosis (Bouley et al., 2001; Hoff et al., 2011) to our knowledge this has not yet been directly demonstrated *in situ.* Initial killing of *Mycobacterium tuberculosis* (MTB) by neutrophils in early tuberculosis has been suggested by *in vitro* experiments (Korbel et al., 2008), but at later stages granulomas contain live bacteria within permissive macrophages (Pieters, 2008). Application of our method could give new insights into the killing dynamics inside MTB granulomas and progression of the disease. Similar to our observations that *Salmonella* adapts to heterogeneous microenvironments, Fenhalls et al. observed differential expression patterns of MTB in granulomas (Fenhalls et al., 2002). This suggests that our observations may be applicable to other models of disease that are less well investigated.

In summary, we have shown that heterogeneous host environments promote strikingly different fates of *Salmonella* including partial killing and local adaptation of distinct subpopulations among the survivors.

3.4 Conclusion

The data presented in this thesis give evidence of dramatic heterogeneity at various levels within infected host tissues. In particular, granulomas have a distinct metabolism that supports potent inflammatory response causing stress and even killing of local *Salmonella* subpopulations.

Granulomas are hotspots of NADPH production which locally aids antimicrobial effector mechanisms, including NADPH oxidase and iNOS activities. ROS and RNS induced stress is high in these areas, rendering granulomas centers of bacterial killing (see figure 1). Bacteria that survive these hostile conditions can adapt to certain host-induced stresses as shown for the response to NO. With respect to the variety of stresses and antimicrobial defense mechanisms within granulomas, we can assume that the bacterial heterogeneity detected in our approach represents only the 'top of the iceberg' of differently adapted bacterial subpopulations. This may have important medical implications, as antibiotics and vaccine strategies may target only subpopulations with distinct properties and thus might fail to control infection.

Our general approach combining enzyme histochemistry, immunostaining, pathogen biosensors, flow cytometry, and proteomics to correlate local metabolism, inflammation, and pathogen activities, might be applicable also for other infectious diseases such as tuberculosis, that involve heterogeneous host tissues.

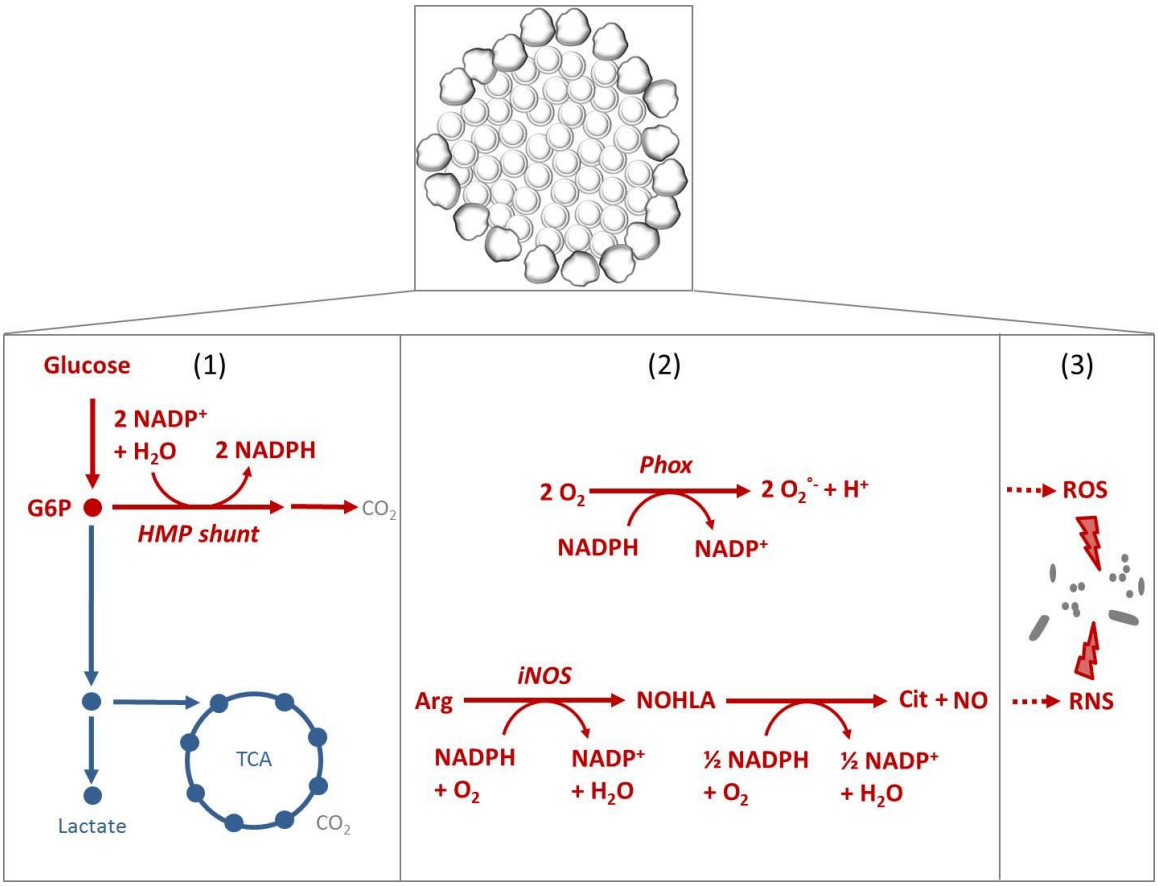

Figure 1. Interconnection of metabolic profile, antibacterial effector mechanisms at killing at inflammatory foci.
Highly used pathways/enzymatic reactions are indicated in red, others in blue.
1: NADPH production via the HMP shunt in granuloma cells. 2: NADPH consumption and superoxide and nitric oxide generation by NADPH oxidase and iNOS. 3: Formation of ROS and RNS lead to or contribute to enhanced killing inside granulomas.
G6P: glucose-6-phosphate; Phox: NADPH oxidase; Arg: L-arginine; NOHLA: N^{ω}-hydroxy-L-arginine; Cit: citrulline.

4. Outlook

In this work, the outstanding features of granulomas and their effects on *Salmonella* have been described. However, granulomas are formed by single cells that transmigrate from blood and spleen reservoirs into the infected host tissues. Single inflammatory macrophages and neutrophils are abundantly present in the infected tissues, but their metabolic, inflammatory and bactericidal properties have not been studied in comparison to the united cell structure of the granulomas. Does granuloma-organization change single cell physiology? Is bacterial killing more effective upon synergistic and cumulative effects due to granuloma organization? We want to answer these questions in the future by selectively isolating and sorting granuloma cells and analysing their proteomes and enzymatic activities.

The exact mechanism by which bacteria are killed in granulomas remains to be elucidated. We want to visualize the relative contribution of NADPH oxidase-derived ROS, by using a $Phox^{-/-}$ mouse model which lacks a functional NADPH oxidase. We plan to analyse tissue sections and compare fractions of dead bacteria within granulomas to controls.

Our data suggest that Kupffer cells do respond to the infection by protecting themselves against collateral damage, but do not exhibit a pro-inflammatory profile. We want to test, if Kupffer cells are already primed and reside in a state of low-level activation in uninfected liver and if they generally exhibit less potential for oxidative burst than inflammatory macrophages. We therefore plan to measure ROS production in fresh, *ex vivo* sorted Kupffer cells and compare them to inflammatory macrophages.

5. References

2010. Retraction. The large-conductance Ca(2+)-activated K(+) channel is essential for innate immunity. *Nature*. 468:122.

Abrahams, G.L., and M. Hensel. 2006. Manipulating cellular transport and immune responses: dynamic interactions between intracellular Salmonella enterica and its host cells. *Cell Microbiol*. 8:728-737.

Alam, M.S., T. Akaike, S. Okamoto, T. Kubota, J. Yoshitake, T. Sawa, Y. Miyamoto, F. Tamura, and H. Maeda. 2002. Role of nitric oxide in host defense in murine salmonellosis as a function of its antibacterial and antiapoptotic activities. *Infect Immun*. 70:3130-3142.

Antunes, L.C., E.T. Arena, A. Menendez, J. Han, R.B. Ferreira, M.M. Buckner, P. Lolic, L.L. Madilao, J. Bohlmann, C.H. Borchers, and B.B. Finlay. 2011. Impact of salmonella infection on host hormone metabolism revealed by metabolomics. *Infect Immun*. 79:1759-1769.

Aussel, L., W. Zhao, M. Hebrard, A.A. Guilhon, J.P. Viala, S. Henri, L. Chasson, J.P. Gorvel, F. Barras, and S. Meresse. 2011. Salmonella detoxifying enzymes are sufficient to cope with the host oxidative burst. *Mol Microbiol*. 80:628-640.

Balce, D.R., B. Li, E.R. Allan, J.M. Rybicka, R.M. Krohn, and R.M. Yates. 2011. Alternative activation of macrophages by IL-4 enhances the proteolytic capacity of their phagosomes through synergistic mechanisms. *Blood*. 118:4199-4208.

Banchereau, J., and R.M. Steinman. 1998. Dendritic cells and the control of immunity. *Nature*. 392:245-252.

Barcia, A.M., and H.W. Harris. 2005. Triglyceride-rich lipoproteins as agents of innate immunity. *Clin Infect Dis*. 41 Suppl 7:S498-503.

Bechmann, L.P., R.A. Hannivoort, G. Gerken, G.S. Hotamisligil, M. Trauner, and A. Canbay. 2011. The interaction of hepatic lipid and glucose metabolism in liver diseases. *J Hepatol*.

Becker, D., M. Selbach, C. Rollenhagen, M. Ballmaier, T.F. Meyer, M. Mann, and D. Bumann. 2006. Robust Salmonella metabolism limits possibilities for new antimicrobials. *Nature*. 440:303-307.

Benjamin, W.H., Jr., P. Hall, S.J. Roberts, and D.E. Briles. 1990. The primary effect of the Ity locus is on the rate of growth of Salmonella typhimurium that are relatively protected from killing. *J Immunol*. 144:3143-3151.

Bilzer, M., F. Roggel, and A.L. Gerbes. 2006. Role of Kupffer cells in host defense and liver disease. *Liver Int*. 26:1175-1186.

Borregaard, N. 2010. Neutrophils, from marrow to microbes. *Immunity*. 33:657-670.

Borregaard, N., and T. Herlin. 1982. Energy metabolism of human neutrophils during phagocytosis. *J Clin Invest*. 70:550-557.

Bouley, D.M., N. Ghori, K.L. Mercer, S. Falkow, and L. Ramakrishnan. 2001. Dynamic nature of host-pathogen interactions in Mycobacterium marinum granulomas. *Infect Immun*. 69:7820-7831.

Brinkmann, V., U. Reichard, C. Goosmann, B. Fauler, Y. Uhlemann, D.S. Weiss, Y. Weinrauch, and A. Zychlinsky. 2004. Neutrophil extracellular traps kill bacteria. *Science*. 303:1532-1535.

Bryk, R., B. Gold, A. Venugopal, J. Singh, R. Samy, K. Pupek, H. Cao, C. Popescu, M. Gurney, S. Hotha, J. Cherian, K. Rhee, L. Ly, P.J. Converse, S. Ehrt, O. Vandal, X. Jiang, J. Schneider, G. Lin, and C. Nathan. 2008. Selective killing of nonreplicating mycobacteria. *Cell Host Microbe*. 3:137-145.

Calder, P.C. 1995. Fuel utilization by cells of the immune system. *Proc Nutr Soc*. 54:65-82.

Calder, P.C., G. Dimitriadis, and P. Newsholme. 2007. Glucose metabolism in lymphoid and inflammatory cells and tissues. *Curr Opin Clin Nutr Metab Care*. 10:531-540.

Casteleijn, E., J. Kuiper, H.C. Van Rooij, J.A. Kamps, J.F. Koster, and T.J. Van Berkel. 1988. Endotoxin stimulates glycogenolysis in the liver by means of intercellular communication. *J Biol Chem*. 263:6953-6955.

Catron, D.M., Y. Lange, J. Borensztajn, M.D. Sylvester, B.D. Jones, and K. Haldar. 2004. Salmonella enterica serovar Typhimurium requires nonsterol precursors of the cholesterol biosynthetic pathway for intracellular proliferation. *Infect Immun*. 72:1036-1042.

Cerny, L. 1980. Histopathology and Histochemistry of Yersin Type Tuberculosis in Rabbits - Enzyme-Histochemical Study of Development of the Disease after Infection with Mycobacterium-Avium. *Acta Vet Brno*. 49:75-83.

Chakravortty, D., I. Hansen-Wester, and M. Hensel. 2002. Salmonella pathogenicity island 2 mediates protection of intracellular Salmonella from reactive nitrogen intermediates. *The Journal of experimental medicine*. 195:1155-1166.

Cheminay, C., D. Chakravortty, and M. Hensel. 2004. Role of neutrophils in murine salmonellosis. *Infect Immun*. 72:468-477.

Co, D.O., L.H. Hogan, S. Il-Kim, and M. Sandor. 2004. T cell contributions to the different phases of granuloma formation. *Immunol Lett*. 92:135-142.

Conlan, J.W. 1997. Critical roles of neutrophils in host defense against experimental systemic infections of mice by Listeria monocytogenes, Salmonella typhimurium, and Yersinia enterocolitica. *Infect Immun*. 65:630-635.

Costa Rosa, L.F., R. Curi, C. Murphy, and P. Newsholme. 1995. Effect of adrenaline and phorbol myristate acetate or bacterial lipopolysaccharide on stimulation of pathways of macrophage glucose, glutamine and O2 metabolism. Evidence for cyclic AMP-dependent protein kinase mediated inhibition of glucose-6-phosphate dehydrogenase and activation of NADP+-dependent 'malic' enzyme. *Biochem J*. 310 (Pt 2):709-714.

Cramer, T., Y. Yamanishi, B.E. Clausen, I. Forster, R. Pawlinski, N. Mackman, V.H. Haase, R. Jaenisch, M. Corr, V. Nizet, G.S. Firestein, H.P. Gerber, N. Ferrara, and R.S. Johnson. 2003. HIF-1alpha is essential for myeloid cell-mediated inflammation. *Cell*. 112:645-657.

D'Autreaux, B., and M.B. Toledano. 2007. ROS as signalling molecules: mechanisms that generate specificity in ROS homeostasis. *Nat Rev Mol Cell Biol*. 8:813-824.

Davis, S.L., E.L. Nuermberger, P.K. Um, C. Vidal, B. Jedynak, M.G. Pomper, W.R. Bishai, and S.K. Jain. 2009. Noninvasive pulmonary [18F]-2-fluoro-deoxy-D-glucose positron emission tomography correlates with bactericidal activity of tuberculosis drug treatment. *Antimicrob Agents Chemother*. 53:4879-4884.

Dhainaut, J.F., N. Marin, A. Mignon, and C. Vinsonneau. 2001. Hepatic response to sepsis: interaction between coagulation and inflammatory processes. *Crit Care Med*. 29:S42-47.

Dhar, A., and L. Castillo. 2011. Insulin resistance in critical illness. *Curr Opin Pediatr*. 23:269-274.

Dougan, G., V. John, S. Palmer, and P. Mastroeni. 2011. Immunity to salmonellosis. *Immunol Rev*. 240:196-210.

Erkkila, L., M. Jauhiainen, K. Laitinen, K. Haasio, T. Tiirola, P. Saikku, and M. Leinonen. 2005. Effect of simvastatin, an established lipid-lowering drug, on pulmonary Chlamydia pneumoniae infection in mice. *Antimicrob Agents Chemother*. 49:3959-3962.

Fang, F.C. 2011. Antimicrobial actions of reactive oxygen species. *MBio*. 2.

Feingold, K.R., I. Hardardottir, and C. Grunfeld. 1998. Beneficial effects of cytokine induced hyperlipidemia. *Z Ernahrungswiss*. 37 Suppl 1:66-74.

Fenhalls, G., L. Stevens, L. Moses, J. Bezuidenhout, J.C. Betts, P. Helden Pv, P.T. Lukey, and K. Duncan. 2002. In situ detection of Mycobacterium tuberculosis transcripts in human lung granulomas reveals differential gene expression in necrotic lesions. *Infect Immun*. 70:6330-6338.

Ferreira, A.S., M.A. de Souza, N.R. Barbosa, and S.S. da Silva. 2008. Leishmania amazonensis: xylitol as inhibitor of macrophage infection and stimulator of macrophage nitric oxide production. *Exp Parasitol*. 119:74-79.

Flynn, J.L. 2004. Mutual attraction: does it benefit the host or the bug? *Nat Immunol*. 5:778-779.

Fossati, G., D.A. Moulding, D.G. Spiller, R.J. Moots, M.R. White, and S.W. Edwards. 2003. The mitochondrial network of human neutrophils: role in chemotaxis, phagocytosis, respiratory burst activation, and commitment to apoptosis. *J Immunol*. 170:1964-1972.

Frazier, W.J., X. Wang, L.M. Wancket, X.A. Li, X. Meng, L.D. Nelin, A.C. Cato, and Y. Liu. 2009. Increased inflammation, impaired bacterial clearance, and metabolic disruption after gram-negative sepsis in Mkp-1-deficient mice. *J Immunol*. 183:7411-7419.

Funk, J.L., K.R. Feingold, A.H. Moser, and C. Grunfeld. 1993. Lipopolysaccharide stimulation of RAW 264.7 macrophages induces lipid accumulation and foam cell formation. *Atherosclerosis*. 98:67-82.

Galli, S.J., N. Borregaard, and T.A. Wynn. 2011. Phenotypic and functional plasticity of cells of innate immunity: macrophages, mast cells and neutrophils. *Nat Immunol*. 12:1035-1044.

Gao, B., W.I. Jeong, and Z. Tian. 2008. Liver: An organ with predominant innate immunity. *Hepatology*. 47:729-736.

Garedew, A., S.O. Henderson, and S. Moncada. 2010. Activated macrophages utilize glycolytic ATP to maintain mitochondrial membrane potential and prevent apoptotic cell death. *Cell Death Differ*. 17:1540-1550.

Garedew, A., and S. Moncada. 2008. Mitochondrial dysfunction and HIF1alpha stabilization in inflammation. *J Cell Sci*. 121:3468-3475.

Geddes, K., F. Cruz, and F. Heffron. 2007. Analysis of cells targeted by Salmonella type III secretion in vivo. *PLoS Pathog*. 3:e196.

Gordon, S., and F.O. Martinez. 2010. Alternative activation of macrophages: mechanism and functions. *Immunity*. 32:593-604.

Grant, A.J., O. Restif, T.J. McKinley, M. Sheppard, D.J. Maskell, and P. Mastroeni. 2008. Modelling within-host spatiotemporal dynamics of invasive bacterial disease. *PLoS Biol*. 6:e74.

Grossart, H.P., C. Dziallas, F. Leunert, and K.W. Tang. 2010. Bacteria dispersal by hitchhiking on zooplankton. *Proc Natl Acad Sci U S A*. 107:11959-11964.

Helaine, S., J.A. Thompson, K.G. Watson, M. Liu, C. Boyle, and D.W. Holden. 2010. Dynamics of intracellular bacterial replication at the single cell level. *Proc Natl Acad Sci U S A*. 107:3746-3751.

Henard, C.A., and A. Vazquez-Torres. 2011. Nitric oxide and salmonella pathogenesis. *Front Microbiol*. 2:84.

Hoff, D.R., G.J. Ryan, E.R. Driver, C.C. Ssemakulu, M.A. De Groote, R.J. Basaraba, and A.J. Lenaerts. 2011. Location of intra- and extracellular M. tuberculosis populations in lungs of mice and guinea pigs during disease progression and after drug treatment. *PLoS One*. 6:e17550.

Holub, M., C.W. Cheng, S. Mott, P. Wintermeyer, N. van Rooijen, and S.H. Gregory. 2009. Neutrophils sequestered in the liver suppress the proinflammatory response of Kupffer cells to systemic bacterial infection. *J Immunol*. 183:3309-3316.

Hormaeche, C.E. 1980. The in vivo division and death rates of Salmonella typhimurium in the spleens of naturally resistant and susceptible mice measured by the superinfecting phage technique of Meynell. *Immunology*. 41:973-979.

Hsu, H.S. 1989. Pathogenesis and immunity in murine salmonellosis. *Microbiol Rev*. 53:390-409.

Jungermann, K., and T. Kietzmann. 1996. Zonation of parenchymal and nonparenchymal metabolism in liver. *Annu Rev Nutr*. 16:179-203.

Kantari, C., M. Pederzoli-Ribeil, and V. Witko-Sarsat. 2008. The role of neutrophils and monocytes in innate immunity. *Contrib Microbiol*. 15:118-146.

Khovidhunkit, W., M.S. Kim, R.A. Memon, J.K. Shigenaga, A.H. Moser, K.R. Feingold, and C. Grunfeld. 2004. Effects of infection and inflammation on lipid and lipoprotein metabolism: mechanisms and consequences to the host. *J Lipid Res*. 45:1169-1196.

Kim, M.J., H.C. Wainwright, M. Locketz, L.G. Bekker, G.B. Walther, C. Dittrich, A. Visser, W. Wang, F.F. Hsu, U. Wiehart, L. Tsenova, G. Kaplan, and D.G. Russell. 2010. Caseation of human tuberculosis granulomas correlates with elevated host lipid metabolism. *EMBO Mol Med*. 2:258-274.

Klion, A.D., and T.B. Nutman. 2004. The role of eosinophils in host defense against helminth parasites. *J Allergy Clin Immunol*. 113:30-37.

Knolle, P.A., and G. Gerken. 2000. Local control of the immune response in the liver. *Immunol Rev*. 174:21-34.

Kobayashi, S.D., and F.R. DeLeo. 2009. Role of neutrophils in innate immunity: a systems biology-level approach. *Wiley Interdiscip Rev Syst Biol Med*. 1:309-333.

Korbel, D.S., B.E. Schneider, and U.E. Schaible. 2008. Innate immunity in tuberculosis: myths and truth. *Microbes Infect*. 10:995-1004.

Kumar, H., T. Kawai, and S. Akira. 2011. Pathogen recognition by the innate immune system. *Int Rev Immunol*. 30:16-34.

Laskin, D.L., B. Weinberger, and J.D. Laskin. 2001. Functional heterogeneity in liver and lung macrophages. *J Leukoc Biol*. 70:163-170.

Levine, A.J., and A.M. Puzio-Kuter. 2010. The control of the metabolic switch in cancers by oncogenes and tumor suppressor genes. *Science*. 330:1340-1344.

Liu, S., D.J. Gallo, A.M. Green, D.L. Williams, X. Gong, R.A. Shapiro, A.A. Gambotto, E.L. Humphris, Y. Vodovotz, and T.R. Billiar. 2002. Role of toll-like receptors in changes in gene expression and NF-kappa B activation in mouse hepatocytes stimulated with lipopolysaccharide. *Infect Immun*. 70:3433-3442.

Maitra, S.R., S. Wang, C.E. Brathwaite, and M.R. El-Maghrabi. 2000. Alterations in glucose-6-phosphatase gene expression in sepsis. *J Trauma*. 49:38-42.

Mastroeni, P. 2002. Immunity to systemic Salmonella infections. *Curr Mol Med*. 2:393-406.

Mastroeni, P., A. Vazquez-Torres, F.C. Fang, Y. Xu, S. Khan, C.E. Hormaeche, and G. Dougan. 2000. Antimicrobial actions of the NADPH phagocyte oxidase and inducible nitric oxide synthase in experimental salmonellosis. II. Effects on microbial proliferation and host survival in vivo. *The Journal of experimental medicine*. 192:237-248.

Meszaros, K., J. Bojta, A.P. Bautista, C.H. Lang, and J.J. Spitzer. 1991. Glucose utilization by Kupffer cells, endothelial cells, and granulocytes in endotoxemic rat liver. *Am J Physiol*. 260:G7-12.

Molteni, R., M. Fabbri, J.R. Bender, and R. Pardi. 2006. Pathophysiology of leukocyte-tissue interactions. *Curr Opin Cell Biol*. 18:491-498.

Mosser, D.M., and J.P. Edwards. 2008. Exploring the full spectrum of macrophage activation. *Nat Rev Immunol*. 8:958-969.

Muller, W.A. 2003. Leukocyte-endothelial-cell interactions in leukocyte transmigration and the inflammatory response. *Trends Immunol*. 24:327-334.

Nathan, C. 2003. Specificity of a third kind: reactive oxygen and nitrogen intermediates in cell signaling. *J Clin Invest*. 111:769-778.

Nemeth, E., A.W. Baird, and C. O'Farrelly. 2009. Microanatomy of the liver immune system. *Semin Immunopathol*. 31:333-343.

Netea, M.G., L.A. Joosten, M. Keuter, F. Wagener, A.F. Stalenhoef, J.W. van der Meer, and B.J. Kullberg. 2009. Circulating lipoproteins are a crucial component of host defense against invasive Salmonella typhimurium infection. *PLoS One*. 4:e4237.

Newsholme, P., L.F. Costa Rosa, E.A. Newsholme, and R. Curi. 1996. The importance of fuel metabolism to macrophage function. *Cell Biochem Funct*. 14:1-10.

Nizet, V., and R.S. Johnson. 2009. Interdependence of hypoxic and innate immune responses. *Nat Rev Immunol*. 9:609-617.

Oberholzer, A., C. Oberholzer, and L.L. Moldawer. 2001. Sepsis syndromes: understanding the role of innate and acquired immunity. *Shock*. 16:83-96.

Odegaard, J.I., R.R. Ricardo-Gonzalez, M.H. Goforth, C.R. Morel, V. Subramanian, L. Mukundan, A. Red Eagle, D. Vats, F. Brombacher, A.W. Ferrante, and A. Chawla. 2007. Macrophage-specific PPARgamma controls alternative activation and improves insulin resistance. *Nature*. 447:1116-1120.

Pastor, C.M., T.R. Billiar, M.R. Losser, and D.M. Payen. 1995. Liver injury during sepsis. *J Crit Care*. 10:183-197.

Peachman, K.K., D.S. Lyles, and D.A. Bass. 2001. Mitochondria in eosinophils: functional role in apoptosis but not respiration. *Proc Natl Acad Sci U S A*. 98:1717-1722.

Pieters, J. 2008. Mycobacterium tuberculosis and the macrophage: maintaining a balance. *Cell Host Microbe*. 3:399-407.

Richter-Dahlfors, A., A.M. Buchan, and B.B. Finlay. 1997. Murine salmonellosis studied by confocal microscopy: Salmonella typhimurium resides intracellularly inside macrophages and exerts a cytotoxic effect on phagocytes in vivo. *The Journal of experimental medicine*. 186:569-580.

Robinson, J.M. 2009. Phagocytic leukocytes and reactive oxygen species. *Histochem Cell Biol*. 131:465-469.

Rock, F.L., G. Hardiman, J.C. Timans, R.A. Kastelein, and J.F. Bazan. 1998. A family of human receptors structurally related to Drosophila Toll. *Proc Natl Acad Sci U S A*. 95:588-593.

Rodriguez-Prados, J.C., P.G. Traves, J. Cuenca, D. Rico, J. Aragones, P. Martin-Sanz, M. Cascante, and L. Bosca. 2010. Substrate fate in activated macrophages: a comparison between innate, classic, and alternative activation. *J Immunol*. 185:605-614.

Sakaguchi, O., C.C. Hsu, and S. Sakaguchi. 1980. Metabolic aspects in mice administered live Salmonella typhimurium. *Microbiol Immunol*. 24:789-802.

Santos, R.L., S. Zhang, R.M. Tsolis, R.A. Kingsley, L.G. Adams, and A.J. Baumler. 2001. Animal models of Salmonella infections: enteritis versus typhoid fever. *Microbes Infect*. 3:1335-1344.

Segal, A.W. 2005. How neutrophils kill microbes. *Annu Rev Immunol*. 23:197-223.

Shapiro, H., A. Lutaty, and A. Ariel. 2011. Macrophages, meta-inflammation, and immuno-metabolism. *ScientificWorldJournal*. 11:2509-2529.

Sheppard, M., C. Webb, F. Heath, V. Mallows, R. Emilianus, D. Maskell, and P. Mastroeni. 2003. Dynamics of bacterial growth and distribution within the liver during Salmonella infection. *Cell Microbiol*. 5:593-600.

Silva, M.T. 2011. Macrophage phagocytosis of neutrophils at inflammatory/infectious foci: a cooperative mechanism in the control of infection and infectious inflammation. *J Leukoc Biol*. 89:675-683.

Simon, L.M., E.D. Robin, J.R. Phillips, J. Acevedo, S.G. Axline, and J. Theodore. 1977. Enzymatic basis for bioenergetic differences of alveolar versus peritoneal macrophages and enzyme regulation by molecular O2. *J Clin Invest*. 59:443-448.

Slauch, J.M. 2011. How does the oxidative burst of macrophages kill bacteria? Still an open question. *Mol Microbiol*. 80:580-583.

Snyder, I.S. 1971. Enzyme activities of the livers of mice infected with Salmonella typhimurium. *Infect Immun*. 4:411-415.

Somashekar, B.S., A.G. Amin, C.D. Rithner, J. Troudt, R. Basaraba, A. Izzo, D.C. Crick, and D. Chatterjee. 2011. Metabolic profiling of lung granuloma in Mycobacterium tuberculosis infected guinea pigs: ex vivo 1H magic angle spinning NMR studies. *J Proteome Res*. 10:4186-4195.

Spitzer, J.J., G.J. Bagby, K. Meszaros, and C.H. Lang. 1988. Alterations in lipid and carbohydrate metabolism in sepsis. *JPEN J Parenter Enteral Nutr*. 12:53S-58S.

Splettstoesser, W.D., and P. Schuff-Werner. 2002. Oxidative stress in phagocytes--"the enemy within". *Microsc Res Tech*. 57:441-455.

Spolarics, Z. 1998. Endotoxemia, pentose cycle, and the oxidant/antioxidant balance in the hepatic sinusoid. *J Leukoc Biol*. 63:534-541.

Spolarics, Z., G.J. Bagby, C.H. Lang, and J.J. Spitzer. 1991. Up-regulation of glucose metabolism in Kupffer cells following infusion of tumour necrosis factor. *Biochem J*. 278 (Pt 2):515-519.

Svec, F., and J.R. Porter. 1998. The actions of exogenous dehydroepiandrosterone in experimental animals and humans. *Proc Soc Exp Biol Med*. 218:174-191.

Swirski, F.K., M. Nahrendorf, M. Etzrodt, M. Wildgruber, V. Cortez-Retamozo, P. Panizzi, J.L. Figueiredo, R.H. Kohler, A. Chudnovskiy, P. Waterman, E. Aikawa, T.R. Mempel, P. Libby, R. Weissleder, and M.J. Pittet. 2009. Identification of splenic reservoir monocytes and their deployment to inflammatory sites. *Science*. 325:612-616.

Takada, Y., X. Ye, and S. Simon. 2007. The integrins. *Genome Biol*. 8:215.

Theilgaard-Monch, K., S. Knudsen, P. Follin, and N. Borregaard. 2004. The transcriptional activation program of human neutrophils in skin lesions supports their important role in wound healing. *J Immunol*. 172:7684-7693.

Thrasher, A.J., and A.W. Segal. 2011. A phagocyte dilemma. *Nat Immunol*. 12:201-202.

Trager, K., D. DeBacker, and P. Radermacher. 2003. Metabolic alterations in sepsis and vasoactive drug-related metabolic effects. *Curr Opin Crit Care*. 9:271-278.

Umezawa, K., T. Akaike, S. Fujii, M. Suga, K. Setoguchi, A. Ozawa, and H. Maeda. 1997. Induction of nitric oxide synthesis and xanthine oxidase and their roles in the antimicrobial mechanism against Salmonella typhimurium infection in mice. *Infect Immun*. 65:2932-2940.

Van Noorden, C.J. 2010. Imaging enzymes at work: metabolic mapping by enzyme histochemistry. *J Histochem Cytochem*. 58:481-497.

Varin, A., and S. Gordon. 2009. Alternative activation of macrophages: immune function and cellular biology. *Immunobiology*. 214:630-641.

Vats, D., L. Mukundan, J.I. Odegaard, L. Zhang, K.L. Smith, C.R. Morel, R.A. Wagner, D.R. Greaves, P.J. Murray, and A. Chawla. 2006. Oxidative metabolism and PGC-1beta attenuate macrophage-mediated inflammation. *Cell Metab*. 4:13-24.

Vazquez-Torres, A., J. Jones-Carson, A.J. Baumler, S. Falkow, R. Valdivia, W. Brown, M. Le, R. Berggren, W.T. Parks, and F.C. Fang. 1999. Extraintestinal dissemination of Salmonella by CD18-expressing phagocytes. *Nature*. 401:804-808.

Vazquez-Torres, A., Y. Xu, J. Jones-Carson, D.W. Holden, S.M. Lucia, M.C. Dinauer, P. Mastroeni, and F.C. Fang. 2000. Salmonella pathogenicity island 2-dependent evasion of the phagocyte NADPH oxidase. *Science*. 287:1655-1658.

Vidal, S.M., D. Malo, K. Vogan, E. Skamene, and P. Gros. 1993. Natural resistance to infection with intracellular parasites: isolation of a candidate for Bcg. *Cell*. 73:469-485.

Wallington, J., J. Ning, and M.A. Titheradge. 2008. The control of hepatic glycogen metabolism in an in vitro model of sepsis. *Mol Cell Biochem*. 308:183-192.

Walton, K.A., A.L. Cole, M. Yeh, G. Subbanagounder, S.R. Krutzik, R.L. Modlin, R.M. Lucas, J. Nakai, E.J. Smart, D.K. Vora, and J.A. Berliner. 2003. Specific phospholipid oxidation products inhibit ligand activation of toll-like receptors 4 and 2. *Arterioscler Thromb Vasc Biol*. 23:1197-1203.

Watson, K.G., and D.W. Holden. 2010. Dynamics of growth and dissemination of Salmonella in vivo. *Cell Microbiol*. 12:1389-1397.

Weber, C., L. Fraemohs, and E. Dejana. 2007. The role of junctional adhesion molecules in vascular inflammation. *Nat Rev Immunol*. 7:467-477.

Wertheimer, F.W. 1967. Enzyme histochemistry of giant-cell reparative granulomas. *Oral Surg Oral Med Oral Pathol*. 23:464-469.

West, A.P., I.E. Brodsky, C. Rahner, D.K. Woo, H. Erdjument-Bromage, P. Tempst, M.C. Walsh, Y. Choi, G.S. Shadel, and S. Ghosh. 2011. TLR signalling augments macrophage bactericidal activity through mitochondrial ROS. *Nature*. 472:476-480.

6. Acknowledgements

First of all I would like to thank my PhD supervisor, Prof. Dirk Bumann, for his inexhaustible support and enthusiasm about my project and the good supervision. Many thanks for all the time you invested.

I would like to thank my PhD committee, Prof. Christoph Dehio and Prof. Markus Heim for their time and valuable suggestions.

Many thanks to Alex Schmidt and Timo Glatter at the proteomics core facility for help with proteome analysis and to Julien Limenitakis for visualization of the data.

Thanks to past and present members of the Bumann lab for suggestions, help and a nice atmosphere.

Special thanks to Bea and Alain for taking care of me in the lab when I started and many, many mice infections. Thanks to Neil for mice infections and cooperation on the iNOS project. Thanks to Janine and Bea for sorting. Thanks to Hesso for telling funny stories and giving cell culture advise from the distance. Thanks to Nikki for the cheerful Christmas parties. Thanks to Mauricio 'mROS' for nice discussions about macrophages and monkeys. Thanks to Anna, Mauricio and Julien for drinkable/edible PhD student support.

Thanks to my fellow PhD students in the lab, I really enjoyed the time with both of you.

I enjoyed our Mensa club, so thanks to Benni, Some, Olivier, Ramona, Hesso, Carolina and Mauricio for the cheerful time.

Thanks to all the people on the floor, for your smiling faces and your help on many occasions.

Special thanks to Elli, Kathrin, Lucie, Matthias and Uli for distractions from work.

Thanks to my friends back home, for welcoming me with open arms, whenever I am there.

Thanks to my parents and my brother for their support.

Thank you Benni, for always picking me up by car, when the last train home was already gone. And for so much more.

7. List of abbreviations

4-HNE	4-Hydroxynonenal
AP	Activator protein
APC	Antigen presenting cell
Arg	L-arginine
ATP	Adenosine triphosphate
CD	Cluster of differentiation
CE	Cholesterol ester
CHO	Free cholesterol
Cit	Citrulline
CPS-1	Carbamoyl phosphate synthetase
DNA	Desoxyribonuleic acid
FA	Fatty acid
FACS	Fluorescence-activated cell sorting
FFA	Free fatty acid
GAPDH	Glyceraldehyde-3-phosphate dehydrogenase
G6PDH	Glucose-6-phosphate dehydrogenase
G6P	Glucose-6-phosphate
G6Pase	Glucose-6-phosphatase
G6PI	Glucose-6-phosphate isomerase
GFP	Green fluorescent protein
GK	Glucokinase
GLUT	Glucose transporter
GSH	Glutathione
GSSG	Glutathione disulfide
H_2O_2	Hydrogen peroxide
Hi	High
HIF-1α	Hypoxia-inducible factor alpha
HK	Hexokinase
HMP shunt	Hexose monophosphate shunt
ICAM	Intercellular adhesion molecule

IDH	Isocitrate dehydrogenase
IFN	Interferon
IL	Interleukin
iNOS	Inducible nitric oxide synthase
i.p.	Intraperitoneal
i.v.	Intravenous
KC	Kupffer cell
LBP	Lipopolysaccharide binding protein
LDH	Lactate dehydrogenase
Lo	Low
LPS	Lipopolysaccharide
MDH	Malate dehydrogenase
MHC	Major histocompatibility complex
Me	Medium
M cells	Microfold cells
mRNA	Messenger ribonucleic acid
mROS	Mitochondrial reactive oxygen species
MTB	*Mycobacterium tuberculosis*
NADH	Nicotinamide adenine dinucleotide
NADPH	Nicotinamide adenine dinucleotide phosphate
NBT	Nitro blue tetrazolium chloride
NFκB	Nuclear factor kappa B
NET	Neutrophil extracellular trap
NO	Nitric oxide
NOD	Nucleotide-binding oligomerization domain-containing protein
NOHLA	N^{ω}-hydroxy-L-arginine
Nramp	Natural resistance-associated macrophage protein
NT	Nitrotyrosine
oxLDL	Oxidized low density lipoprotein
OXPHOS	Oxidative phosphorylation
O_2	Oxygen

PAMP	Pathogen-associated molecular pattern
PET	Positron emission tomography
PGC	Peroxisome proliferator-activated receptor-gamma coactivator
PGDH	6-Phosphogluconate dehydrogenase
Phox	Phagocytic oxidase (= NADPH oxidase)
PMA	Phorbol-12-myristate-13-acetate
PMN	Polymorphonuclear leukocyte
PPAR	Peroxisome proliferator-activated receptors
PRR	Pattern-recognition receptor
ROS	Reactive oxygen species
RNS	Reactive nitrogen species
SCV	*Salmonella*-containing vacuole
SDH	Succinate dehydrogenase
SOD	Superoxide dismutase
SPI1	*Salmonella* pathogenicity island one
SPI2	*Salmonella* pathogenicity island two
STAT	Signal Transducer and Activator of Transcription
T3SS	Type three secretion system
TCA cycle	Tricarboxylic acid cycle
TG	Triglyceride
Th	T helper cell
TLR	Toll-like receptor
TNBT	Tetranitro blue tetrazolium
TNF-α	Tumor necrosis factor alpha
VCAM	Vascular cell adhesion protein
Vs.	Versus